



Universiteit  
Leiden  
The Netherlands

## Single-Molecule Probes in Organic Field-Effect Transistors

Nicolet, A.A.L.

### Citation

Nicolet, A. A. L. (2007, October 4). *Single-Molecule Probes in Organic Field-Effect Transistors. Casimir PhD Series*. Retrieved from <https://hdl.handle.net/1887/12366>

Version: Corrected Publisher's Version

License: [Licence agreement concerning inclusion of doctoral thesis in the Institutional Repository of the University of Leiden](#)

Downloaded from: <https://hdl.handle.net/1887/12366>

**Note:** To cite this publication please use the final published version (if applicable).

# Single-Molecule Probes in Organic Field-Effect Transistors

PROEFSCHRIFT

ter verkrijging van  
de graad van Doctor aan de Universiteit Leiden,  
op gezag van Rector Magnificus prof.mr. P.F. van der Heijden,  
volgens besluit van het College voor Promoties  
te verdedigen op woensdag 4 oktober 2007  
klokke 13.45 uur

door

**Aurélien Armel Louis Nicolet**

geboren te La Tronche

in 1977

**Promotiecommissie:**

Promotor: Prof. Dr. M. A. G. J. Orrit  
Referent: Prof. Dr. B. Lounis (Université Bordeaux)  
Overige Leden: Prof. Dr. A. Morpurgo (TU Delft)  
Prof. Dr. J. M. van Ruitenbeek  
Prof. Dr. J. Aarts  
Prof. Dr. E. J. J. Groenen  
Prof. Dr. S. Völker

The presented work is part of the research program of the Stichting voor Fundamenteel Onderzoek der Materie (FOM), which is financially supported by the Nederlandse Organisatie voor Wetenschappelijk Onderzoek (NWO).

Casimir PhD Series, Delft-Leiden, 2007-12  
ISBN: 978-90-8593-035-8

# Contents

<b>1</b>	<b>Introduction</b>	<b>1</b>
1.1	Towards nanoprobes for conduction in molecular crystals . . .	2
1.1.1	Organic field-effect transistors . . . . .	3
1.1.2	Single-molecule spectroscopy and nano-probes . . . . .	4
1.2	Outline of the thesis . . . . .	7
<b>2</b>	<b>Terrylene in anthracene: Intermolecular intersystem-crossing</b>	<b>11</b>
2.1	Introduction . . . . .	12
2.2	Experimental . . . . .	13
2.3	Results . . . . .	15
2.4	Discussion . . . . .	22
2.5	Conclusion . . . . .	25
<b>3</b>	<b>Dibenzoterrylene in anthracene: I. Spectroscopy and photo- physics</b>	<b>27</b>
3.1	Introduction . . . . .	28
3.2	Experimental . . . . .	29
3.2.1	Sample preparation . . . . .	29
3.2.2	Optical setup . . . . .	30
3.2.3	Signal acquisition . . . . .	30
3.3	Results and discussion . . . . .	31
3.4	Conclusion . . . . .	39
<b>4</b>	<b>Dibenzoterrylene in anthracene: II. Main insertion sites</b>	<b>41</b>
4.1	Introduction . . . . .	42
4.2	Experimental and results . . . . .	44
4.2.1	Experimental . . . . .	44
4.2.2	Temperature and pressure dependence . . . . .	44
4.2.3	Orientation . . . . .	46
4.2.4	Stark effect . . . . .	47
4.3	Simulations . . . . .	50
4.3.1	Molecular modelling . . . . .	50
4.3.2	Identification of the insertion sites . . . . .	51

4.4	Discussion . . . . .	55
4.5	Conclusion . . . . .	57
<b>5</b>	<b>The transistors</b>	<b>59</b>
5.1	Introduction . . . . .	60
5.2	Experimental . . . . .	62
5.3	Result and discussion . . . . .	63
5.4	Conclusion . . . . .	67
<b>6</b>	<b>Probing charges</b>	<b>69</b>
6.1	Charge injection . . . . .	70
6.2	Transistors and single-molecule . . . . .	72
6.2.1	DC regime . . . . .	73
	Model with a single jump . . . . .	75
	The continuous-time random walk . . . . .	77
6.2.2	AC regime . . . . .	82
	Resonances . . . . .	83
	Discussion . . . . .	86
6.3	Conclusion . . . . .	88
<b>7</b>	<b>Conclusions and perspectives</b>	<b>91</b>
	<b>Bibliography</b>	<b>95</b>
	<b>Samenvatting</b>	<b>109</b>
	<b>List of publications</b>	<b>115</b>
	<b>Curriculum vitae</b>	<b>117</b>
	<b>Nawoord</b>	<b>119</b>

# 1 Introduction

**B**UILDING and integrating more and more electronic structures on a smaller and smaller area is one of the fascinating technological challenges of today. In the end, the ultimate limit is only given by the finite size of atoms and molecules. The description of the physical processes in these structures goes much beyond the simple interpolation between the well-known worlds of macroscopic physics on the one hand and of the quantum mechanics of atoms and small molecules on the other hand. It is, therefore, necessary to find a way to study and understand the electric processes at these mesoscopic and nanometric scales in order to predict the function of new nanoscale devices. The nano-instruments which are needed for this purpose could be simple nano-objects that are placed in the vicinity of the device under study. By measuring the perturbations exerted by the device on the nano-instrument, information could be obtained about the working of the device. Amongst the possible nano-instruments, single molecules have proved to be very sensitive nanoprobles for processes in their local neighbourhood. Their use could bring new insight into electronic processes at nanometer scales.

## 1.1 Towards nanoprobes for conduction in molecular crystals

Considering their electric properties, materials can be divided in four different categories. The two first categories consist of materials for which charges can travel with ease, either with a small resistance in the case of conductors, or without any, in the case of superconductors. As a third category are the insulators, for which the charges are localised and, as a consequence, conduction is not possible. A last category consists of semiconductors, which present a situation in between conductors and insulators. Under certain conditions, these materials can be either insulators or conductors.

Excluding the case of superconductivity, the electrical properties of these materials can be described according to a band theory, with a conduction-band and a valence-band, separated by a gap. In conductors, the charges are completely filling the valence-band and partly the conduction-band. In the case of semiconductors and insulators, the conduction-band is empty, and no charges can travel through the materials at zero temperature. The main difference between semiconductors and insulators is the width of the gap between the two bands: a large gap does not permit charges to travel in insulators, while a small gap in semiconductors makes conduction possible when an electric field is applied. Conductors and semiconductors are generally made of inorganic materials.

However, in 1977, the first report on electrical conduction in organic material showed that polymers, which were considered as insulators, could turn to a metallic behaviour when correctly doped [1]. Following this result, numerous studies were motivated by the potential advantages of organic materials: a low cost of production and several interesting mechanical properties such as strength and flexibility. The combination of the advantages of organic materials with properties of metals or semiconductors has opened the way for many new applications. Nowadays, new polymer devices have been successfully developed, such as large-area displays, light-emitting devices and solar cells.

The electronic properties of Van der Waals bonded organic semiconductors and those of their covalently/ionically bonded inorganic counterpart are very different. Organic semiconductors are characterised by a strong electron-phonon coupling and a small inter-molecular hopping amplitude. This results in the formation of polarons [2,3], which determine the transport properties of these materials. Polaron formation involves many-particle interactions, therefore, this complicated problem has mainly been treated phenomenologically.

Additionally, basic aspects of the problem have not been addressed yet and a satisfactory microscopic description is still missing [4].

While most of these applications involve polymers, which are characterised by disorder and complexity, for fundamental research, it is a natural choice to look for assemblies of smaller molecules with a higher degree of structural ordering such as molecular crystals. A similar description in terms of band-gap theory can be achieved in the case of organic crystals. The conduction-band is then replaced by the lowest unoccupied molecular orbitals (LUMO) and the valence-band by the highest occupied molecular orbitals (HOMO). However, reality is far more complex and in general, the gap contains numerous intermediate states created by impurities and defects of the crystals, which will act as traps for electrons or holes. These traps will play a critical role in the conduction phenomena.

The electrical properties are usually studied measuring the mobility, which represents the ease for charges to travel through the material. The measurement of this parameter gives ideas about the possible physical processes involved in the conduction phenomenon. Its temperature dependence gives important information about the energy distribution of the traps. However, the mobility is an ensemble parameter, and the values obtained result from an average of microscopic events. It is then difficult from the macroscopic measurement to distinguish between several possible mechanisms involved in the conduction processes. A solution to this problem would consist in measuring locally the electric field with a nanoprobe inserted inside the material.

In order to have a satisfactory control over the measurements, the probes should be embedded in a well defined structure, such that the conduction paths can be easily identified. Field-effect transistors are good candidates for this purpose.

### 1.1.1 Organic field-effect transistors

An organic field-effect transistor (FET) consists of three electrodes contacted to an organic semiconductor material. The source and the drain are co-planar and are directly connected to the semiconductor. We will consider from now on that the semiconductor is an organic molecular crystal. Applying a voltage to the drain will induce a displacement of charges inside the crystal and, consequently, a current will be detected. However, in order to have a current, it is necessary to inject charges into the crystal. This is one of the main advantages of a FET: it is possible to vary the charge density in the organic material via a transverse gate electrode, separated from the crystal by an insulator layer. Applying a gate-voltage will then inject charges inside the



conducting layer, creating in this way charges available for conduction. Hence, the number of charges moving inside the crystal when applying a source-drain voltage will increase, and so will the current.

The characterisation of a FET is done by measuring the current-voltage or  $I - V$  curves. We can measure the source-drain current either as a function of the source-drain voltage or of the gate voltage. From these measurements, it is then possible to extract the mobility, which, in principle, is an intrinsic property of the conducting material.

Unfortunately, the extrapolation from the measured mobility to the intrinsic one is not always straightforward. Indeed, the contact effects between the electrodes and the conducting material are not easy to take into account. Moreover, the contributions of charge injection, conduction and trapping are not decorrelated and the measured parameter results from an interplay of all these phenomena.

In order to keep the advantages of a FET, we propose to insert nano-objects inside the material. Being sensitive to the electric field, those local probes could 'feel' changes and heterogeneities of the local field. We propose to use individual molecules, which can be optically addressed by means of single-molecule spectroscopy (SMS).

### 1.1.2 Single-molecule spectroscopy and nano-probes

When interacting with matter, light can excite an electron from an occupied energy level to a higher empty energy level. In general, this can happen when the energy difference between the two levels is exactly the amount of energy provided by the incident photon. Following this process, the electron can either relax to its ground state by transforming the energy into heat (phonon assisted), or by emitting back a photon of a lower energy than the excitation one. In the most general case, a combination of the two processes will take place. In the case of emission of light, the latter is called fluorescence.

Let us imagine a particular molecule which can fluoresce. If we dilute these molecules in such a way, that we have at most one molecule in a confocal volume, we can, in principle, detect a single molecule. This is called single-molecule microscopy. It is the basis of many applications, especially in biology, where fluorescent molecules are attached to an object (a protein for example; in that case we will say that the protein is labelled). Then, the detection of the fluorescence allows one to track the movements of this object inside the cell. In solid samples at cryogenic temperatures, there is another way to select a molecule than the spatial one. Tuning carefully the wavelength of the excitation light, it is possible to select a molecule spectrally as well. In the latter

case, we will speak about single-molecule spectroscopy (SMS). SMS usually requires to have the molecules inserted into a matrix. Optically addressed, single fluorescent molecules have proved to be very sensitive spectral probes of small perturbations in their vicinity.

When inserted into a matrix (the host), the fluorophores (the guests) are exposed to different local constraints. Because of the high sensitivity to small differences in their environment, each guest molecule will absorb (and emit) photons at different wavelengths. Hence, the signal from an ensemble, which is the average over all individual molecules, is much broader than the one from a single molecule. At liquid-helium temperatures the zero-phonon lines (ZPL) of typical dye molecules are very narrow with widths of typically 10–100 MHz (about  $10^{-3} \text{ cm}^{-1}$ ). At low temperatures, zero-phonon lines can, therefore, be used as very sensitive probes for processes in the molecules' neighbourhood, up to several nm away, as induced shifts of the order of  $10^{-7}$  of the absolute optical frequency can easily be detected.

In various high-resolution studies, single-molecule probes have been used as thermometers via the broadening of the single-molecule lines [5–7], as manometers, via the pressure induced shift of the lines [8, 9], as magnetometers, via the effects of the triplet states of the chromophore [10–13], or as voltmeters via the Stark shift of the energy levels of the molecule [14–18].

An electric field will change the absorption frequency of the molecule via the Stark effect [14, 15]. Figure 1.1 shows the energy levels of a molecule with and without an electric field. In the presence of an electric field, the shift induced by the field on the energy levels is not the same for the excited and the ground states. The Stark shift is the difference of the shifts of the two levels.

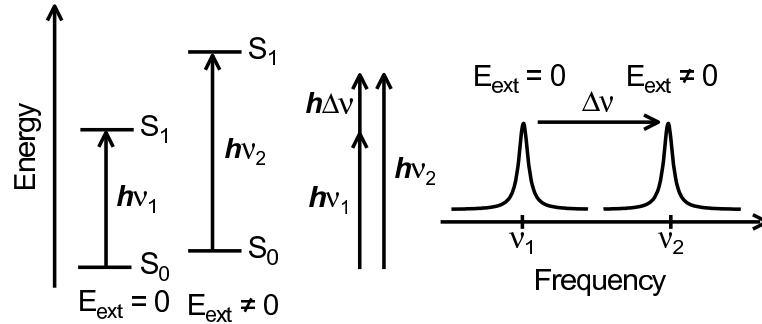


**Figure 1.1:** Influence of an electric field over the energy levels of a chromophore: Stark effect.

In a pure insulator, the probe molecules are only affected by electrostatic

fields as no movement of charge carriers occurs. The observed shift will be just the Stark shift. However, materials in which charge transport occurs are expected to show a richer variety of interaction mechanisms [19–22], as a charge will create an additional local field in the environment of the chromophore. Therefore, we can also probe local movements of charges in the vicinity of the molecules.

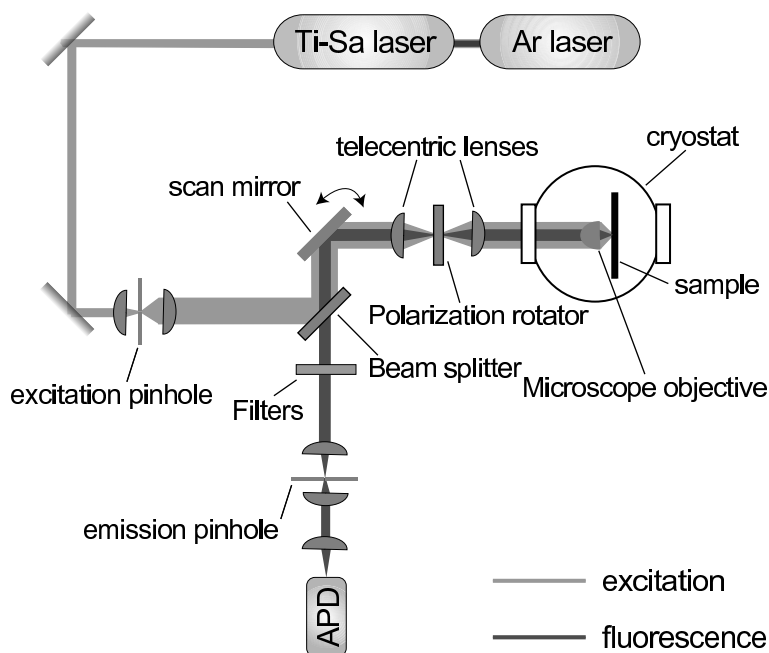


**Figure 1.2:** Confocal microscopy and spectroscopy setup.

High spectroscopic resolution can be obtained for probe molecules inserted into an organic molecular crystal at low temperatures, as no additional phonon-induced broadening of the ZPL occurs. Single-molecule studies are performed with the confocal microscopy and spectroscopic techniques. Figure 1.2 shows, as an example, the experimental setup used in the studies presented in Chapters 3, 4 and 6. A titanium sapphire (Ti-Saph) laser, pumped by an argon (Ar) laser, produces the excitation light with a precisely defined wavelength tunable from 700 to 800 nm. The laser light is then focused on the sample by means of a microscope objective, with a focal spot area of about  $1 \mu\text{m}^2$ . The sample is kept inside a cryostat in superfluid He. A scanning mirror allows us to move the focal point over an area of the sample of 200 times

200  $\mu\text{m}^2$ . Changing the wavelength of the laser and the position of the focal point onto the sample makes it possible to select a molecule both spectrally and spatially. The reflected laser light is then blocked by a long-pass filter, which is transparent for the red-shifted fluorescence. The strength of confocal microscopy resides in the use of an emission pinhole that eliminates all out-of-focus light, increasing considerably the signal to noise ratio. Finally, the fluorescence signal is detected by means of an avalanche photodiode (APD).

We propose to use single molecules as nanoprobe to investigate electric transport phenomena in organic crystals.

## 1.2 Outline of the thesis

Applying SMS in a well-defined micro-structure configuration should allow us to correlate optical and electrical properties on comparable scales and to distinguish between effects induced by the applied electric field, by the movement of individual charge carriers, and those due to the macroscopic current. Using confocal microscopy as well as spectroscopy will allow us to relate different spectral properties of the probe molecules with their spatial position in the nanostructure. The use of small well-defined micro-fabricated structures such as FET structures forces the current in a limited spatial spot and facilitates the identification of particular conduction paths.

Such a study brings together both the constraints of SMS and of FET. The first step of this work therefore consisted in finding a suitable guest-host combination, favourable for SMS, with a matrix which should act as a conducting material for the FET.

Chapter 2 of this thesis stresses a novel fundamental requirement for SMS concerning the energy levels of the guest with respect to the host. Taking the example of terrylene (Tr) molecules embedded in an anthracene (Ac) crystal, we show that, when the triplet of the host is in between the first singlet excited state and the first triplet excited state of the guest molecule, the intersystem crossing can be dramatically enhanced via an intermolecular process. This effect can be extremely strong so as to prevent single-molecule detection. This result led us to the choice of a different system.

Following the results of Chapter 2, we propose another guest-host system for SMS. Chapters 3 and 4 are devoted to studies of this new system which consists of dibenzoterrylene (DBT) molecules inserted in an Ac crystal. In Chapter 3, we focus on the photophysics of this combination. The system presents two dominant insertion sites. We show that DBT in an Ac crystal fulfills all the requirements for high-resolution spectroscopy at cryogenic temperatures: a

narrow ZPL (around 30 MHz), a high count rate (the detected fluorescence rates at saturation reach 100,000 cps), a low ISC yield (lower than  $10^{-7}$ ), and a very good photostability.

Chapter 4 concentrates on the description of the insertion of the molecules inside the crystal. We perform molecular simulations and compare them to experiments. With both experimental results and simulations, we find two dominant insertion sites. Data on the temperature dependence of the linewidth of single DBT molecules, the distributions of their transition dipole moments and their Stark coefficients allow us to unambiguously attribute the two predominant insertion sites to the replacement of three Ac molecules by one of DBT, inserted with a small angle (of about 5 degrees or less) with respect to the 'b'-axis of the Ac crystal.

As a last requirement for this study, we need to verify whether Ac is an adequate conducting material at cryogenic temperatures or not. In Chapter 5, we characterise the Ac-FET by measuring the current as a function of the applied voltages (gate and source-drain). These  $I-V$  curves exhibit a power law dependence, with high values of the exponents. This is a typical behaviour of trap-filling in the space-charge limited conducting regime. From the previous measurements, we extract a lower bound of the mobility and plot it as a function of temperature. We obtain a non-monotonous temperature dependence, with first an increase of the mobility while decreasing temperature and second, after a maximum, a decrease of the mobility with decreasing temperature. We compare these results with previous experimental data. The value of the mobility is of the same order of magnitude than that measured for other systems at low temperatures. Though Ac is not a very good conducting material, it is possible to inject charges and measure a current, which indicates that the number of charges inside the crystal is high enough to be detected locally by means of SMS.

Chapter 6 presents single-molecule data in a FET for dc and ac-regimes. The dc-regime shows different behaviours depending on whether the source-drain voltage is on or off. Without a source-drain voltage, we observe drifts of the frequencies of the absorption lines of the molecules over long durations. These drifts vary roughly as the log of time. We propose a phenomenological model in order to explain these long-time shifts. With a source-drain voltage, the data become more complicated. A similar drift of the frequencies of the molecules is still present. However, a stretched exponential is not satisfactory anymore. In that case, we use of a power law. Additionally to these drifts, some molecules exhibit very complex features with strong correlations from molecule to molecule. The ac-regime presents interesting phenomena such

as the unexpected presence of resonances for specific frequencies of the ac-voltage. We describe the properties of these effects. In order to rule out some possible explanations, we have performed a series of experiments, changing many parameters such as the matrix, the temperature, the applied voltages, etc. A possible explanation is proposed.



## 2 Terrylene in anthracene: Intermolecular intersystem-crossing

WE present a spectroscopic study of terrylene in anthracene crystals at the ensemble and single-molecule levels. In this matrix, single-molecule fluorescence is reduced by three orders of magnitude. Correlation measurements allow us to identify a new relaxation channel, matrix-enhanced intersystem-crossing. This process starts with a singlet-to-triplet energy transfer from guest to host, after which the triplet exciton is transferred back to the guest. Intermolecular intersystem-crossing is expected whenever the lowest triplet state of the host is located between the lowest singlet  $S_1$  and lowest triplet  $T_1$  excited states of the guest. It must be considered when searching for new host-guest systems for single-molecule spectroscopy<sup>1</sup>.

---

<sup>1</sup> The content of this chapter is published in: A. Nicolet, M. A. Kol'chenko, B. Kozankiewicz, M. Orrit "Intermolecular inter-system-crossing in single-molecule spectroscopy: Terrylene in anthracene crystal" *J. Chem. Phys.* **124**, 164711 (2006).



## 2.1 Introduction

Following the first detection of a single fluorescent molecule, more than 15 years ago [23,24], the high-resolution spectroscopy of single molecules at cryogenic temperatures (SMS) has become a powerful tool for investigating the properties of matter. Since the first experiments on pentacene in p-terphenyl crystal, a good deal of effort has been devoted to extending the range of suitable host-guest systems. A candidate system requires guest molecules with a large absorption cross-section, a high quantum yield of fluorescence, a strong and narrow zero-phonon line (ZPL), a low efficiency of irreversible photo-induced reactions, i.e. a good photo-stability. Fluorescence is generated by an electronic transition from the molecule's first excited singlet state ( $S_1$ ) to its ground singlet state ( $S_0$ ). The first excited triplet state ( $T_1$ ) is energetically situated between  $S_0$  and  $S_1$ . Radiationless transitions between states of different spin multiplicity are called intersystem crossing. In the following, we restrict the term "intersystem crossing (ISC)" to transitions from the excited singlet level  $S_1$  to the triplet level  $T_1$ . The probability of such a spin-forbidden transition is usually very low. Because the  $T_1$  to  $S_0$  transition is also spin-forbidden, the lifetime of the triplet state is rather long compared to the singlet's one. Excluding the unlikely case where a fluorescent  $T_1 \rightarrow T_2$  transition would be in resonance with the  $S_0 \rightarrow S_1$  transition, the molecule does no longer absorb photons in its triplet state and, thus, does not emit light either. For this reason, the triplet state is also called dark state. Fluorescence from an individual molecule is therefore emitted in bunches of photons separated by dark periods [25]. Consequently, an additional and important requirement for a good host-guest system for SMS is that the guest molecule should have a low ISC rate and a short triplet lifetime.

In order to monitor single-molecule lines for extended observation times, one has to choose host-guest systems in which photo-induced jumps and spectral diffusion [26,27] are minimal. This is often the case for crystalline host matrixes with well-defined insertion sites for the guest, a condition that is usually met when host and guest molecules have compatible size and shape. For instance, one guest molecule substitutes one host molecule for pentacene [28] and terrylene [29] in p-terphenyl crystals, but a guest could also substitute more than one host molecule. Irrespective of the molecular sizes, an obvious additional condition is that the host singlet should be at higher energy than that of the guest, to avoid fluorescence quenching.

The present work was started as a search for a convenient system to probe the movement of charge carriers in molecular materials. Because of the sensitivity of a guest molecule to interactions with its immediate surroundings,

SMS is an appealing method to probe conduction at nanometer scales [19]. Moreover, molecular crystals have recently attracted widespread interest as basic models for organic conductors [30], as well as for their potential applications [31]. A single-molecule investigation of conduction in an organic crystal requires a convenient host-guest combination, in which the host crystal at the same time supports conduction and maintains the guest probe in a stable position.

Anthracene (Ac) crystals have recently been used as active materials in organic FET [32]. Because the photophysical properties of terrylene (Tr) as a guest molecule are very favourable to single-molecule studies, Tr in Ac crystals was an appealing candidate for this project. This system fulfils all of the previously mentioned criteria of spectral ranges and stability. We therefore started to characterise this new system with ensemble and single-molecule experiments. Surprisingly, although the fluorescence lines were sharp and stable at low temperature, as expected in a crystal environment, the fluorescence signal was extremely weak. We found that intersystem crossing of Tr is strongly enhanced in Ac crystals, and attribute this to a singlet-to-triplet energy transfer from guest to host, a previously observed effect known as intermolecular ISC. Intermolecular ISC is followed by a triplet-triplet (Dexter) energy transfer back to the guest. This new intermolecular ISC channel imposes a further restriction for the choice of a SMS system: The guest fluorescent singlet should not only lie below the host's lowest singlet state, but also below the host's lowest triplet state<sup>2</sup>.

In the first part of this chapter (Section 2.2), we briefly describe our experimental setups and the techniques we used. We then present (see Section 2.3) our detailed spectroscopic study of Tr in Ac, and discuss (Section 2.4) the mechanism of intermolecular ISC and its consequences for SMS.

## 2.2 Experimental

We studied Tr in two crystal hosts, anthracene and naphthalene, the latter one for comparison purposes. Starting from commercial material (Aldrich scintillation grade  $\geq 99.0\%$ ), we purified the host compounds in a home-built zone-refiner for about 4000 passes. We couldn't detect any impurity-related fluorescence in the zone-refined materials. Polycrystalline samples were pre-

---

<sup>2</sup> Another possibility would be to choose a host with a triplet lower than that of the guest, which would shorten the guest's triplet lifetime via Dexter transfer. However, this configuration is difficult to realize, and the host triplet may quench the guest's fluorescence.

pared by first melting the purified host doped with a small amount of Tr (purchased from Laboratory for PAH Research, Greifenberg, Germany). The melt was quenched in a small glass test tube quickly dipped into water. The resulting samples were deep red, indicating a high concentration of the guest Tr molecules ( $\sim 10^{-4}$  M) in the two matrices. Single crystals were grown by co-sublimation in a home-built device under a 150 mbar nitrogen atmosphere. Under these conditions, the sublimation "flakes" developed along the (a,b) plane, and had diameters as large as a few millimetres and thicknesses of a few tens of micrometres.

Experiments on ensembles of molecules (bulk measurements) were performed on two different setups. In the first setup, the excitation spectra of Tr in Ac were measured for both polycrystalline and single-crystal samples by scanning the wavelength of a dye laser (Coherent 700, operated with Rh6G and pumped by a mode-locked Antares 76 Nd:YAG) with pulses of 10 ps duration and 76 MHz repetition rate. The fluorescence emitted perpendicular to the excitation beam was filtered by a monochromator (McPherson 207) set at the first vibronic component of the fluorescence (at  $247\text{ cm}^{-1}$  from the ZPL) and scanned synchronously with the laser, in order to reduce background. The fluorescence intensity was recorded with an EMI 9659 photomultiplier. The same laser system, but operating with a 7.6 MHz repetition rate, was used to measure fluorescence decays [33] with the time-correlated single photon counting (TCSPC) technique. Other components of the set-up in this mode of operation were: an avalanche photodiode (APD) for the start signals and a Hamamatsu R8090-07 microchannel plate photomultiplier for the stop signals, a Tennelec TC 454 quad constant fraction discriminator, a TC 864 time-to amplitude converter, and a Nucleus PCA-II multichannel analyser. The two experiments were performed at 5 K. With the second setup, we also measured bulk fluorescence spectra of single crystals of Tr in Ac or naphthalene. We excited the ZPL of Tr (main site at 579.1 nm for Ac and 574.5 nm for naphthalene) with a tunable single mode dye laser (Coherent 899-21, operated with Rh6G), and recorded the fluorescence by means of a system composed of a spectrometer (Spectrapro 500i; Acton Research) coupled to a nitrogen-cooled CCD camera (Spec-10; Roper Scientific). The same setup was used to measure bulk saturation. The laser was focused with a lens ( $f = 100\text{ mm}$ ) onto the edge of the crystals (beam lying in the a-b plane), using the same path for excitation as for emission. During these experiments, the sample was kept at 4.2 K.

Single-molecule (SM) measurements were performed with a home-built confocal microscope [34]. We used the same single-mode dye laser as for the latter bulk experiments. The laser was tightly focused onto the surface of a single-

crystal sample (beam perpendicular to the (a,b)-plane) in both cases of Ac and naphthalene by means of a single aspheric lens ( $f_{obj}=1.45$  mm, NA=0.55, from Thorlabs). The fluorescence signal was collected by the same lens, and monitored with an APD (SPCM-AQ-161; EG&G). The position of the focus on the sample was controlled by means of a high precision home-built scanning mirror [35]. To obtain ensemble fluorescence spectra, we scanned the frequency of the dye laser over the resonance of the molecules. Auto-correlation curves were obtained using a special data acquisition card (TimeHarp 200) and its associated software (MicroTime 200; both from PicoQuant GmbH). Due to a drift of the laser frequency, the acquisition time during autocorrelation experiments was limited to about 10 to 20 minutes. All single-molecule experiments were performed in superfluid helium at 1.5 K.

## 2.3 Results

Figure 2.1 shows the excitation spectra of Tr in single-crystal (upper panel) and polycrystalline (lower panel) Ac. The several absorption peaks are attributed to guest molecules in different insertion sites. Some of the sites in the single crystal spectrum do not exist in the polycrystalline spectrum and vice versa. The single-crystal spectrum presents three main sites at 579.1 nm, 581.0 nm, and 584.7 nm. However, there are also weaker spectral sites at 576.7 nm, 578.4 nm and 585.2 nm. Similar differences in site intensities for crystals grown by different methods are frequently observed (see perylene in biphenyl for example [36]). In the polycrystal, the relative intensities of the sites are probably related to the free energies of insertion at the melting temperature. The sublimation flake is grown far from thermodynamic equilibrium, and the guest molecules have a well-defined orientation in the resulting single crystal. Therefore, growth kinetics and crystal orientation may affect the site intensities in the latter case.

We measured the fluorescence lifetimes of Tr in Ac for several sites. They presented slightly different values (see Figure 2.1), but all of them were within 0.2 ns of a central value, 3.15 ns. This value is significantly shorter than the fluorescence lifetime of Tr in *p*-terphenyl crystals, 4.2 ns [37]. This shorter lifetime could result from new relaxation channels, from a different radiative rate due to the somewhat higher refractive indexes of the Ac crystal (ranging from 1.6 to 2.2 for the different crystal axes at  $\lambda=546$  nm [38], versus 1.6 to 2.1 in *p*-terphenyl), or from a different orientation of the guest with respect to crystal axes [39]. The first hypothesis will be discussed later. We will now concentrate on measurements of the spectral site at 579.1 nm. A bulk fluores-

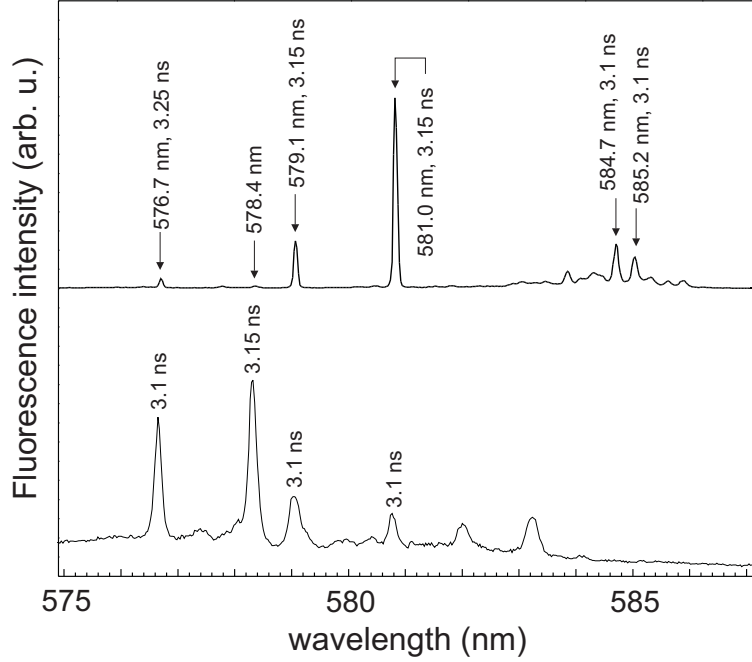


**Figure 2.1:** Bulk fluorescence excitation spectra of Tr in single sublimation-grown Ac crystal (top) and in a polycrystalline sample (bottom) at 5 K. The wavelengths of the main spectral sites and the corresponding lifetimes are indicated.

cence spectrum of Tr in a single sublimation-grown Ac crystal excited at the ZPL wavelength, 579.1 nm, is presented on Figure 2.2. The several peaks seen in this spectrum are attributed to the vibronic lines of Tr, in good agreement with previous work [40]. The weakness of the phonon sidebands indicates a weak electron-phonon coupling, favourable to single-molecule studies.

Motivated by the promising results of the bulk measurements, we attempted single-molecule detection on Tr in single sublimation-grown Ac crystals. This proved very difficult. The fluorescence excitation lines of single molecules were spectrally very stable, but surprisingly weak (less than a few hundreds of counts per second). The count rate depends not only on the host-guest system, but also on the detection efficiency of the setup. In order to compare this count rate to those of other host-systems, we recorded saturation curves for single Tr molecules in Ac and naphthalene single-crystals with the same setup (Figure 2.3).

The fully saturated count rate of Tr in Ac crystal was always lower than

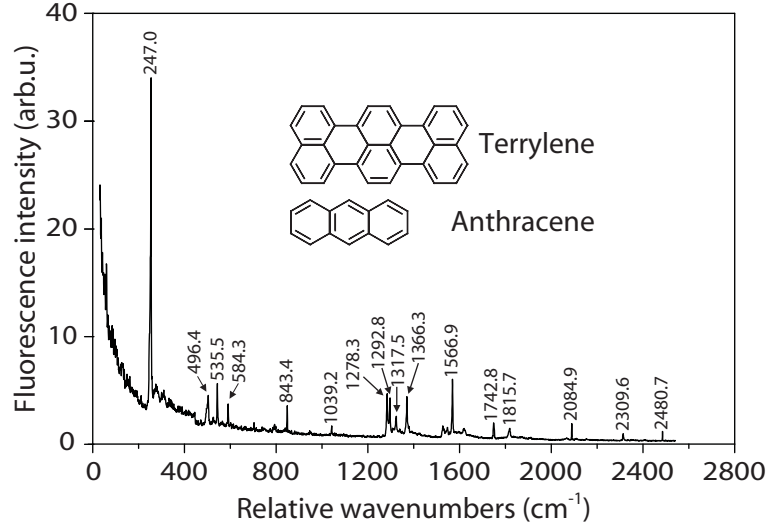


**Figure 2.2:** Bulk fluorescence spectrum of Tr molecules in an Ac single sublimated crystal, excited at 579.1 nm at 4.2 K. The spectral positions of the vibronic components are given in relative wavenumbers from the ZPL.

300 cps. Tr is a well known fluorophore which usually gives a high rate of fluorescence in a wide variety of matrices [41]. Saturated Tr molecules in *p*-terphenyl crystals can give up to 600,000 cps [42]. We checked that, with our setup, we could record almost 200,000 cps at saturation for single Tr molecules in naphthalene crystal [43], indicating again a strong difference between the two systems. The measurements on the same setup of Tr in Ac on one hand and in naphthalene on the other allowed us to compare the parameters of Tr via Eq. 2.1 which gives the fully saturated fluorescence emission rate defined as [26]:

$$R_{\infty} = (k_{21} + k_{23}) \frac{\phi_f}{2 + \frac{k_{23}}{k_{31}}} = \frac{k_{21}^r}{2 + \frac{k_{23}}{k_{31}}}, \quad (2.1)$$

where  $k_{21}$  is the rate for the  $S_1 \rightarrow S_0$  transition,  $k_{23}$  for  $S_1 \rightarrow T_1$  and  $k_{31}$  for  $T_1 \rightarrow S_0$ .  $\phi_f$  is the fluorescence quantum yield and  $k_{21}^r$  the radiative decay rate. What is measured experimentally is  $\eta \times R_{\infty}$  where  $\eta$  is the detection efficiency of the setup, which is presently the same for the two systems under consideration. If we assume in first approximation that  $k_{21}^r$  doesn't change dramatically from one system to the other and that  $k_{31}$  is similar in Ac and

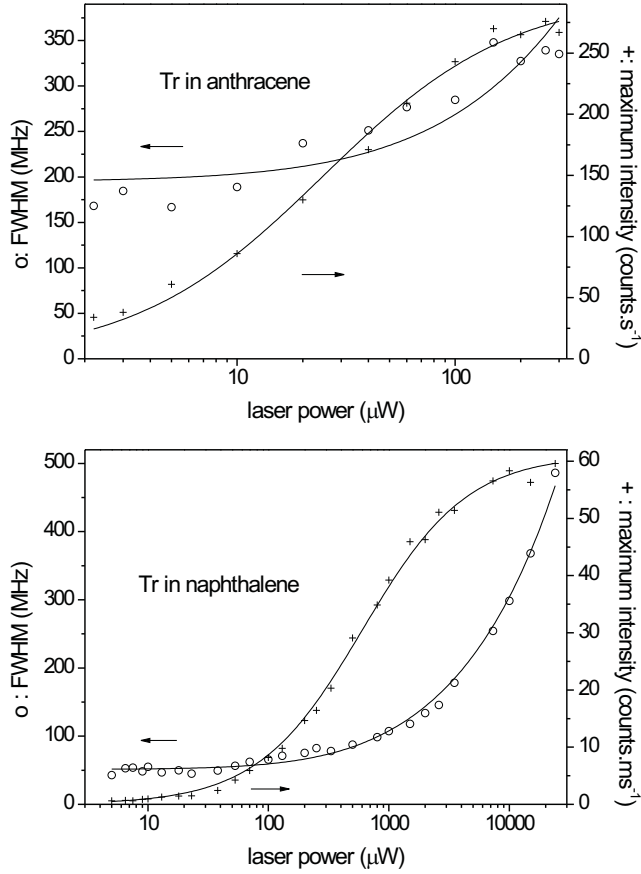


**Figure 2.3:** Upper panel: saturation of a single terrylene molecule in a single Ac crystal. This particular molecule was probably broadened by spectral diffusion. Lower panel: same plot for a single Tr molecule in a single naphthalene crystal shown for comparison purposes.

naphthalene, we should have an ISC yield almost three orders of magnitude larger in the case of Tr in Ac than for Tr in naphthalene. It has to be pointed out that we didn't measure the orientation of the molecules in the matrices. An unfavourable orientation of the molecules could indeed lead to a less efficient excitation and detection if the dipole moment of the molecules is nearly perpendicular to the polarisation of the laser, or if it is oriented along the observation direction. The lower saturation intensity for Ac than for naphthalene rules out orientation as the only cause for this difference [44]. As the fluores-

cence rate of a fluorophore appears to be determined mainly by intramolecular properties (ISC rate, triplet lifetime, fluorescence yield and radiative rate), a difference by three orders of magnitude in fluorescence intensity upon a change of host was highly intriguing.

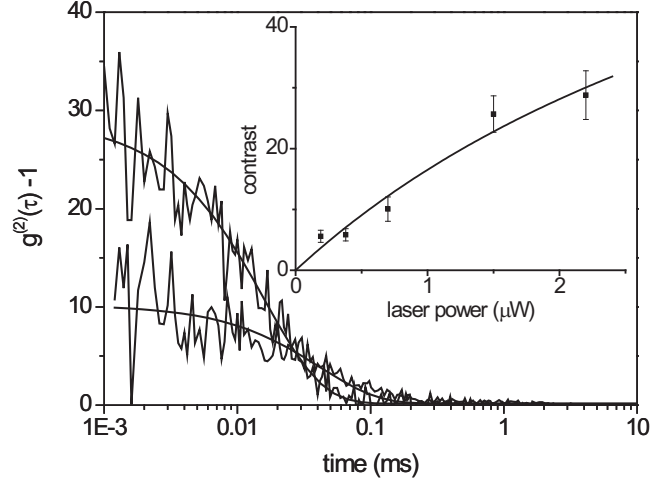


**Figure 2.4:** Two auto-correlation functions of a single Tr molecule in an Ac crystal, for two different laser powers ( $P=0.7 \mu W$  and  $P=2.2 \mu W$ ). The smooth thin lines are fits with single exponentials. The insert shows the contrast  $C$  versus the laser power and the thick line is a fit with Eqs. 2.3 and 2.4.

A possible cause for a large reduction in fluorescence rate is an enhanced ISC channel. In order to determine the ISC yield of Tr molecules in Ac single crystal we used the correlation method [25, 45]. We measured the auto-correlation functions  $g^{(2)}(\tau)$  of the fluorescence intensity of single Tr molecules (Figure 2.4). All data are compatible with single-exponential decays, although a weak tail with a lifetime of 1 ms cannot be excluded. Under the assumption that ISC only populates one triplet spin sublevel [25], the single-exponential correlation function is given by:

$$g^{(2)}(\tau) = 1 + Ce^{-\lambda\tau}, \quad (2.2)$$

where  $\lambda$  is the decay parameter and  $C$  the contrast of the correlation. Following references [25, 45], these parameters are related to the transition rates to and from the triplet state, via the relations:



$$C = \frac{(\lambda - k_{31})}{k_{31}}, \quad (2.3)$$

$$\lambda = k_{31} \left[ 1 + \frac{\frac{I}{I_S}}{1 + \frac{2k_{31}}{k_{23}} \left( 1 + \frac{I}{I_S} \right)} \right], \quad (2.4)$$

where  $I$  is the excitation intensity,  $I_S$  is the usual saturation intensity defined as [46]:

$$I_S = n \frac{\epsilon_0 c}{4} \left( \frac{\hbar}{\mu_{eg}} \right)^2 \frac{\Gamma^2}{1 + \frac{k_{23}}{2k_{31}}}, \quad (2.5)$$

where  $n$  is the refractive index of the medium,  $\epsilon_0$ , the vacuum permittivity,  $c$  the velocity of light,  $\mu_{eg}$  the transition dipole moment between excited and ground state (we have neglected local field corrections of  $\mu_{eg}$  [47]), assumed to be parallel to the exciting polarisation, and  $\Gamma$ , the rate of the decay, assumed to be purely radiative (pure dephasing is neglected, see below). In the present case, due to the weakness of the fluorescence signal, it was very important to correct the autocorrelation contrast value for the background. The true value for the contrast was obtained by multiplying the experimental value by  $(1 + b/s)^2$ , where  $b$  and  $s$  are the average background and the signal values, respectively [25]. Then, we used Eq. 2.3 to find the rate of the  $T_1 \rightarrow S_0$  transition. We obtained a value of  $k_{31} = (1.8 \pm 0.3) \cdot 10^3 s^{-1}$ . This corresponds to a triplet lifetime of about 500  $\mu s$ , comparable to that of the shorter component previously found for Tr in para-terphenyl crystal. Subsequently, the value of  $k_{23}$  was found by replacing that of  $k_{31}$  in Eq. 2.4, and by fitting the result for different excitation intensities. We obtained a value of  $k_{23} = (1.0 \pm 0.5) \cdot 10^6 s^{-1}$ . To obtain the ISC yield, we deduced the decay rate of  $S_1$  from the previously measured fluorescence lifetime:  $(k_{21} + k_{23}) = 3.1 \cdot 10^8 s^{-1}$ . We found an ISC yield  $k_{23}/(k_{21} + k_{23}) = (3 \pm 2) \cdot 10^{-3}$ . This value is three orders of magnitude larger than that measured for Tr in either *p*-terphenyl [42] or naphthalene crystals, and is consistent with the large difference in fluorescence rate at saturation previously reported.

As a last result, we measured the linewidths of single Tr molecules in Ac. Figure 2.5 shows the histogram of measured widths for 50 molecules. Because of the weakness of the signals, these widths were directly measured on the

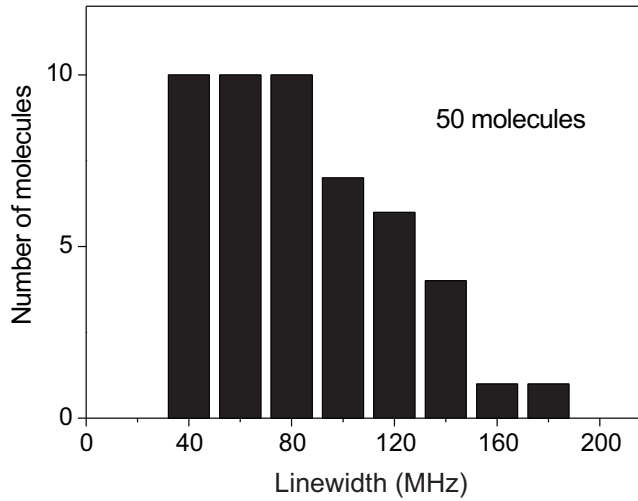


**Figure 2.5:** Linewidth distribution of 50 single terrylene molecules in an anthracene single crystal. The tail of the distribution for large widths partly results from saturated molecules and partly from spectral diffusion.

spectra recorded at the lowest possible excitation intensity, without extrapolation to zero intensity. Correlation measurements show that some molecules had extremely low saturation intensities. These molecules were probably saturated in the width measurements. The narrowest lines we found, on the other hand, about 45 MHz broad, must stem from unsaturated molecules. Equation 2.6 gives the relation between the lifetime  $T_1$  of the excited state and the linewidth  $\gamma_{SM}$  of the molecules [37], where  $T_2^*$  is the pure dephasing time.

$$\gamma_{SM} = \frac{1}{\pi} \left( \frac{1}{2T_1} + \frac{1}{T_2^*} \right). \quad (2.6)$$

At low temperature and in crystals, this last term can be neglected due to a low population of phonons. The linewidth does not change dramatically with temperature below 1.5 K as shown in the case of Tr in naphthalene [48]. According to Eq. 2.6 and to the last considerations, the narrowest linewidth of 45 MHz is consistent with the lifetime of  $\sim 3.15 \pm 0.2$  ns that we found previously. However, the molecule of Figure 2.3 (upper part) still presents a width of more than 150 MHz at low excitation intensity, although it is not saturated. This shows that at least some molecules seem to undergo spectral diffusion.

This histogram of linewidths is completely different from the one reported in a previous work [49] where the system of Tr in Ac had been investigated. In this work, the crystal had been fixed to a fibre using immersion oil which had probably dissolved Ac and partially destroyed the matrix. Therefore, the remaining terylene molecules were not measured in a crystal of Ac anymore but in oil, which explains the difficulties to find photo-stable molecules during this experiment and the very broad distribution of linewidths.

## 2.4 Discussion

First, we would like to rule out alternative explanations for an enhancement of the triplet yield. Molecular distortions away from planarity are known to enhance ISC by sigma-to-pi orbital mixing. A heavily distorted geometry of Tr in Ac could also enhance ISC. Similarly, coincidences of levels might enhance ISC in the Tr/Ac system. However, Tr consistently shows a high fluorescence rate and very low ISC rate in a wide variety of matrixes, including aromatics (p-terphenyl, naphthalene, benzophenone) and saturated molecules (n-alkanes, polymers). It seems therefore unlikely that distortions or coincidences of levels would solely occur in the Ac matrix. Ac being the only matrix with its triplet state below the singlet of Tr, it is reasonable to assume that ISC enhancement is a consequence of this feature<sup>3</sup>.

We now discuss the matrix-induced enhancement of ISC. The mechanism that we propose is based on the opening of a new relaxation channel from the Tr guest to the Ac host via intermolecular ISC. Intermolecular ISC has been already described in 1971 by *Zimmermann et al.* [50] in a bulk study on molecular crystals. It results from an interaction between two different molecules and consists of a transition from an excited state of a first molecule (or donor) to a state of different spin multiplicity of a second molecule (acceptor).

Let us first consider regular intramolecular ISC (see Fig. 2.6, path A). The first excited singlet state of Tr relaxes to the first triplet state ( $S_1 \rightarrow T_1$ ) via spin-orbit coupling and creation of intramolecular vibrations by non-adiabatic coupling terms. The rate of such a transition is:

$$k_{S_1 \rightarrow T_1}^{(1)} = \frac{2\pi}{\hbar} |\langle S_1 | H_{SO} | T_1 \rangle|^2 \rho_{T_1}(E_{S_1}), \quad (2.7)$$

---

<sup>3</sup> Moreover, we have recently measured the ISC rate of dibenzoterylene, a heavier analog of Tr, in Ac crystals (see Chapter 3). In spite of the strong guest distortions found in molecular mechanics simulations, the ISC rate is very low, consistent with the guest singlet (785 nm) lying below the Ac triplet (680 nm).

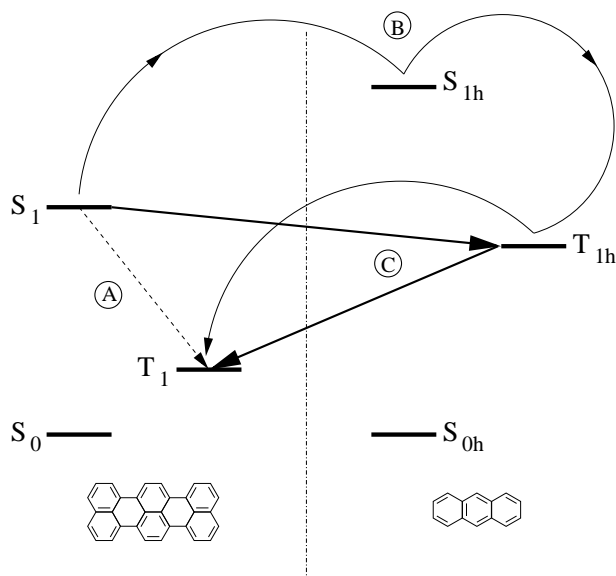


**Figure 2.6:** Possible mechanisms for matrix-induced enhancement of ISC of Tr in Ac crystal. (A) indicates a usual ISC, with a transition  $S_1 \rightarrow T_1$ . (B) is a process involving a virtual passage through the first singlet and triplet excited states of Ac (the host), respectively  $S_{1h}$  and  $T_{1h}$  and (C) is the direct two-step transition  $S_1 \rightarrow T_{1h} \rightarrow T_1$ . The process (C) dominates (A) and (B) for Tr in Ac.

where we considered the spin-orbit coupling operator between the two Tr states  $S_1$  and  $T_1$  and where  $\rho_{T_1}(E_{S_1})$  represents the density of coupled vibronic states of  $T_1$  at the energy  $E_{S_1}$ . The probability of intramolecular ISC is very low in the isolated Tr molecule and for Tr in previously used matrices like p-terphenyl, naphthalene or n-alkanes.

We now consider intermolecular ISC as a first step in the  $S_1 \rightarrow T_1$  relaxation of Tr. This first step is a relaxation from  $S_1$  of Tr to the first triplet  $T_{1h}$  of the host Ac. Since this triplet state lies at  $14,736 \text{ cm}^{-1}$  [51], a direct transition  $S_1 \rightarrow T_{1h}$  is energetically possible (Fig. 2.6, path C). In a second step, the Ac triplet must transfer back to the Tr triplet, by a Dexter process. If this did not happen, the host triplet would either migrate away as a triplet exciton of Ac (in this case Tr fluorescence would not be changed), or remain on a nearby Ac molecule<sup>4</sup>. There, it would act as a quencher for the Tr singlet, because the

<sup>4</sup> *Bach et al* [52] have shown, in the case of Tr in an isotopically mixed crystals of naphthalene, that the triplet exciton of naphthalene  $h_8$  is trapped by a potential funnel created by the terylene molecule (used as a probe).

second excited triplet  $T_{2h}$  of Ac lies only  $11,200\text{ cm}^{-1}$  above the first one [53]. Tr fluorescence would then be quenched during the Ac triplet lifetime, about 50 ms, whereas the lifetime indicated by our correlation measurements is that of Tr, 500  $\mu\text{s}$ .

We now proceed to estimate the transfer rate  $S_1 \rightarrow T_{1h}$ . This can be seen as dipole-dipole coupling between Ac and Tr singlet states, combined with spin-orbit coupling between the singlet and triplet states of Ac. An alternative way is to see it as a Förster energy transfer between the Tr donor singlet and the Ac acceptor triplet, the weak triplet absorption being determined by spin-orbit coupling within Ac. In either case, we obtain:

$$k_{S_1 \rightarrow T_{1h}}^{(2)} = \frac{2\pi}{\hbar} \left| \frac{\langle S_1 | V | S_{1h} \rangle \langle S_{1h} | H_{SO}^h | T_{1h} \rangle}{(E_{S_1} - E_{S_{1h}})} \right|^2 \rho_{T_{1h}}(E_{S_1}), \quad (2.8)$$

where  $V$  is the dipole-dipole coupling operator between the host and guest excited singlet states. In this situation, the system is 'really' passing through the  $T_{1h}$  state of Ac. The second step is the Dexter transfer  $T_{1h} \rightarrow T_1$ , which is fast because the transition is spin-allowed and the molecules are close neighbours. We can safely assume that the inverse rate of this process is shorter than 1 ns. The rate of the  $S_1 \rightarrow T_{1h} \rightarrow T_1$  transition therefore is that of the slow limiting step  $k_{S_1 \rightarrow T_{1h}}$  calculated above. We can estimate the ratio of the two rates  $k_{S_1 \rightarrow T_{1h}}^{(2)}/k_{S_1 \rightarrow T_1}^{(1)}$ :

$$\frac{k_{S_1 \rightarrow T_{1h}}^{(2)}}{k_{S_1 \rightarrow T_1}^{(1)}} = \left| \frac{\langle S_1 | V | S_{1h} \rangle}{E_{S_1} - E_{S_{1h}}} \right|^2 \left| \frac{\langle S_{1h} | H_{SO}^h | T_{1h} \rangle}{\langle S_1 | H_{SO} | T_1 \rangle} \right|^2 \frac{\rho_{T_{1h}}(E_{S_1})}{\rho_{T_1}(E_{S_1})}. \quad (2.9)$$

Using typical values of  $1000\text{ cm}^{-1}$  for the dipole-dipole interaction,  $10000\text{ cm}^{-1}$  for the energy separation between the Tr and Ac singlet states, the known intramolecular ISC rates of  $\sim 1000\text{ s}^{-1}$  [42] for Tr and  $1.1 \cdot 10^8\text{ s}^{-1}$  [54] for Ac, and assuming that  $\rho_{T_{1h}}(E_{S_1})$  does not differ too much from  $\rho_{T_{1h}}(E_{S_{1h}})$ , we find a ratio  $k_{S_1 \rightarrow T_{1h}}^{(2)}/k_{S_1 \rightarrow T_1}^{(1)}$  of about 1000, consistent with our measurements.

There is an alternative, matrix-induced way of relaxing from the Tr excited singlet to its excited triplet. In this alternative mechanism (Fig. 2.6, path B), the transition to  $T_{1h}$  is considered as 'virtual'. In other words, we involve the coupling matrix elements to the Ac triplet state in higher-order perturbation theory, but do not assume a real population of Ac triplet to arise. In this case, the rate will be expressed as:

$$k_{S_1 \rightarrow T_1}^{(3)} = \frac{2\pi}{\hbar} \left| \frac{\langle S_1 | V | S_{1h} \rangle \langle S_{1h} | H_{SO}^h | T_{1h} \rangle \langle T_{1h} | V | T_1 \rangle}{(E_{S_1} - E_{S_{1h}})(E_{S_1} - E_{T_{1h}})} \right|^2 \rho_{T_1}(E_{S_1}). \quad (2.10)$$

However, we can expect this process to be negligible as compared to the first one. Indeed, forming the ratio of Eqs. 2.8 and 2.10, we obtain the following quantity:

$$\frac{k_{S_1 \rightarrow T_1}^{(3)}}{k_{S_1 \rightarrow T_{1h}}^{(2)}} = \left| \frac{\langle T_{1h} | V | T_1 \rangle}{E_{S_1} - E_{T_{1h}}} \right|^2 \frac{\rho_{T_1}(E_{S_1})}{\rho_{T_{1h}}(E_{S_1})}. \quad (2.11)$$

The density of states  $\rho_{T_1}(E_{S_1})$  is expected to be lower than  $\rho_{T_{1h}}(E_{S_1})$  because the gap of energy is lower between  $S_1$  and  $T_{1h}$  than between  $S_1$  and  $T_1$ , but their orders of magnitude should be the same. The real difference will consequently come from the other part of Eq. 2.11.  $\langle T_{1h} | V | T_1 \rangle$  is around  $1 \text{ cm}^{-1}$  while  $E_{S_1} - E_{T_{1h}}$  is  $3000 \text{ cm}^{-1}$ . Therefore, the virtual process is expected to be a million times weaker than the real one.

The comparison with the case of Tr in naphthalene is interesting because the triplet state of naphthalene lies at  $21,200 \text{ cm}^{-1}$  [55], much above the singlet  $S_1$  of Tr. The real intermolecular ISC channel is therefore blocked, whereas the virtual process, which would still be active, remains negligible. The absence or weakness of intermolecular ISC is consistent with the high fluorescence count rates observed for Tr in naphthalene. We can also consider the case of perylene in Ac crystal [36]. For this system, the Ac triplet ( $14,736 \text{ cm}^{-1}$ ) lies below the perylene singlet ( $22,265 \text{ cm}^{-1}$ ) but still above the perylene triplet ( $12,844 \text{ cm}^{-1}$ ). As in the case of Tr in Ac, perylene in Ac shows an enhanced ISC, large enough to measure perylene phosphorescence [36]. Similarly, the fluorescence of perylene is dramatically quenched in crystalline naphthalene, a phenomenon we also attribute to singlet ( $22,265 \text{ cm}^{-1}$ ) to triplet ( $21,200 \text{ cm}^{-1}$ ) energy transfer. In order to suppress the real channel for intermolecular ISC, one just has to choose a guest with its singlet state below the triplet of the Ac host. Indeed, we have recently shown [56] that single dibenzoterrylene molecules (singlet at  $12,740 \text{ cm}^{-1}$ ) give rise to high count rates in Ac crystal, with a very weak ISC channel.

## 2.5 Conclusion

In the present work, we have investigated the spectroscopy of Tr in Ac crystals with bulk and single-molecule measurements. The weakness of single-molecule

fluorescence was attributed to a matrix-enhanced ISC, involving a singlet-to-triplet excitation transfer via the triplet state of the Ac matrix. This unusual intermolecular ISC channel can be expected whenever the lowest triplet state of the host is located between the lowest singlet  $S_1$  and lowest triplet  $T_1$  excited states of the guest. This effect can be strong enough to prevent single molecule detection, as in the case of perylene in Ac, or to make it very difficult, as in the case of Tr in Ac. It also probably rules out SMS in isotopically mixed crystals such as protonated naphthalene as a guest in a deuterated naphthalene host<sup>5</sup>. Intermolecular ISC can be prevented by choosing a guest with its singlet below the triplet state of the host, as in the case of dibenzoterrylene in Ac. Intermolecular ISC will have to be taken into account in future searches for new host-guest systems suitable for single-molecule spectroscopy.

---

<sup>5</sup> An additional issue are resonant excitonic interactions, which, for strong allowed transitions, would delocalise the guest exciton into the host band.

### 3 Dibenzoterrylene in anthracene: I. Spectroscopy and photophysics

WE study single dibenzoterrylene molecules in an anthracene single-crystal at 1.4 K in two insertion sites at 785.1 and 794.3 nm. The single-molecule zero-phonon lines are narrow (about 30 MHz), intense (the detected fluorescence rates at saturation reach 100,000 counts/s) and very photostable. The intersystem-crossing yield is extremely low ( $10^{-7}$  or lower). All these features are hallmarks of an excellent system for high-resolution spectroscopy and nanoscale probing at cryogenic temperatures<sup>6</sup>.

---

<sup>6</sup> The content of this chapter is published in: A. A. L. Nicolet, C. Hofmann, M. A. Kol'chenko, B. Kozankiewicz, M. Orrit, "Single Dibenzoterrylene Molecules in an Anthracene Crystal: Spectroscopy and Photophysics", *ChemPhysChem* **8**, 1215 (2007).



### 3.1 Introduction

Since the first detection of a single fluorescent molecule [23,24], one of the main applications of high-resolution single-molecule spectroscopy (SMS) has been to probe the properties of matter at nanometer scales [57,58]. The first class of dynamical processes investigated with single molecules were tunnelling events of atoms or groups of atoms in crystals and polymers at low-temperatures [59–61]. Another, very important class of dynamical processes in solids is the motion of charge carriers which is responsible for conduction. Single-molecule techniques may provide insight into conduction processes at nanometer scales in complex and disordered materials, which may differ from those in standard semiconductor crystals. In earlier studies, the single molecules were included in an organic matrix, while the charge carriers were moving in an inorganic semiconductor material. Experiments were done at room temperature [62] or at cryogenic conditions [19, 21, 22].

The motivation of the present work is to study conduction in the same matrix material in which the single molecules are imbedded [56]. For this study, molecular crystals are attractive matrices. They give rise to well-defined insertion sites for suitable guest molecules, and to narrow and stable zero-phonon lines, which are very sensitive to any dynamics in the surroundings of each single molecule. Electrical transport in various molecular crystals has been initially studied by photoconduction and time-of-flight methods [63]. More recently, conduction has been studied in organic field-effect transistor (OFET) structures, which enable independent control of charge carrier injection and of conduction [4, 64]. Various molecular single crystals have been used as active materials in OFET structures: sexithiophene [65], rubrene [66], pentacene [67], tetracene [68, 69], anthracene [32]. We therefore propose to perform single-molecule studies of conduction at nanometer scales in OFET structures [56], which requires a suitable guest-host system. Among the different organic crystals previously used in OFET's, anthracene (Ac) has several advantages. It is cheap, it can be easily purified and handled, it is stable at room temperature, it is easy to grow as single crystals [70], and does not present any phase transition upon cooling. We therefore have to find a guest fluorophore detectable as single molecules in an Ac single crystal.

High-resolution SMS in crystalline matrices requires a "good" fluorescent guest (presenting both a large absorption cross-section and a high fluorescence yield), and a good insertion of the guest in the host lattice, giving rise to a strong and narrow zero-phonon line (ZPL). Because SMS studies require acquisition over extended periods, photo-induced jumps should be minimal. The guest's ZPL should be very stable, both against photochemistry (photo-

bleaching), which is usually suppressed at cryogenic temperatures, and against spectral diffusion processes, which may obscure the interesting spectral shifts induced by electrical or other dynamical processes. Finally, in order to achieve a high rate of fluorescence, intersystem crossing (ISC) should be weak: The guest's triplet yield should be low, and its triplet state should be short-lived. A first idea was to use a standard single-molecule chromophore such as terrylene (Tr) [42], or dibenzanthanthrene (DBATT) [71] as a guest in Ac. We showed in the previous chapter, however, that it is very important to consider also the respective energetic positions of the guest's singlet and of the host's triplet [72]. Indeed, if the host's triplet lies below the guest's singlet, the guest's ISC can be spectacularly enhanced, thus dramatically decreasing fluorescence and making SMS close to impossible. Therefore, the first singlet excited state of the fluorophore should be lower than the triplet state of the host. The first excited triplet state of Ac being located at about  $14,700\text{ cm}^{-1}$  [51], good guest candidates should have their first singlet state at a lower energy. The first excited singlet state of dibenzoterrylene (DBT) lies around  $12,740\text{ cm}^{-1}$  [56]. We found that the guest-host system DBT in Ac crystals is very well suited to high-resolution single-molecule studies, and we propose to use it in the future for studies of charge transport phenomena in OFET structures.

Here, we present a spectroscopic and photophysical study of this system. Chapter 4 will report on the properties induced by interactions between the chromophore and the Ac crystal, as well as discuss the structure of the insertion sites of the guest in the matrix. Section 3.2 describes the experimental set-up and procedures used for this study. In Section 3.3, we report a general spectroscopic study of single molecules in the DBT/Ac system, antibunching and bunching measurements, and fluorescence spectra. In the same Section, we discuss the relaxation rates between the singlet and triplet levels and their consequences for spectroscopic measurements.

## 3.2 Experimental

### 3.2.1 Sample preparation

Anthracene (Ac) (Aldrich, scintillation grade, purity  $\geq 99.0\%$ ) was purified in a home-built zone-refiner for about 4000 passes. 7,8,15,16-dibenzoterrylene (DBT) was purchased from Dr. W. Schmidt (Laboratory for PAH Research, Greifenberg, Germany). Samples were single crystals of Ac as a host, doped with DBT. Flat crystals (flakes) were grown by co-sublimation in a home-built device under a 150 mbar nitrogen atmosphere. This co-sublimation device consists of a large tube (30 mm diameter) containing a load of Ac powder,

heated by resistant wires. Crystals grow on a collector plate at a slightly lower temperature than the load [70]. Within this tube, a small crucible containing the guest, DBT, is heated with resistant wires wrapped around it, up to an adjustable temperature. We thus can control the concentration of probe molecules in the matrix. The sublimation flakes develop along the (a-b) plane and reach diameters of a few millimeters and thicknesses from a few micrometers to a few tens of micrometers. They are optically contacted to a glass substrate or glued to it by a small amount of vacuum grease, mounted and cooled down to 1.4 K in a helium bath cryostat.

### 3.2.2 Optical setup

The single-molecule (SM) measurements were performed with a home-built confocal microscope. The samples were illuminated with a single-frequency Ti-Sapphire laser (Coherent 899-21 with Auto-scan option) pumped by an Argon ion laser (Coherent Innova 200). The tightly focused laser beam (diameter about 1  $\mu\text{m}$ ) was brought onto the surface of the single-crystal, the beam axis being perpendicular to the (a-b) plane, by means of a microscope objective [60 $\times$ , (NA)=0.85, Edmund Optics]. Everything was immersed in superfluid helium. A fast steering mirror (Newport FSM-300-01) outside the cryostat allowed us to move the focused beam in the plane of the sample over an area of about 150 $\times$ 200  $\mu\text{m}^2$ . Fluorescence was detected after suitable long-pass filters (810 nm, Chroma) which blocked the residual laser light. Fluorescence-excitation spectra were obtained by scanning the laser frequency over the molecular resonance lines of DBT and recording the fluorescence signal from an avalanche photodiode (SPCM-AQR-15, Perkin-Elmer). For the bulk fluorescence-excitation spectrum, we defocused the laser beam with respect to the sample in order to increase the number of illuminated DBT molecules. We recorded fluorescence spectra by collecting the fluorescence by means of a system composed of a spectrometer (Spectrapro 500i; Acton Research) coupled to a nitrogen-cooled charge-coupled device (CCD) (Spec-10; Roper Scientific). The spectrometer's resolution was about 4  $\text{cm}^{-1}$ .

### 3.2.3 Signal acquisition

Auto-correlation and cross-correlation functions were obtained with a special data acquisition card (TimeHarp 200) and its associated software (MicroTime 200; both from PicoQuant). The antibunching measurement was performed with a Hanbury Brown and Twiss setup [73]. By performing a start-stop measurement between two APD detectors, one efficiently removes all after-pulse

and dead-time effects of the devices, at the cost of a reduced correlation signal. One of the signals was delayed by 120 ns in order to measure the correlation for negative times. Bunching was also measured as a cross-correlation between two APD's with the same setup, because of the exceeding low level of the correlation and of the short bunching time.

### 3.3 Results and discussion

Figure 3.1 shows the fluorescence-excitation spectrum of a small ensemble of DBT molecules in a single-crystal of Ac, recorded by scanning the frequency of the laser from  $12,500\text{ cm}^{-1}$  to  $12,800\text{ cm}^{-1}$ . The laser beam was slightly defocused in order to increase the number of DBT molecules sampled. The spectrum presents at least four absorption peaks which we attribute to different insertion sites. The two dominant sites are at  $12,737\text{ cm}^{-1}$  and  $12,590\text{ cm}^{-1}$ . Their corresponding energies differ by about  $147\text{ cm}^{-1}$ . We can also distinguish two weaker sites at  $12,700\text{ cm}^{-1}$  and  $12,775\text{ cm}^{-1}$ . In the following, we will only concentrate on the two dominant insertion sites, from now on called main site (at  $12,737\text{ cm}^{-1}$ , or  $785.1\text{ nm}$ ) and red site (at  $12,590\text{ cm}^{-1}$ , or  $794.3\text{ nm}$ ). We can clearly see in Fig. 3.1 some narrow lines from single-molecules, especially in the red site. The number of molecules in the main site is considerably greater than in the red site (at least 100 times more). We think that the insertion probability during growth is higher in the main site and therefore, that the main site is probably energetically lower than the red site. This will be discussed in more detail in Chapter 4. Single-molecule lines in the red site show a more intense fluorescence, which is probably mainly due to the efficiency of the detection filter. Indeed, in order to reject the scattered laser light, we use a long-pass filter that transmits light with wavelengths above  $810\text{ nm}$  (i.e. wavenumbers below  $12,345\text{ cm}^{-1}$ ), removing more fluorescence from the main site than from the red one. Finally, the inhomogeneous width of the main site (around  $5\text{ cm}^{-1}$ ) is much smaller than that of the red site (around  $20\text{ cm}^{-1}$ ). This difference might indicate larger fluctuations of the insertion position of DBT molecules into the lattice in the case of the red site (see Chapter 4).

One can compare these absorption frequencies with that ( $13,198\text{ cm}^{-1}$ , or  $757.7\text{ nm}$ ) of the same DBT molecule embedded in a naphthalene single-crystal [74]. As a first approximation, the polarizability of unsaturated molecules is expected to increase proportionally to the volume of the molecules [18]. An increase of the polarizability of the solvent molecules will tend to stabilize the solute's excited state more than its ground state, and will consequently give

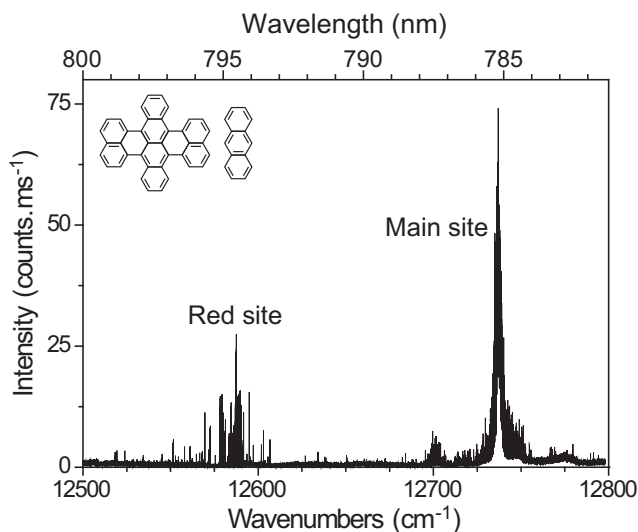


**Figure 3.1:** Bulk fluorescence-excitation spectrum of DBT molecules in a single-crystal of Ac at 1.4 K. The laser beam was defocused in order to increase the number of DBT molecules sampled. Two peaks are clearly dominant. The narrow spikes are single-molecule lines. The inset shows the structures of the DBT and the Ac molecules.

rise to a red shift of the solute's optical transition. Therefore, the absorption frequency of DBT molecules is red-shifted in Ac, with respect to naphthalene (with shifts of  $461\text{ cm}^{-1}$  and  $608\text{ cm}^{-1}$  for the two main peaks, respectively). This effect was already found for terrylene (Tr) in the two same matrices [48, 72]. However, the shift from naphthalene to Ac is larger for DBT than for Tr ( $461\text{ cm}^{-1}$  against  $138\text{ cm}^{-1}$ ), and the ratio of the shifts is larger than what could be expected from molecular volumes only.

Using a single molecule as a highly sensitive probe requires guest molecules with a narrow absorption line in order to detect small shifts of this line. An additional requirement is a high fluorescence signal. We obtained saturation curves of the fluorescence excitation lines by plotting the width and the fluorescence count rate at resonance as functions of the excitation intensity. Figure 3.2 shows these saturation curves for two DBT molecules, one excited at  $12,720\text{ cm}^{-1}$ , in the main site, and the other one at  $12,593\text{ cm}^{-1}$ , in the red site. The two curves show the full width at half maximum (FWHM)  $\gamma_{SM}$  measured on the single-molecule line (left side of the graph) and the maximum fluorescence intensity (right side of the graph) as functions of the excitation

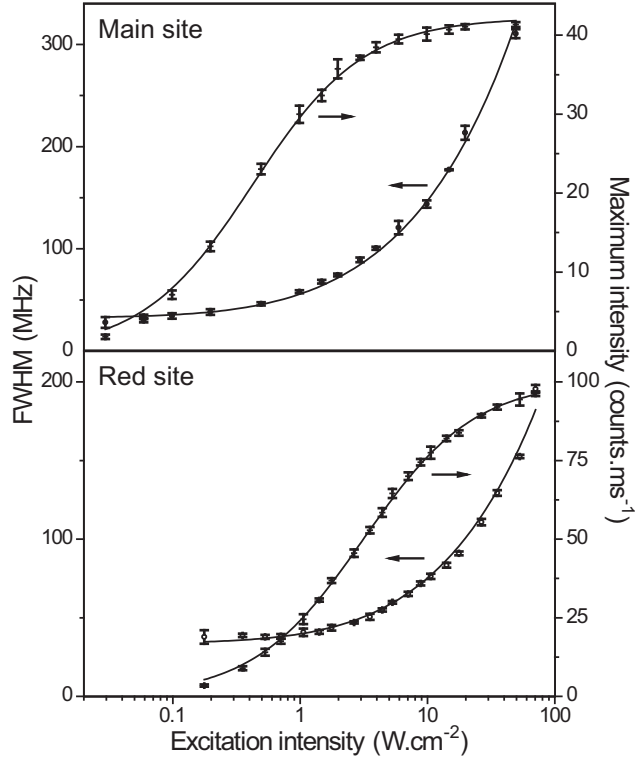


**Figure 3.2:** Saturation curves for two DBT molecules, in the main site (upper panel) and in the red site (lower panel) in a single-crystal of Ac at 1.4 K. The curves are fits of the FWHM and the maximum intensity as functions of the excitation intensity according to Eqs. 3.1 and 3.2, which provide the parameters  $\gamma_{hom}$ ,  $I_S$  and  $R_\infty$ .

intensity  $I$ . Neglecting a possible spectral diffusion, as a first approximation, the FWHM is equal to the homogeneous width  $\gamma_{hom}$ . Under this assumption, we found perfect agreement with the expected saturation laws [26]:

$$\gamma_{hom}(I) = \gamma_{hom}(0)(1 + I/I_S)^{1/2}, \quad (3.1)$$

$$R(I) = R_\infty \frac{I/I_S}{1 + I/I_S}, \quad (3.2)$$

where  $I_S$  is the saturation intensity,  $R(I)$  is the fluorescence detection rate and  $R_\infty$  the fully saturated fluorescence detection rate. For the molecule in the

main site, we find  $\gamma_{hom}(0) = 32$  MHz,  $I_S = 0.5 \pm 0.1$  W/cm<sup>2</sup>,  $R_\infty = 40,000$  cps. For the one in the red site, we find  $\gamma_{hom}(0) = 34$  MHz,  $I_S = 3.0 \pm 0.5$  W/cm<sup>2</sup>,  $R_\infty = 100,000$  cps (the detection efficiencies are about  $10^{-3}$  for the red site and  $0.5 \times 10^{-3}$  for the main site). These values have been already compared to those of other systems [56]. The higher fully saturated fluorescence emission rate of the red site calculated from the spectrum is probably mainly due to the efficiency of the detection filter, as mentioned above. The saturation intensity of this specific molecule in the main site is about six times smaller than that of the one in the red site. This large difference could be due to different orientations of the transition dipole moment of the molecules (it will be discussed in Chapter 4) or to different depths of the molecules inside the crystal.

The FWHM has been measured for many molecules at 0.1 W/cm<sup>2</sup> for the main site and 0.2 W/cm<sup>2</sup> for the red one. At these intensities, the molecules are far from saturation, which allows us to obtain the width  $\gamma_{SM}(0)$  directly without any need for extrapolation at zero intensity. Figure 3.3 shows the histograms of measured widths for 72 molecules of the main site (upper panel) and 75 molecules of the red one (lower panel) at 1.4 K. The relation between the linewidth  $\gamma_{SM}$  and the lifetime  $T_1$  of the excited state of the molecules is given by Eq. 3.3, where  $T_2^*$  is the pure dephasing time [37] and  $\Delta\omega_{SD}(t_w)$  represents the broadening by spectral diffusion over the waiting time  $t_w$ :

$$\gamma_{SM} = \gamma_{hom} + \Delta\omega_{SD}(t_w) = \frac{1}{\pi} \left( \frac{1}{2T_1} + \frac{1}{T_2^*} \right) + \Delta\omega_{SD}(t_w). \quad (3.3)$$

$1/T_2^*$  can be neglected due to the low population of phonons at low temperature in the crystal, as confirmed by the temperature dependence of the broadening (see Chapter 4). The widths of the distributions are narrow, around 10 MHz, as expected in a crystal at low temperature. The distributions show a low-width cut-off around 26 MHz for the main site and 29 MHz for the red one.

The fluorescence lifetime  $\tau_{21}$  can be obtained from a start-stop measurement [75], which gives the probability to detect a second fluorescence photon after a first one has already been detected. Figure 3.4 shows such an antibunching measurement for two molecules excited at 12,721 cm<sup>-1</sup> and at 12,585 cm<sup>-1</sup>, in the main and red sites, respectively. The curves were fitted according to [75]. We found a lifetime  $\tau_{21}$  of  $6.0 \pm 0.5$  ns for the main site and of  $5.4 \pm 0.5$  ns for the red one. These numbers are in very good agreement with the values found from the cut-offs of the linewidth distributions (see Fig. 3.3). They give a lifetime-limited linewidth of around 26.5 MHz for the main site and 29.5 MHz for the red one. We believe that lines broader than the cut-off of the distributions are broadened by spectral diffusion. This spectral diffusion might

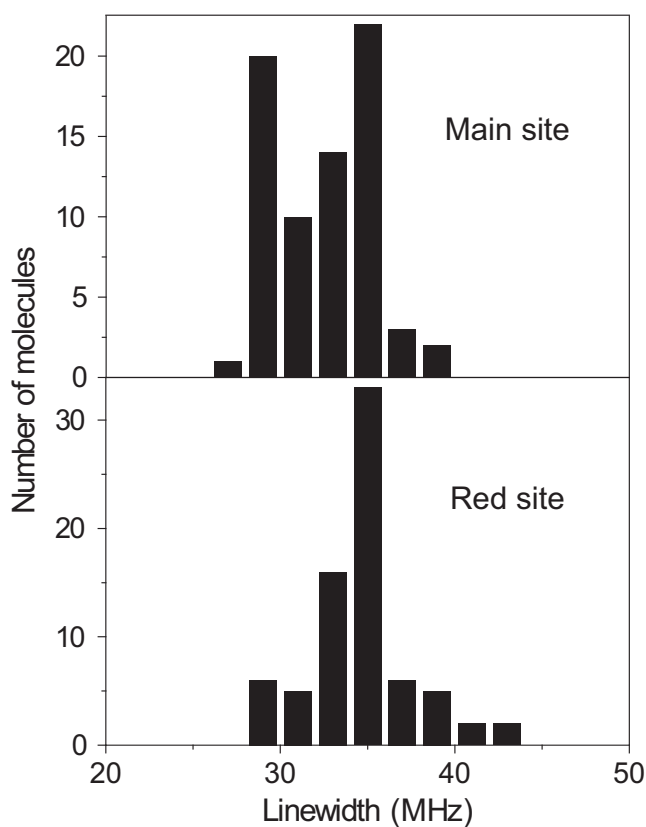


**Figure 3.3:** Linewidth histogram for 72 molecules of the main site (upper panel) and 75 molecules for the red site (lower panel) at 1.4 K. These histograms were recorded at low enough power in order to avoid any saturation effect. The low-width cut-offs of the two histograms are consistent with the lifetimes measured (see Figure 3.4). Molecules with a broader linewidth than the cut-off might undergo spectral diffusion.

result from crystal defects arising upon cooling down (the thermal expansion coefficients of the substrate and the crystal differ), or from thermally activated migration of charges [76].

In order to obtain stable and intense fluorescence signals of single molecules on an extended period of time, one would need a system with a low ISC yield. This ISC yield can be determined with a bunching measurement. Figure 3.5 shows the bunching measurement for a single molecule in the main site excited at  $12,729\text{ cm}^{-1}$  (upper panel) and the corresponding measurement for the background (lower panel). These measurements were performed for sev-



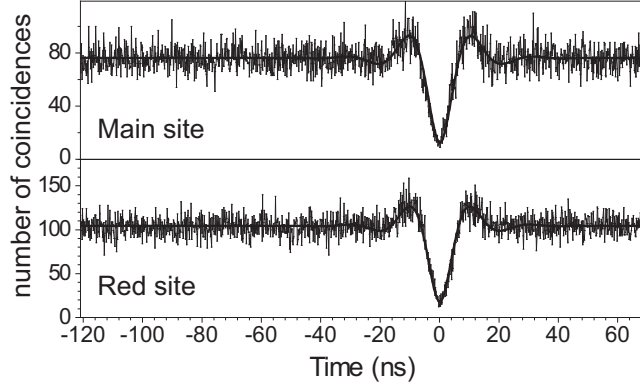


**Figure 3.4:** Antibunching measurement for two single DBT molecules in the main site (upper panel) and in the red site (lower panel). The two measurements were recorded with an intensity of 120 nW, at 1.4 K. The signal is in grey. A fit according to [75] is given by the thick line, which allows us to determine the lifetime of the first excited singlet state, from the width of the dip. Rabi oscillations are also distinguishable.

eral excitation intensities (from 0.6 to 3 W/cm<sup>2</sup>). They required a very long integration time (several hours in total, recorded in several runs) because of the extreme weakness of the correlation signal. The correlation signal was even lower for the red site, therefore we could not satisfactorily fit it. In the case of the main site, the correlation signal  $g^{(2)}(\tau)$  has been fitted with a single exponential, under the assumption that ISC only populates one triplet spin sub-level [25]:

$$g^{(2)}(\tau) = 1 + Ce^{-\lambda\tau}, \quad (3.4)$$

where  $\lambda$  is the decay parameter and  $C$  the contrast of the correlation. From the analysis, we obtained a contrast value of  $0.002 \pm 0.001$ . From the relation  $C = (\lambda - k_{31})/k_{31}$ , we estimated the rate  $k_{31}$  of the transitions from the first triplet excited state to the ground state ( $T_1 \rightarrow S_0$ ) to be of about  $2.5 \times 10^4 \text{ s}^{-1}$ , which corresponds to a triplet lifetime of about 40  $\mu\text{s}$ . We measured the triplet lifetime for different molecules. The values ranged from 40 to 200  $\mu\text{s}$ . Such short lifetimes may indicate a small energy gap between  $T_1$  and  $S_0$  according to the energy gap law [77]. From the analysis, we also obtain an upper bound of the ISC yield ( $\phi_T = k_{23}/(k_{21} + k_{31})$ ) around  $10^{-7}$ , which is more than one order of magnitude lower than the one of terrylene in *p*-terphenyl ( $6 \times 10^{-6}$ ) [42] and consistent with previous studies of DBT in naphthalene [74]. This extremely

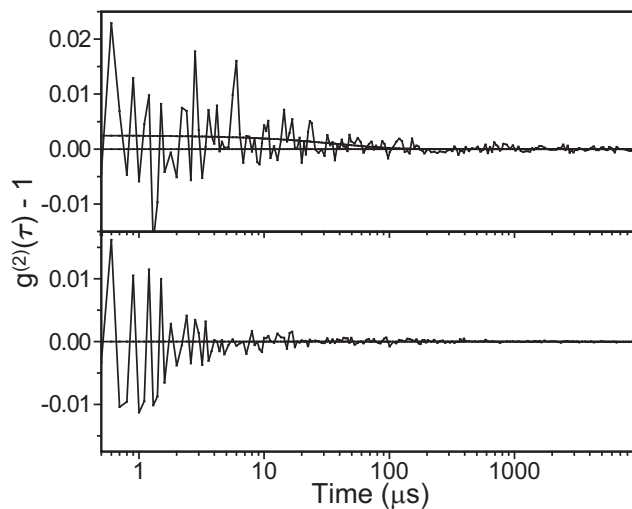


**Figure 3.5:** Bunching measurement for a DBT molecule in the main site (upper panel) and for scattered light (lower panel) at 1.4 K. The single-exponential fit of the signal coincides with the base-line for the scattered light. We obtain an upper bound for the ISC yield of  $10^{-7}$ , and a triplet lifetime of 40  $\mu\text{s}$ .

low ISC yield is, to our knowledge, the lowest ever measured for an organic molecule. This value is four orders of magnitude lower than the one of the system Tr in Ac where the ISC was strongly enhanced by intermolecular energy transfer from the Tr singlet guest to the Ac triplet host [72].

As a last experiment, we recorded the fluorescence spectra of DBT ensembles and single molecules in Ac for both sites. We found no significant differences between bulk and single-molecule spectra in each site. The vibrational frequencies and intensities were more reproducible from molecule to molecule (and from single molecules to ensembles) in the main site than in the red site. Figure 3.6 shows the fluorescence spectra of single DBT molecules in the main site (upper part) and in the red site (lower part) plotted as functions of the frequency relative to excitation. We did not find any Raman scattering line of the Ac crystal [78] in these spectra. As mentioned previously, the transmission of the detection filter is lower for the red site than for the main site. Therefore, the first vibronic components (lower than  $413\text{ cm}^{-1}$ ) are only visible for the red site. We first compared the positions of the vibronic lines between the two sites. There are more lines in the spectrum of the main site than in that of the red site, particularly at  $587\text{ cm}^{-1}$ , at  $974\text{ cm}^{-1}$ , and at  $998\text{ cm}^{-1}$ . The vibration frequencies of the two triplets of lines around  $460\text{ cm}^{-1}$  and  $780$

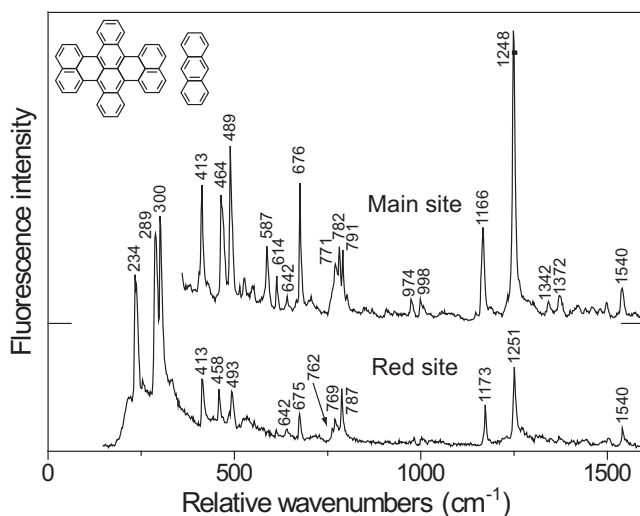


**Figure 3.6:** Fluorescence spectra of a single DBT in Ac at 1.4 K for the main site (excited at  $12,730\text{ cm}^{-1}$ ) and for the red site (excited at  $12,592\text{ cm}^{-1}$ ). The relative frequencies of the main lines are indicated with a resolution of about  $4\text{ cm}^{-1}$ . The intensities have not been corrected for instrument response. The intensity of the main site has been increased for clarity purposes.

$\text{cm}^{-1}$  are very different for the two sites and are probably very sensitive to any distortion of the molecules. It is also interesting to compare these spectra to the one of DBT in a naphthalene single crystal [74]. While lines at  $235\text{ cm}^{-1}$  and  $675\text{ cm}^{-1}$  for naphthalene are rather well reproduced in Ac, the one at  $1,259\text{ cm}^{-1}$  is slightly shifted to lower frequencies. More interesting is the single line at  $787\text{ cm}^{-1}$ , which splits as a triplet (around  $780\text{ cm}^{-1}$ ) when the molecule is embedded in Ac. The same happens to the single line at  $292\text{ cm}^{-1}$  which is largely split into two lines at  $289\text{ cm}^{-1}$  and at  $300\text{ cm}^{-1}$ . However, the two lines in naphthalene at  $403\text{ cm}^{-1}$  and at  $410\text{ cm}^{-1}$  merge into a single one at  $413\text{ cm}^{-1}$  for both sites in Ac (unless these lines are originally part of the triplet which would be largely shifted to lower frequencies in the case of naphthalene). These examples of lines that split when going from one matrix to another indicate that the symmetry of the DBT molecule is probably broken in different ways in the two matrices. Simulations and molecular dynamics would be required for the assignment of the different vibrational modes of the molecules, leading to a better understanding of the insertion of the DBT molecules into the matrix.

### 3.4 Conclusion

In the present chapter, we have investigated the photophysics of DBT single molecules in an Ac crystal. This system shows a strong and narrow ZPL (minimum widths of 26 MHz and 29 MHz for the main and the red sites, respectively), a high detection rate of fluorescence (40,000 and 100,000 counts/s for the main and the red sites, respectively), a good photostability and a very low ISC yield (less than  $10^{-7}$ ). Although the molecules seem to undergo some limited spectral diffusion, these characteristics make this system a very good candidate for many applications of high-resolution SMS at cryogenic temperatures. The next chapter will focus on the properties determined by the interactions between the DBT molecules and the Ac matrix.



## 4 Dibenzoterrylene in anthracene: II. Main insertion sites

WE find two main spectroscopic sites of dibenzoterrylene molecules in an anthracene crystal. We compare the experimental data (orientation of the transition dipole moment, temperature and pressure dependence of the linewidth, and electric field effects) with molecular dynamics simulations and with simulated annealing. From the simulations, we find two possible substitutions of three anthracene molecules by one dibenzoterrylene molecule. The very good agreement between molecular dynamics data and experimental results allows us to unambiguously attribute the two spectroscopic sites<sup>7</sup>.

---

<sup>7</sup> The content of this chapter is accepted for publication in: A. A. L. Nicolet, P. Bordat, C. Hofmann, M. A. Kol'chenko, B. Kozankiewicz, R. Brown, M. Orrit, "Single Dibenzoterrylene Molecules in an Anthracene Crystal: Main Insertion Sites", *ChemPhysChem* **8**, in press (2007).

## 4.1 Introduction

Cryogenic single-molecule spectroscopy is a powerful tool for detailed investigation of the structure and dynamics of condensed matter at nanometer scales [23, 24, 57, 58]. This high-resolution spectroscopic technique has shown all its relevance in studies of dynamical processes such as tunnelling of atoms or molecules in polymers and crystals at cryogenic temperatures [59–61]. A completely different kind of dynamical processes are the motions of charge carriers involved in conduction [79], whose study at nanometer scales has only started [19, 21, 22, 62]. The long-term goal of the present work is to investigate molecular conduction processes using single molecules as local probes [56]. In Chapter 3, we have identified a suitable guest-host system for this study: 7,8,15,16-dibenzoterrylene (DBT) in an anthracene (Ac) crystal. Here, we discuss the insertion of the guest in the host lattice, and the associated spectroscopic properties.

Probing dynamical processes with single molecules requires very stable fluorophores in stable insertion sites, in order to focus on the effects of interest. The stability of single-molecule lines critically depends on the insertion of the fluorophore in the matrix. Three main classes of organic matrices have served as hosts for single molecules [41]: polymers, which often lack short-range order, crystal-like Shpol'skii matrices, which present mostly short-range order with some orientational long-range order [80], and mixed molecular crystals, where the guest usually replaces one or a few host molecules, and which present short-range as well as long-range order.

Polymers, as matrices, present the advantages of being easy to handle and of having a good optical quality. Perylene, terrylene and some of their derivatives have been studied as single molecules in several polymers, including polyethylene [15, 81–83], polyvinylbutyral, polymethylmethacrylate, polystyrene [49], poly(isobutylene) [84]. In polymer matrices, single molecules are usually prone to various dynamical phenomena, such as photoinduced jumps [81], and spectral diffusion [59, 85] even at superfluid helium temperatures. A consequence of these processes is that molecules present spectral jumps and a broadened absorption line, which make these systems unpractical for high-resolution spectroscopy.

A particular class of materials are the Shpol'skii matrices consisting of  $n$ -alkane chains. Various guest chromophores (terrylene and perylene derivatives, diphenyloctatetraene, 2,3,8,9-dibenzanthanthrene (DBATT), pentacene, benzodiphenantrobisanthene (BDBP)) have been studied in  $n$ -nonane [86],  $n$ -dodecane [87],  $n$ -tetradecane [87–90],  $n$ -hexadecane [71, 82, 91]. Single molecules are more stable in these matrices than in polymers and often present narrow

zero-phonon lines, but they still undergo many spontaneous and light-induced spectral jumps, in particular via interactions with two-level systems. These jumps limit spectral resolution and acquisition times.

Finally, a last class of materials are mixed molecular crystals. Provided the guest matches the voids left by one or a few adjacent host molecules, these host-guest systems usually give rise to well-defined and stable insertion sites. Past studies include terrylene [42] and pentacene [23,24] in *p*-terphenyl, DBATT [5], pentacene [92], dibenzoterrylene [74], and terrylene [48,93] in naphthalene and in isotopically mixed naphthalene crystals [52], and terrylene in Ac [72]. In most of these systems, single molecules appear to be indefinitely stable and photostable, with lifetime-limited widths at low enough temperatures (often below 3 K). In some cases, photo-excitation of the guest can lead to a reversible change of insertion. The best documented case of such a switch is that of the X<sub>1</sub> site of terrylene in *p*-terphenyl, where single-molecule lines shift by 27 cm<sup>-1</sup> upon a photoinduced jump [94]. The switching has been shown to arise from a flip of a neighbour *p*-terphenyl molecule [29], and is related to the antiferro-elastic phase transition of *p*-terphenyl. The crystal's phase transition, which has been simulated by molecular dynamics [95], gives rise to a new unit cell with four inequivalent molecules, leading to four different insertion sites for the guests pentacene [28] and terrylene [29]. Therefore, for high-resolution spectroscopy, one would preferably select molecular crystals which do not undergo a phase transition upon cooling.

In Chapter 3, we have shown that single dibenzoterrylene (DBT) molecules in an anthracene single crystal are extremely favourable for nanoscale probing. We have discussed the photophysical properties of the two principal insertion sites at 785.1 and 794.3 nm. The single-molecule zero-phonon lines are narrow (about 30 MHz), intense (the detected fluorescence rates at saturation reach 100,000 counts/s), and very photostable. The intersystem-crossing yield is extremely low (10<sup>-7</sup> or lower). The present chapter reports on the properties induced by interactions between the chromophore and the Ac crystal, then compares and discusses the structures of the two principal insertion sites. Section 4.2 describes the experimental setup and procedures, and reports measurements of the temperature dependence of the linewidth, of the orientation of the transition dipole moments with respect to the crystallographic axes, and of the Stark effect. Section 4.3 is devoted to molecular dynamics simulations of the insertion sites of DBT molecules in Ac crystal. Finally, Section 4.4 compares experimental results and simulations. Their excellent agreement leads us to an unambiguous attribution of the two principal insertion sites of DBT in Ac.



## 4.2 Experimental and results

### 4.2.1 Experimental

Samples consisted of single crystals of Ac, doped with DBT. The sample preparation, as well as the home-built confocal microscope used for the single-molecule study have been described in Chapter 3.

We performed temperature-dependent measurements on the system, in the range of 1.4 to 4.0 K, monitoring the temperature with a calibrated resistor (Cernox Resistor CX-1050-AA-1.4L, LakeShore, Westerville, OH). It has to be pointed out that our bath cryostat did not allow us to independently vary temperature and pressure.

The orientation of the crystallographic axes 'a' and 'b' of the Ac crystals were determined by a polarisation transmission measurement, rotating the polarisation of the incident light and recording the minimum intensity transmitted by an analyser placed behind the crystal. A reflection measurement allowed us to distinguish between the 'a' and 'b' axes.

The Stark coefficients were recorded by applying high voltages (from -3000 to 3000 V), with a crystal carefully placed in between two copper electrodes, with a spacing of 3 mm. The Stark cell had been designed so as to avoid any contact between the crystal and the electrodes in order to rule out any charge injection effects. The electric field was applied in the (a,b) plane of the Ac crystal, with an angle of 60° with respect to the 'b' axis.

### 4.2.2 Temperature and pressure dependence

We first studied the influence of temperature on the single-molecule lines. As a first effect, a broadening of the molecule lines is expected, when temperature rises, because of an increase of the population of phonons [96, 97]. Figure 4.1 shows the widths of two single DBT molecules, one in the main site and one in the red site, versus temperature. Experimental data were fitted with an Arrhenius law [98]:

$$\gamma_{hom}(T) = \gamma_{hom}(0) + Ae^{-\frac{E_a}{k_B T}}, \quad (4.1)$$

where  $\gamma_{hom}(0)$  is the linewidth at zero temperature,  $k_B$  is the Boltzmann constant,  $E_a$  is the activation energy, equal to the energy  $\hbar\omega_{LP}$  of the local phonon [7] and  $A$  is a constant depending of the electron-phonon coupling. The inset of Fig. 4.1 shows the plot of the logarithm of Eq. 4.1 for the molecule of the red site. We obtained an activation temperature  $T_a$  of  $16 \pm 4$  K. Measurements over 19 molecules of the red site showed an activation temperature

ranging from 10 to 40 K, with a maximum of the distribution around 25 K. The lines of molecules in the main site do not broaden significantly between 1 and 4 K, which is the range accessible to our bath cryostat. Assuming an electron-phonon coupling value equal to the average value for the red site, the fit gives a lower bound for the activation temperature of 35 K, which may be largely conservative.

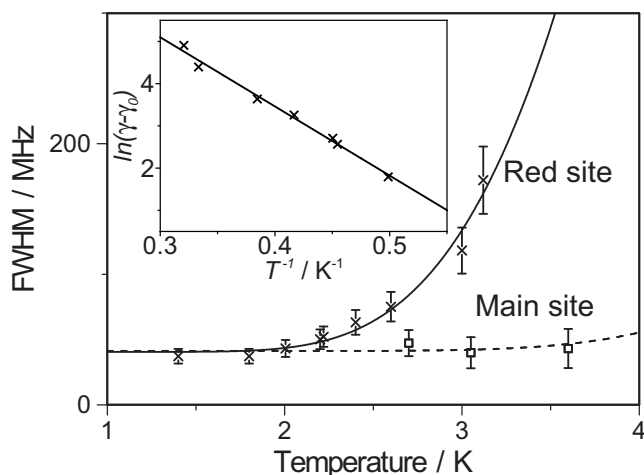


**Figure 4.1:** Linewidth versus temperature for two molecules, one in the red site and one in the main site. The temperature-dependence has been fitted by an Arrhenius function for both sites. The fit of the main site allows us to give a minimum value for the activation energy, assuming that the electron-phonon coupling constant is similar for both sites. The inset shows a linear fit of  $\ln(\gamma(T) - \gamma(0))$  versus  $T^{-1}$  for the molecule of the red site.

A change of pressure should induce a shift of the molecular lines. We expect that a variation of temperature should also cause such a shift. However, the temperature effect in the range of temperatures explored (from 1 to 4 K) is much smaller than the associated pressure effect (change from a few mbar to 1 bar). As a consequence, the observed shift of the molecular lines is mainly due to changes of pressure, the temperature effect being negligible. All molecules investigated exhibited a linear and reversible red-shift with increasing pressure, ranging from 0.7 to 1.1 GHz/bar for the main site and from 0.8 to 1.8 GHz/bar for the red site. These values are comparable to the ones measured for similar systems, such as terrylene [9] or pentacene [8] in *p*-terphenyl.

### 4.2.3 Orientation

In order to investigate the interaction between guest and host molecules, it is useful to know how DBT molecules are inserted in the Ac crystal. We rotated the polarisation of the laser light so as to investigate the orientation of the projection of the transition dipole moment of the DBT molecules in the (a,b) plane of the Ac crystal. Figure 4.2 shows the modulation of the fluorescence intensities of several molecules versus the orientation of the polarisation of the laser light. In an isotropic matrix, we would expect the maximum intensity when the excitation polarisation is parallel to the molecule's transition dipole moment, with a 100% modulation depth. However, the strong birefringence of the anthracene crystal (the refractive indices are 1.6, 1.8 and 2.2 for the different crystal axes at  $\lambda = 546$  nm [38]) can shift the angular position of the maximum, and decrease the modulation depth [99]. Both effects depend on the depth of the molecule in the crystal, and are difficult to model accurately in the case of a large-aperture excitation beam. In order to minimise the bias due to birefringence in our statistical analysis of Fig. 4.3, we selected molecules with high fluorescence intensities and modulation depths larger than 90%, which are thought to lie closest to the surface.

The lower panel of Fig. 4.2 shows the fluorescence intensity versus the excitation polarisation angle. The minimum fluorescence signal is at background level. We then fitted the modulation with a  $\cos^2$ -function in order to get the orientation of the in-plane component of the transition dipole moment of the molecule. Repeating the same procedure on many individual molecules (63 and 67 molecules for the main and the red sites, respectively), we built histograms of the orientations of the projection of the DBT transition dipole moment in the (a,b) plane of the Ac crystal for the two sites (see Fig. 4.3). We also tried to record the out-of-plane component of the transition dipole moment, but without success, probably due to the small numerical aperture of our microscope objective [(NA)=0.85].

The in-plane component of the DBT transition dipole moment was found to be predominantly along the 'b' axis of the Ac crystal within a few degrees. For both sites, the angular distributions are centred on the *b*-axis. The half-maximum widths of the distributions are 10 and 17 degrees for the main and the red sites, respectively. Some of this width may arise from a distribution of depths and from the birefringence of the crystal. This effect may obscure a double-peaked distribution if the transition dipole moments are not exactly lying along the 'b' symmetry axis. Nevertheless, the double-peaked distribution found for the red site appears clearly enough not to be due to statistical fluctuations.

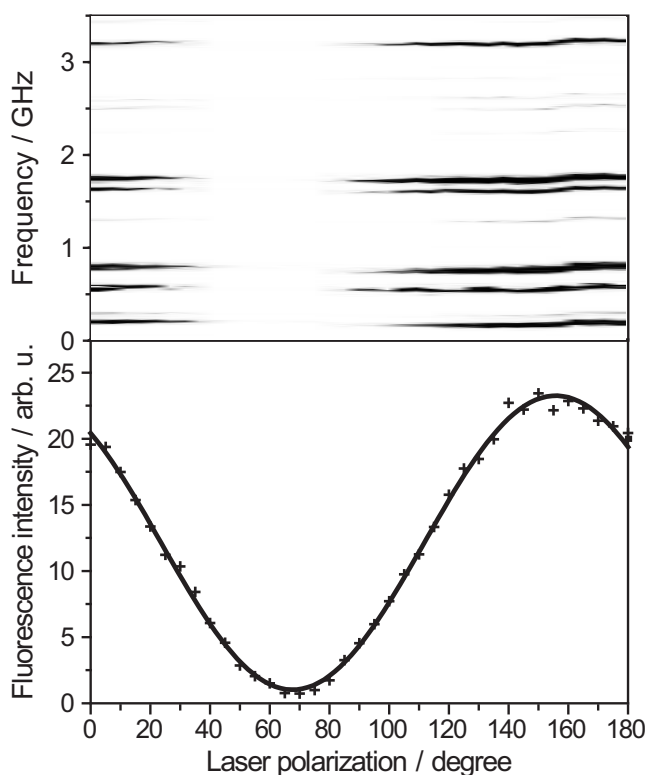


**Figure 4.2:** Upper panel: A few traces of single DBT molecules recorded upon scanning a range of 3.5 GHz over the molecular resonances. The fluorescence intensity is represented on a grey scale. After each scan, we rotated the polarisation of the laser by 5 degrees. Lower panel: Modulation of the fluorescence intensity versus the orientation of the polarisation of the laser. The modulation has been fitted with a  $\cos^2$ -function in order to get the orientation of the projection of the transition dipole moment of the molecule in the (a,b) plane of the crystal.

#### 4.2.4 Stark effect

As a last experiment, we studied the Stark effect. Applying an electric field onto the sample shifts the energies of both ground and excited states. Being different, these shifts lead to a measurable change of the molecular absorption frequency. It was very important in this measurement to avoid any contact between the electrodes and the crystal, so as to prevent any charge injection into the sample. The applied electric field was oriented with an angle of  $60^\circ$  with respect to the 'b' axis of the crystal. For each molecule, we fitted the

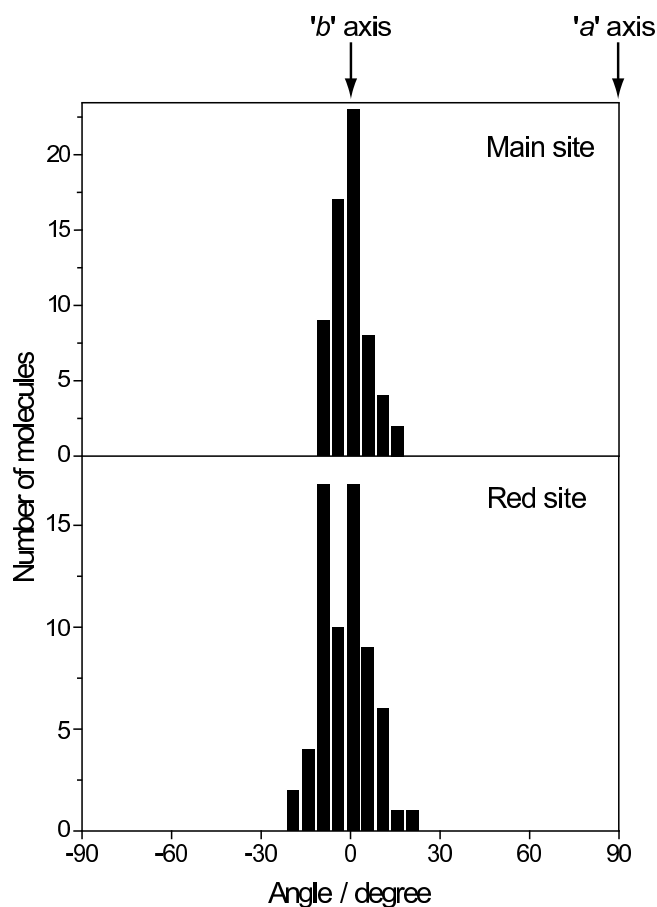


**Figure 4.3:** Histograms of the orientations of the transition dipole moments of 63 DBT molecules of the main site (upper panel) and 67 molecules of the red site (lower panel). The orientation of the crystallographic axes 'a' and 'b' has been determined by transmission and reflection measurements.

measured shift as a sum of two contributions, linear and quadratic in electric field [16]:

$$\delta\nu = aE + bE^2 = \frac{1}{h} \left( -\delta\vec{\mu} \cdot \vec{E} - \vec{E} \cdot \delta\alpha \cdot \frac{\vec{E}}{2} \right), \quad (4.2)$$

where  $\delta\nu$  is the change of the absorption frequency of a single molecule,  $E$  is the applied electric field,  $a$  and  $b$  are the linear and quadratic Stark coefficients,

$\delta\vec{\mu}$  is the dipole moment change and  $\delta\alpha$  is the polarisability tensor change upon excitation.

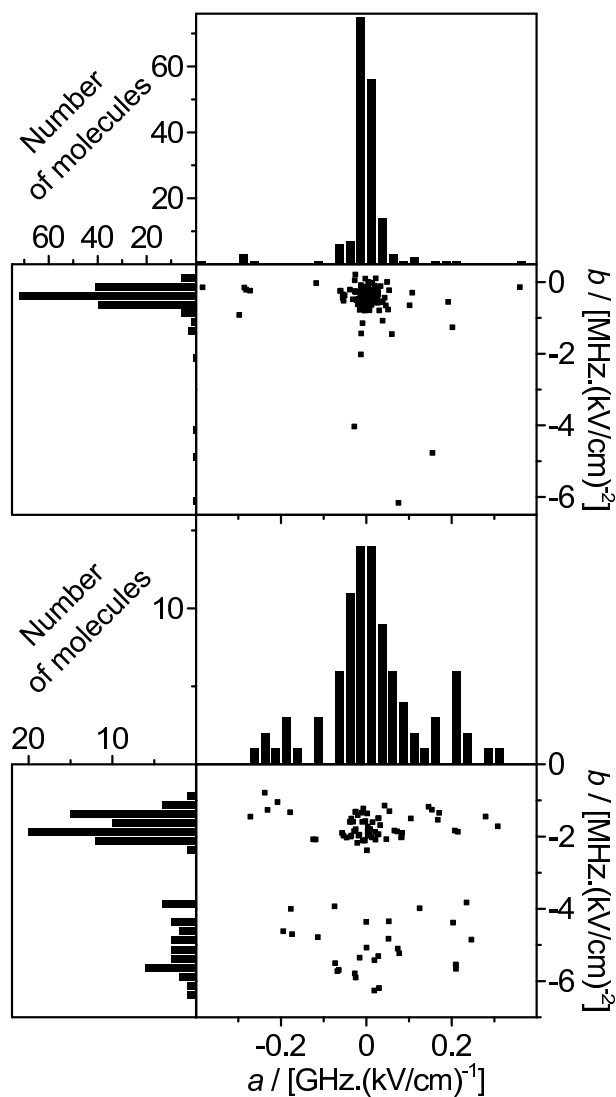


**Figure 4.4:** Linear ( $a$ ) and quadratic ( $b$ ) Stark coefficients for 174 molecules of the main site (upper panel) and for 91 molecules of the red site (lower panel) with scatter plots.

Figure 4.4 shows the distribution of the linear and the quadratic Stark coefficients for 174 and 91 molecules of the main and the red sites, respec-

tively. A scatter plot shows the absence of clear correlation between the two coefficients. The distribution of the linear component of the Stark shift is centred on zero, and has a half-maximum width of 30 MHz/(kV/cm) for the main site and of 90 MHz/(kV/cm) for the red site. Neglecting the local field correction, these values correspond to dipole moment changes of 60 mD and 180 mD, respectively ( $1 \text{ D} = 3.34 \cdot 10^{-30} \text{ C}\cdot\text{m}$ ). The quadratic Stark coefficient was found to be rather high for both sites. For the main site, the average value is about  $-0.4 \text{ MHz}/((\text{kV}/\text{cm})^2)$  (corresponding to a polarisability change of  $400 \text{ \AA}^3$  [16]), and the width of the distribution is about  $0.5 \text{ MHz}/((\text{kV}/\text{cm})^2)$ . The red site presents two populations, one with a centre value of  $-1.7 \text{ MHz}/((\text{kV}/\text{cm})^2)$  (i.e. a polarisability change of  $1700 \text{ \AA}^3$ ) and distribution width of  $0.8 \text{ MHz}/((\text{kV}/\text{cm})^2)$  and another one at  $-5.2 \text{ MHz}/((\text{kV}/\text{cm})^2)$  (i.e. a polarisability change of  $5200 \text{ \AA}^3$ ) with a distribution width around  $1.6 \text{ MHz}/((\text{kV}/\text{cm})^2)$ . All these values are much larger than the molecular volume, which points to significant charge delocalisation in the excited or the ground state of the guest molecules [79].

### 4.3 Simulations

In parallel, we also performed molecular modelling of the system DBT in Ac in order to investigate the substitution of Ac molecules, the conformation of the DBT molecules and the insertion of the guest into the crystal.

#### 4.3.1 Molecular modelling

Substitution sites for one DBT molecule in Ac were investigated by modelling one guest molecule in  $4 \times 5 \times 3$  monoclinic unit cells of the host, with periodic boundary conditions. The force field for the host was optimised from intra- [100–102] and inter- [103] molecular force-fields in the literature. Partial atomic charges were determined from an electrostatic potential (ESP) fit (Gaussian98 [104]). Details of the model, which accurately describes solid and liquid Ac over a wide range of pressures and temperatures, will be provided in a forthcoming paper.

DBT was modelled with the force field developed earlier for terrylene [29, 105], except for the partial charges calculated here with an ESP fit. The model satisfactorily describes the structure and the lowest vibrational frequencies of DBT found in AM1 HF and B3LYP/6-31G DFT geometry optimisations (Gaussian98 [104]). Individual rings in the molecule are closely planar, but owing to steric hindrance, the free molecule has point group  $C_{2h}$  only, like *p*-terphenyl, with the tetracene unit tilted out of the common plane of the

naphthalene units (dihedral  $\theta$  in Table 4.1). The external rings of the tetracene unit are bent out of the plane of the central rings (dihedral  $\psi$ ). Details of the optimised structures and further properties of the present substitution sites will be presented elsewhere.

**Table 4.1:** Out-of-plane deformation (see text) of the optimised geometries of DBT.

	$\theta$ ( $^\circ$ )	$\psi$ ( $^\circ$ )
B3LYP/6-31G	27.6	16.6
HF/AM <sub>1</sub>	28.3	17.1
Classical force-field	28.2	16.3

All classical molecular dynamics simulations were performed in the  $N\sigma T$  (iso-stress, isothermal) ensemble with the Berendsen thermostat and barostat [106], using the DLPOLY suite of MD programmes [107]. The timestep was 0.5 fs and the relaxation times of the thermo - and baro-stat were respectively 0.1 and 0.5 ps. Electrostatic interactions were evaluated with the shifted potential approximation.

### 4.3.2 Identification of the insertion sites

Considering the shape and size of DBT compared to anthracene, we examined substitutions of two or three host molecules. The initial orientation of DBT was parallel to the (b,c) crystal plane, with the long axis close to 'b'. Figure 4.5 shows the substitutions envisaged here, with replacement of two (substitutions III and V) or three (substitutions I, II, and IV) host molecules. Note that, for all of these, equivalent substitutions (noted I'-V') are obtained by symmetry in a glide plane parallel to (b,c). Properties related by this symmetry, e.g. the tilts of the DBT long axis off the host's 'b' axis, will change sign on going from (I)-(V) to (I')-(V'). Substitutions of two molecules along the 'a' crystal axis was rejected on grounds of packing and hindrance by the host molecule at the centre of the (a,b) cell face.

While sublimation crystal growth is a non-equilibrium process, it should be stressed that for the present purposes, it is nonetheless the equilibrium



Gibbs free energy differences between different substitutions under ambient conditions, rather than the minimised energies of optimised structures, that are more appropriate to judge which substitution sites are most likely. These free energies were estimated from 1 ns simulations of a variety of substitutions of two or three hosts by one DBT molecule. The models were subsequently quenched to 1 K (50 ps runs) for comparison with experimental data obtained at helium temperatures. Thus, it turns out that the structures with lowest potential energy at helium temperatures are not always the most probable at room temperature.

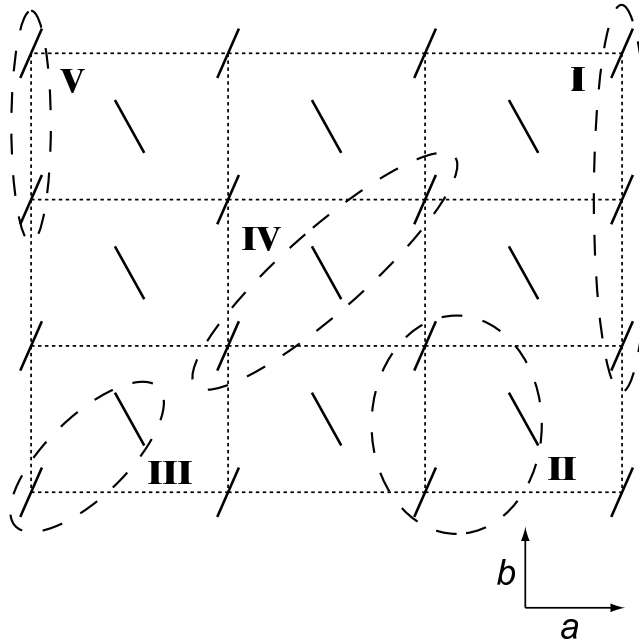


**Figure 4.5:** Schematic representation of the selected substitutions. DBT replaces two (substitutions III and V) or three (substitutions I, II, and IV) anthracene molecules.

Free energy differences between substitutions of the same number of anthracene sites are just the differences in the total internal energies of the simulations. Differences between substitutions of different numbers of host molecules include an entropic contribution, estimated (cf. [105]) by assuming the doped crystal is in equilibrium with anthracene vapour:

$$\Delta G = \Delta E_{doped\ crystal}^{tot} + E_{Ac, gas}^{tot} - 2RT. \quad (4.3)$$

Taking the values of  $\Delta G$  (at 300 K and 1 bar) for the substitution I as a reference, we found substitution II at 1.3 kcal/mol, substitution III at 10.2 kcal/mol, substitution IV at 13.7 kcal/mol, and, finally, substitution V at 19.1 kcal/mol.

**Table 4.2:** Orientational and structural parameters (see text) of site I and II. We added the experimental values of the main and the red site according to the assignment presented in Section 4.4. The uncertainties are taken from the half-width of the distributions (see Fig. 4.3).

Substitution	$\theta$ ( $^\circ$ )	$\psi$ ( $^\circ$ )	$\chi$ ( $^\circ$ )	$\xi$ ( $^\circ$ )	$\xi_{exp}$ ( $^\circ$ )
I	32.5	11.9	-1.2	1.2	0 $\pm$ 5
II	33.7 $\pm$ 0.2	14.0 $\pm$ 0.1	1.0 $\pm$ 0.1	11.4 $\pm$ 0.3	5 $\pm$ 9

From the Gibbs free energy differences we see that replacement of three anthracenes is more favourable than two, with the most probable substitution being I. As expected, substitution II is very similar, both in energy and structure, and close in free energy to substitution I. Substitution IV, 13.7 kcal/mol (6900 K) above I, is very unlikely. We may thus expect that substitution I corresponds to the experimental main site and substitution II to the less populated red site [108]. Figures 4.6(I) and 4.6(II) show insertions I and II. This attribution is supported by the pitch,  $\xi$ , of the projection of the long molecular axis of DBT (also the transition dipole direction) in the (a,b) plane with respect to the 'b' axis (see Table 4.2). The values reported in Table 4.2 are in very good agreement with those deduced from modulation of the laser polarisation, Section 4.2.3.

Two angles describe the orientation of the naphthalene units with respect to the central tetracene. The first angle is the tilt (twist) dihedral  $\theta$  of the naphthalenes around the DBT long axis. The second angle  $\chi$  describes tilts (bends) of the naphthalene units around a direction parallel to the long tetracene axis, measured from the centro-symmetric conformation of DBT in the gas phase. Significant differences are found for these angles in the two substitutions, which may be related to the differences in the experimental vibronic spectra in the main and red sites [108].

We have also performed simulated annealing (with 200 cycles of heating to T=300 K and cooling at T=1 K) to probe the fine structure of insertions I and II. Fig. 4.7 shows a scatter diagram of the intermolecular electrostatic and

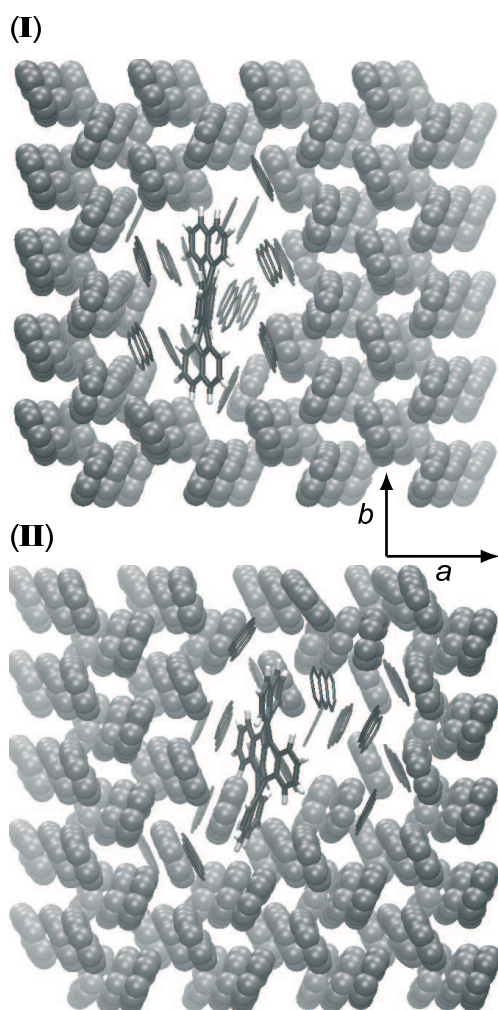


**Figure 4.6:** Orthographic views down the long axis of anthracene, of molecular models of the two lowest free energy substitution sites of DBT (sticks) in Ac (balls): (I) substitution I, (II) substitution II. The Ac molecules represented with wireframes are distorted and/or displaced. The three different colours of the Ac molecules indicate three different planes. The crystallographic axes 'a' and 'b' are indicated with arrows.

repulsion-dispersion energies between DBT and the host crystal. This plot is a way to distinguish different minima of the potential energy landscape. A single cloud of points is obtained for each substitution, consistent with the stability of the sites (absence of large photo-induced spectral jumps). The cloud of

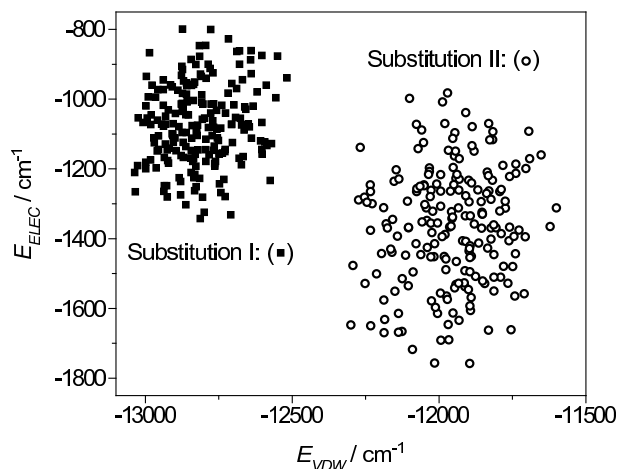


**Figure 4.7:** Scatter diagram of the components of the intermolecular stabilisation (electrostatic versus repulsion-dispersion) obtained in 200 simulated annealing cycles of substitution I (squares) and II (circles).

points from insertion I is however more compact than that of insertion II.

A further element in the identification of the sites is provided by the deviations of the substitution sites from centro-symmetry. Substitution I lies on an inversion centre of the host crystal, whereas substitution II does not. This agrees with the experimental observation that one of the sites displays higher deviations from inversion symmetry than the other.

From our simulations, we expect two-peak distributions of the orientations of the transition dipole moments for each insertion. The peaks on either side of the 'b' axis would correspond to substitutions I and I' (II and II'). The dipole moment change should be exactly zero for the centrosymmetric substitution I. The absence of centro-symmetry of substitution II should lead to a two-peak distribution of its dipole moment changes.

## 4.4 Discussion

We now compare the main results from the experiments and from the simulations. Both present two dominant features, the main and the red sites for the experiments, and insertions I and II for the modelling. How to assign them?

In Chapter 3, we presented the bulk fluorescence excitation spectrum of DBT in Ac. The number of molecules in the main site is considerably greater

than in the red site (at least 100 times larger), indicating that the insertion probability during growth is higher in the main site. The comparison of simulated Gibbs free energies (see Table 4.2, where substitution I presents a lower energy than II) leads us to assign insertion I to the main site. This assignment is supported by the agreement between the experimental inhomogeneous widths (the main site presents a much lower inhomogeneous width - about  $5\text{ cm}^{-1}$  - than the red site - about  $20\text{ cm}^{-1}$ ) and the spreads of simulated scatter plots in Fig. 4.7. Both data point to a larger susceptibility of the red site and of insertion II to disorder and to perturbations. The spread of measured pressure shifts (larger in the red site than in the main site) and the larger temperature dependence in the red site also illustrate the same trend, which is also consistent with the observations in fluorescence spectra [108] of the more reproducible vibrational frequencies and intensities from molecule to molecule (and from single molecules to ensembles) in the main site. The previous discussion therefore strongly supports the assignment of insertion I to the main site.

We now turn to the orientations of the transition dipole moments of the DBT molecules (cf. Table 4.2). The simulations reproduce the nearly perfect alignment of the dipole moments with the 'b' axis of the host crystal for both sites. Even the simulated angles with the 'b' axis are in a fair agreement with the measurements, within error bars. Looking in more detail at the measured angular distributions, we find a single maximum for the main site, and two symmetrical peaks around the 'b' axis for the red site. This is exactly the outcome of the simulations, with a much smaller angle between the projection of the long DBT axis into the (a,b) plane and 'b' for insertion I than for insertion II. This further supports the assignment of insertion I to the main site and of insertion II to the red site.

Finally, the linear Stark coefficients are distributed around zero for both sites, without clear indication of a double maximum for symmetrical values of  $\delta\mu$ . This seems to indicate that both sites are centro-symmetric, in good agreement with the simulations for insertion I, but in disagreement with them for insertion II. The deviation from centro-symmetry of insertion II should lead to a double-peak distribution around two values  $\pm\delta\mu_0$ . This unexpected result can be explained if the center of the distributions ( $\pm\delta\mu_0$ ) is smaller than their width, or if the applied electric field was nearly perpendicular to the dipole moment change. Additional measurements at variable orientations would be needed to answer this question.

## 4.5 Conclusion

In this chapter, we have reported on those spectroscopic properties of the guest-host system DBT in anthracene crystal which depend on the details of the insertion for the two main spectroscopic sites. These properties include the temperature dependence of the linewidth of single molecules, the orientation of their transition dipole moment with respect to crystal axes, and the linear and quadratic Stark effect coefficients. The quadratic coefficient turns out to be very large for all molecules, while the linear coefficients are distributed around zero. We have performed molecular dynamics simulations of the Ac crystal, of the conformation of the isolated DBT, and of the insertion of DBT in the crystal. Molecular dynamics simulations indicate that a DBT molecule replaces three Ac molecules, with a transition dipole moment mainly oriented along the '*b*' axis of the crystal, in full agreement with the experiments, within the experimental error of 5 to 10 degrees. The higher activation energies for phonon-induced broadening, the narrower distributions of the pressure shifts, of the orientation of the transition dipole moments, and of the dipole moment changes (with smaller values) for the main site all indicate that this site is less prone to fluctuations around the optimum insertion position than its red counterpart. These experimental results are all consistent with the better stability (with respect to slight numerical perturbations) of the simulated substitution I. Finally, the very good agreement between experiments and simulations leads us to unambiguously attribute the main site to substitution I (one DBT replaces three host molecules along the '*b*' axis) and the red site to substitution II (one DBT replaces two host molecules along the '*b*' axis and one of their nearest-neighbours in the '*a*' direction).



## 5 The transistors

WE present the characterisation of an anthracene single-crystal organic field-effect transistor in the temperature-range of 4.2 to 290 K. We recorded the source-drain current as a function of the applied voltages (source-drain and gate). The measured curves exhibit a superlinear dependence when plotted on a log-log scale with an exponent larger than two, which is typical in case of a trap-filling regime. At low temperatures, the source-drain current becomes temperature independent and shows a plateau. We estimate a lower bound of the mobility and compare the values we found with former experiments.



## 5.1 Introduction

During the last decades, the interest devoted to the electronic properties of organic  $\pi$ -conjugated materials has grown considerably [4,79,109–111]. On the side of applied research, many promising organic-based devices, including fully flexible devices for large-area displays, light-emitting devices [112], or solar cells have been successfully developed, opening numerous new technological potentialities. However, many basic concepts about electronic transport and charge injection in these materials are still not very well understood, especially at nanometer scales.

The relevant quantity to characterise charge transport at a macroscopic scale is the carrier mobility which represents the ease for charge carriers to move through the material. Various methods have been developed to study this carrier mobility [79]. Among the most popular are the time-of-flight (TOF) measurements, the field-effect transistor (FET) configuration, the diode configuration and the pulse-radiolysis time-resolved microwave conductivity (PR-TRMC) [113,114]. Some of these techniques involve measurements over large areas. Therefore, they are impurity- and defect-dependent and require materials with high purity and high order. Moreover, the mobility is an ensemble parameter. As a consequence, the individual events are completely lost in these measurements.

In a former publication [56], we proposed to study charge transport by means of single-molecule spectroscopy and microscopy at cryogenic temperatures as this technique could ultimately allow us to optically probe displacements of individual charges with a very high accuracy [115]. We previously said (see Chapter 4) that such a study requires a system where the probe molecules are embedded into a rigid matrix in order to increase their photo-stability and therefore the sensitivity of the technique. To keep the advantages of high-resolution spectroscopy, one also has to choose a matrix with as little disorder as possible, the best results being usually obtained with matrices that consist of organic crystals at cryogenic temperatures [41]. We previously showed (see Chapter 3) that DBT in Ac was a promising system for this study.

In organic crystals, the charge carriers have strong interactions with their environment. Their movements generate distortions of the molecules and the lattice, and change the polarisation of the electronic cloud of the surrounding molecules. A movement of the charge carriers will always be accompanied by these perturbations. The strong interaction between the charge carriers and the induced polarisation is described under the model of the polaron [2,3].

Organic crystals of small conjugated molecules can be described with a fully filled valence band which consists of the overlapping of the highest occupied

molecular orbitals (HOMO) of the individual molecules, and an empty conduction band defined by the mixing of the lowest unoccupied molecular orbitals (LUMO). Defects and impurities of the crystal might create some available energy levels in the gap between the HOMO and the LUMO bands, which will act as traps. These traps can be separated into two categories. On the one hand, we have traps with energy levels of the order of a few  $k_B T$ , where  $k_B$  is the Boltzmann constant and  $T$  is the temperature. The detrapping of charges will be thermally activated. For that reason, we will call them shallow traps. On the other hand, some defects or impurities might act as traps out of the range of thermal activation. These traps will be called deep traps. It is clear that the conduction mechanism will not be of the same nature in presence of shallow and/or deep traps. The temperature dependence of the mobility can therefore give crucial information with respect to the processes that are involved in the conduction phenomena.

We already explained that FET is a powerful system to study the different processes of charge carriers transport as it allows one to tune the charge carrier density in a continuous way and therefore to control the working regime of the device via the transverse gate electrode. Several organic crystals have been used as a conducting layer in FET. Among them are sexithiophene [65], rubrene [66], pentacene [67], tetracene [68, 69] or Ac [32]. Thus, the choice of Ac is natural if we consider the single-molecule study that we propose to conduct.

In FET configuration, essential information about conduction can be obtained via the current-voltage  $I - V$  curves, where the current is plotted as a function of the gate-voltage  $V_g$  [116] or of the source-drain voltage  $V_{sd}$ . From these curves, we can either extract or estimate a lower bound of the mobility using the proper formula for the respective regimes of the FET. The temperature dependence of the mobility of Ac-FET has been studied until 100 K [32]. However, a change of the conduction regime is expected at much lower temperatures (about a few tens of kelvins).

Herein, we present the properties of Ac-based FET in the light of the current-voltage characteristics for several temperatures, ranging from 4.2 to 290 K. From these  $I - V$  curves, we give a lower bound of the mobility at room and at low temperatures. In Section 5.2, we describe the experimental setup and procedure. In Section 5.3, we present the experimental results and discuss their main features. We finally comment on the potentialities of Ac-based FET for a better understanding of charge carrier transport in molecular crystals.

## 5.2 Experimental

Anthracene (Ac; Aldrich, scintillation grade, purity  $\geq 99.0\%$ ) was purified in a home-built zone refiner for about 4000 passes. Single crystals of Ac were then grown by sublimation under a 150 mbar nitrogen atmosphere. Sublimation flakes developed along the (a,b) plane with diameters of a few millimetres and a thickness of a few tens of micrometres. The substrates of the FET structures consisted of Si wafers highly p-doped with boron (with a resistivity of 0.001 - 0.01  $\Omega\text{cm}$ ) with a thermally grown  $400 \pm 20$  nm thick layer of  $\text{SiO}_2$ . Interdigitated gold electrodes (30 electrodes with 29 gaps, 40 nm thick) with spaces of 5  $\mu\text{m}$  were deposited (by the Fraunhofer-Institut für Mikroelektrische Systeme und Schaltungen, Munich, Germany) on top of the insulator layer by e-beam lithography, with a 12 nm thick layer of TiW. Before contacting the FET structure to the Ac crystal, electrodes were treated with a solution of 10 mM nitrobenzenethiol in acetonitrile as this treatment significantly reduces the contact resistance, which is crucial for low-temperature measurements [32, 117]. The Ac crystals were then optically contacted on top of the structures.

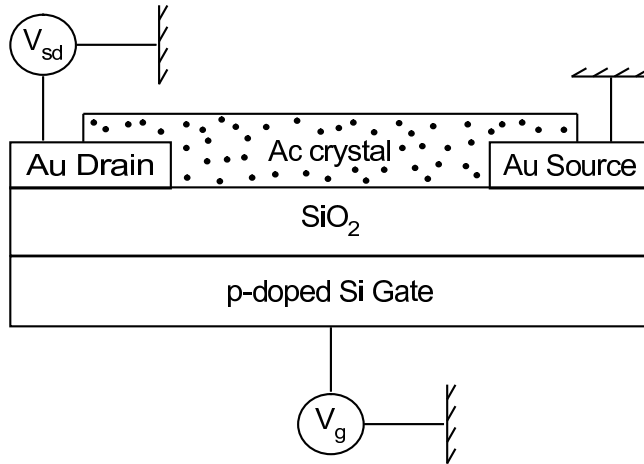


**Figure 5.1:** Schematic drawing of an Ac FET. Dimensions are discussed in the text.

The samples were mounted in a helium bath cryostat and cooled down with liquid nitrogen for temperatures ranging from 290 K to 77 K and with liquid helium for lower temperatures (down to 4.2 K). Source-drain current was detected by means of a home-made ammeter (with several settings of sensitivities, ranging from 0.001 to 0.1  $\mu\text{A}$ ) after applying several source-drain

and gate voltages. Prior to any measurement and before contacting the Ac crystals, we measured the gate-induced leakage current of the gold electrodes. We could not detect any current. It has been shown [118] that, in order to operate the FET with stability, one requires a leakage current lower than  $10^{-9}$  A/cm<sup>2</sup>. We tried to measure this leakage current with a more sensitive ammeter (Keithley, Picoammeter 6487) for other structures, but could not find any current.

### 5.3 Result and discussion

Figure 5.2 shows a typical plot of  $\log I_{sd}$  versus  $\log V_{sd}$  for an Ac-FET at 217 K. The  $I - V$  curves show a power-law dependence as  $I_{sd} \sim V_{sd}^n$ . The values of the exponent  $n$  are ranging from 6 to 12 for different temperatures, consistent with previous measurements (Mark *et al.* found a value of 12, but mentioned traces of tetracene in the crystal [119], and Aleshin *et al.* obtained values ranging from 6 to 16 [32]). At a given temperature, the exponent is only weakly gate-dependent, slightly decreasing when  $V_g$  increases. The space-charge limited current (SCLC) theory describes transport mechanisms with different regimes. From the Ohmic regime (at low voltages), we pass the rather narrow SCLC regime governed by shallow-traps (where we have a dependence as  $I_{sd} \sim V_{sd}^n$ , with  $n \sim 2$ ), to the trap filling (TF) limit (where  $I_{sd} \sim V_{sd}^n$ , with  $n \gg 2$ ). Our measurements exhibit the latter regime of conduction, and the  $I - V$  curves are superlinear over their entire range.

Usually, deep traps prevent the current flow by localising charge carriers. It is yet possible to inject charges via the electrodes and to initiate a current if the amount of charges is sufficient to fill the traps. We can define the voltage of trap-filling limit as [116]:

$$V_{TF} = \frac{eL^2N_t}{\epsilon_r\epsilon_0}, \quad (5.1)$$

where  $e$  and  $N_t$  are respectively the elementary charge and the trap concentration,  $L$  is the length of the channel,  $\epsilon_0$  is the permittivity of free space, and  $\epsilon_r$  the relative dielectric constant of the material (for Ac,  $\epsilon_r=3.2$ ). Unfortunately, we cannot determine  $V_{TF}$  in our measurement, and consequently cannot estimate the number of traps and its variation as a function of temperature and gate-voltage.

Ac is an organic crystal with a rather high band gap  $E_g \sim 4$  eV [120, 121]. The band gap being large, we expect high-purity crystals to act as insulators.

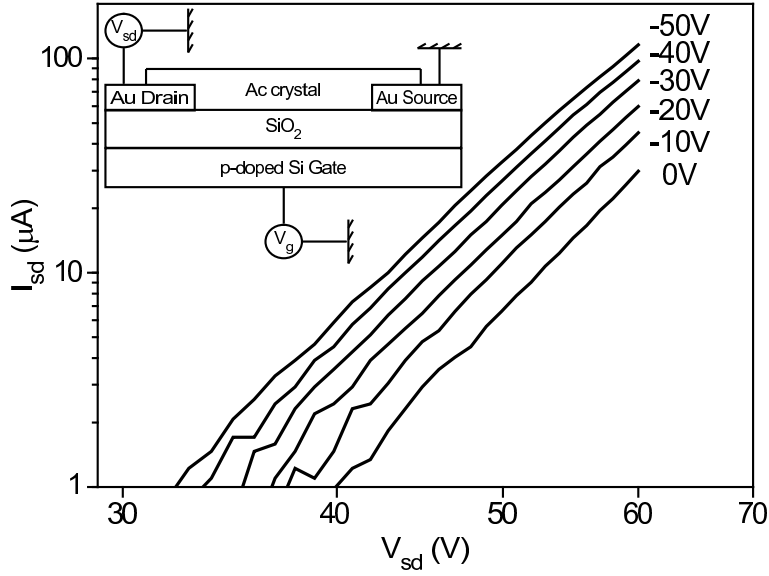


**Figure 5.2:**  $I_{sd}$  as function of  $V_{sd}$  for different  $V_g$  at 217 K, plotted on a log-log scale. The inset shows a drawing of the FET.

Applying a large enough voltage, it is yet possible to pass a current through the crystal if the voltage induces charge injection from the electrodes. It is possible to define an upper bound for the current that can be carried in the SCLC regime. This current corresponds to the maximum amount of charges that can be injected, limited by Coulomb repulsion. In the 1 D case, this current can be expressed as [116]:

$$I = A \frac{9\epsilon_r \epsilon_0 \mu V^2}{8L^3}, \quad (5.2)$$

where  $A$  is the area of the conducting channel, and  $V$  is the applied voltage. This equation, known as the Mott-Gurney law, is directly obtained from the Poisson equation in the 1 D case for a sandwich-type geometry.

However, in a coplanar geometry, a different dependence in gap width is expected, corresponding to a two-dimensional theory [122–124]:

$$I = \frac{2\epsilon_r \epsilon_0 \mu V^2}{\pi L^2}, \quad (5.3)$$

A crossover from one- to two-dimensional SCLC has been measured in pentacene single crystals as a function of the gap width  $L$  and of the thickness  $h$  of the crystal [125] when increasing the ratio  $L/h$ . For low values of the ratio  $L/h$  (typically lower than 15), the current dependence is well described by the Mott-Gurney law (with a dependence in  $L^{-3}$ ) while for high values (typically higher than 250), Geurst's model applies (with a dependence in  $L^{-2}$ ). It is not possible to extrapolate directly the law in case of an Ac crystal from the measurements on pentacene; yet, with a ratio  $L/h < 1$ , one can assume that the Mott-Gurney regime would be a better approximation as an upper bound of the current.

Various models have been put forward to explain the power law observed in Figure 5.2. The most popular ones assume either an exponential (or gaussian) distribution of energy of the trapping states [119, 126] or a field dependence of the mobility [127]. The origin of the mobility field enhancement is related either to the Frenkel-Poole process [128] or to hopping through disorder [129].

In the case of an exponential trap energy distribution, we obtain a voltage dependence of the current as  $I \propto V^{l+1}$ , where  $l = T_c/T$  ( $T_c$  is a characteristic trap distribution parametre and  $T$  is the temperature). From the measured slope at room temperatures, with  $V_G=0$  V, we obtain  $k_B T_c=0.3$  eV, a value similar to the one found by Mark *et al.* [119]. However, at low temperatures, we expect a tunnelling regime, and the law should consequently be temperature independent, as found for a pentacene-based FET [130]. A different law should then be applied.

The upper limit of the current, as defined by Eq. 5.2, is intrinsic. The presence of trap will just decrease the apparent mobility (as not all charges participate to the detected current). In other words, we obtain a lower bound of the intrinsic mobility of the mobile charges from Eq. 5.2:

$$\mu_{min} = \frac{8IL^3}{9A\epsilon_r\epsilon_0V^2}, \quad (5.4)$$

We now look at the temperature dependence of the current. Figure 5.3 shows the temperature dependence of the source-drain current measured for  $V_{sd} = 30$  V and  $V_g = -50$  V in a temperature range between 6 and 280 K. The curve is plotted on a log-log scale. We can see first a sudden increase of the current when we decrease the temperature. After reaching a peak around 100 K, the current then decreases and around 15 K, it reaches a plateau, where the regime is probably only a trapping-detraping mechanism.

We can in principle calculate the lower bound of the mobility (from Eq. 5.4) and plot it as a function of temperature.

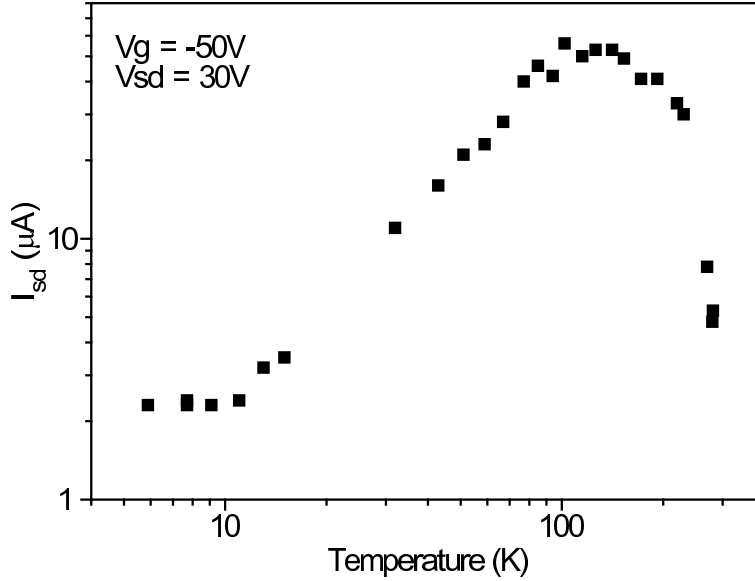


**Figure 5.3:**  $I_{sd}$  versus temperature for  $V_{sd} = 30$  V and  $V_g = -50$  V, plotted on a log-log scale.

We first have an increase of the mobility as the temperature decreases. After a peak, the mobility decreases with temperature decrease. Such a non-monotonous temperature dependence of the mobility is usually a good indication for high-quality crystals in presence of shallow traps [68], with  $\mu \sim T^{-n} \exp(-E_a/k_B T)$  (where  $E_a$  represents an activation energy).

For some samples, we obtained mobility values of  $3.5 \cdot 10^{-3}$   $\text{cm}^2/\text{Vs}$  at 4.2 K, with a maximum around  $10^{-2}$   $\text{cm}^2/\text{Vs}$  at 150 K, for  $V_g = -50$  V, which is of the same order of magnitude as found in a previous study by Aleshin *et al.* [32].

We observed some differences from sample to sample, with variations within one order of magnitude. We always detected a non-monotonous temperature dependence of the mobility, which points to a good quality of the crystals. However, several effects might influence the detected current and therefore the mobility. The most likely one can be due to small differences in the quality of the contact at the crystal-electrode interfaces. Note that, non-isotropic mobility has been reported in the case of rubrene [131]. In our FET, we did not check the orientation of the crystal. The effect of an anisotropy is difficult to estimate. Finally, we have to mention the influence of possible impurities

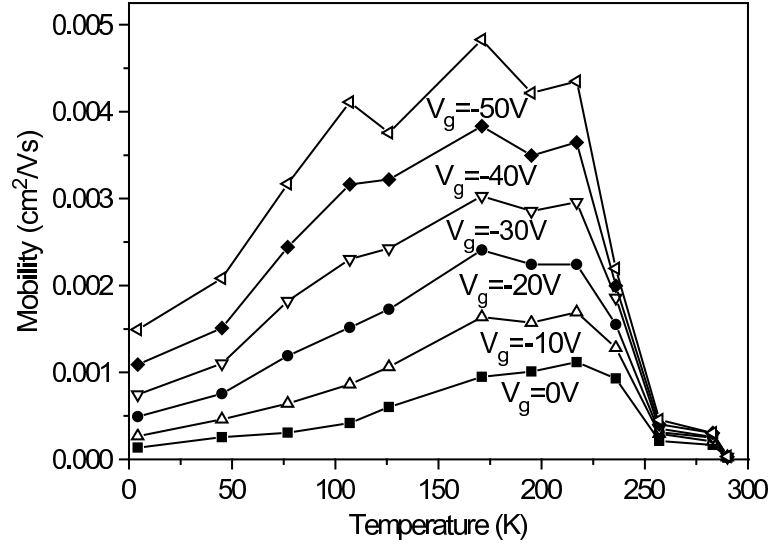


**Figure 5.4:** Lower bound of the mobility plotted as a function of temperature for different gate voltages. We applied a source-drain voltage  $V_{sd} = 60$ .

at the surface of the crystal such as anthraquinone, which might also play a role in these differences. It has been shown that the concentration of such derivatives is larger by one order of magnitude on the surface than in the bulk of the crystals in the case tetracene [132]. These derivatives, with oxygens, usually act as good traps.

Additional measurements are required for a better understanding of the Ac-FET. We propose now to investigate transport phenomenon at the nanometric scale via SMS.

## 5.4 Conclusion

We presented the characteristics of our Ac-based FET for several temperatures ranging from 290 to 4.2 K. The  $I - V$  curves plotted on a log-log scale are linear with an exponent  $n \gg 2$  which is typical for a trap-filling regime. For high temperatures, the current of our FET increases with a decrease of the temperature, indicating the good quality of the crystals. At low temperatures, the current reaches a plateau. This temperature independent process indicates the hopping conduction regime. We calculated a lower bound of the mobility and plotted it as a function of temperature. We obtained values of



$3.5 \cdot 10^{-3} \text{ cm}^2/\text{Vs}$  at 6 K, with a maximum around  $10^{-2} \text{ cm}^2/\text{Vs}$  at 150 K for some samples. A microscopic study of Ac-based FET could bring new insight into the mechanism of charge carrier transport in this system.

## 6 Probing charges

IN order to investigate charge carrier transport phenomena in organic crystals, we now combine single-molecule spectroscopy and microscopy in an organic field-effect transistor configuration. We first study the ‘contact-Stark’ effect, where the crystal is touching the electrodes, but in a configuration without any gate. We then study the Stark shifts induced by the movements of charges inside the crystal by manipulating the two voltages applied to the FET. We apply dc and ac-voltages. The dc-regime shows slow shifts of the molecular lines. In the case of ac-voltages, we observe resonance phenomena for particular frequencies of the modulation.

## 6.1 Charge injection

As a first step in the understanding of the electrical transport phenomena we have studied the ‘contact-Stark’ effect on the DBT molecules in an Ac crystal. This measurement differs from the one in Chapter 4 by the fact that the crystal is now in direct contact with the electrodes. Such a configuration allows charges to get injected into the crystal. For availability reasons, we used Al instead of Au. The sample consisted of a few hundred nm thick layer of Al deposited on a glass surface, with a 60  $\mu\text{m}$  gap in between (see Fig. 6.1).

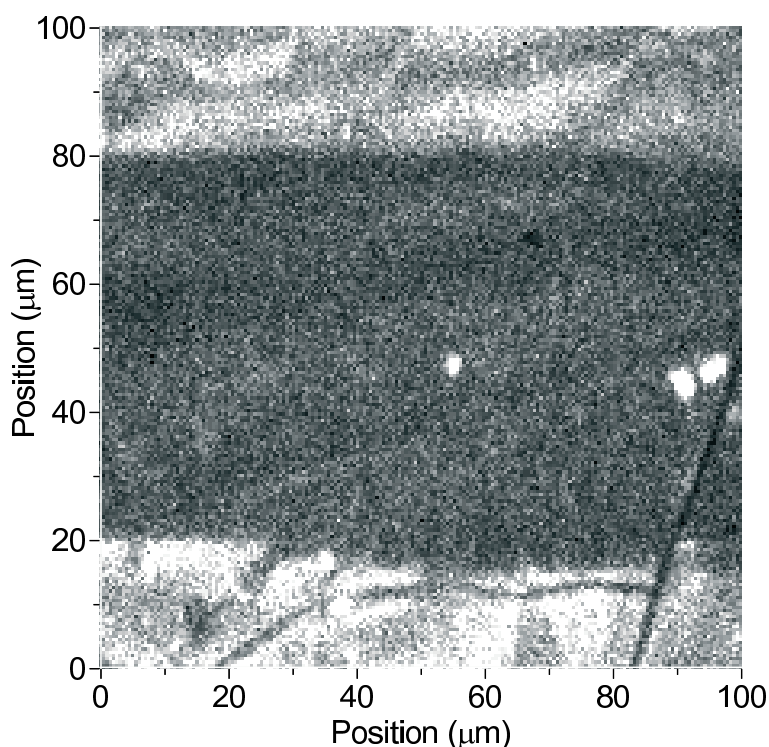


**Figure 6.1:** Image of the slit between Al electrodes. The Al (white part) reflects more light than the glass (dark). We can see some cracks of the crystal and three single molecule spots in between the electrodes.

We then chose molecules close to the centre of the gap so as to avoid boundary effects which create inhomogeneities of the electric field. Figure 6.2 shows such a measurement. We scanned the frequency of the laser over 10 GHz and changed the voltage from -200 to 200 V, with steps of 10 V between each scan.

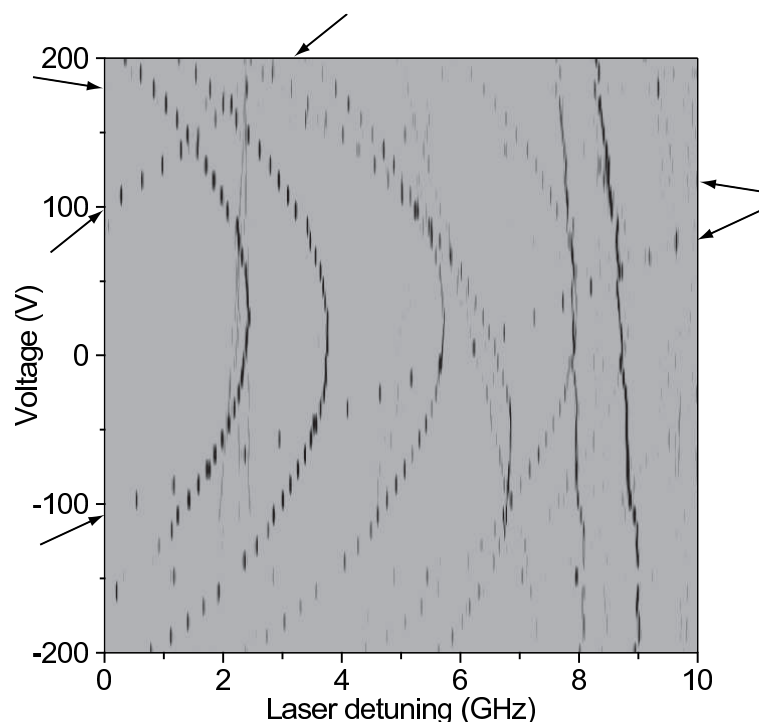


**Figure 6.2:** ‘Contact-Stark’ probing measurement with charge injection. The crystal is placed on the Al electrodes, which leads to charge injection. We can see the presence of large values of the linear Stark coefficients for some molecules (indicated with arrows).

We can see a large variety of Stark shifts from molecule to molecule. Some molecules (along the solid lines) present very large values of their linear Stark component. The distribution of Stark shifts has to be compared to the one presented in Chapter 4 for the red site. It is similar, centred on 0 GHz/(kV/cm), but some molecules exhibit very high values, about 10 times larger [a few GHz/(kV/cm), neglecting the local field correction, this corresponds to a  $\Delta\mu$  of a few D] than what had been recorded for the Stark cell (see Fig. 6.3). These abnormally large values are representative of heterogeneities of the local fields inside the crystal. We explain these heterogeneities by the presence of charges inside the crystal.

Distinct molecules will consequently probe different electric fields, which may locally break the symmetry of the system and, as a consequence, induce strong linear shifts. Examples of such a strong shift can be seen on Fig. 6.2,

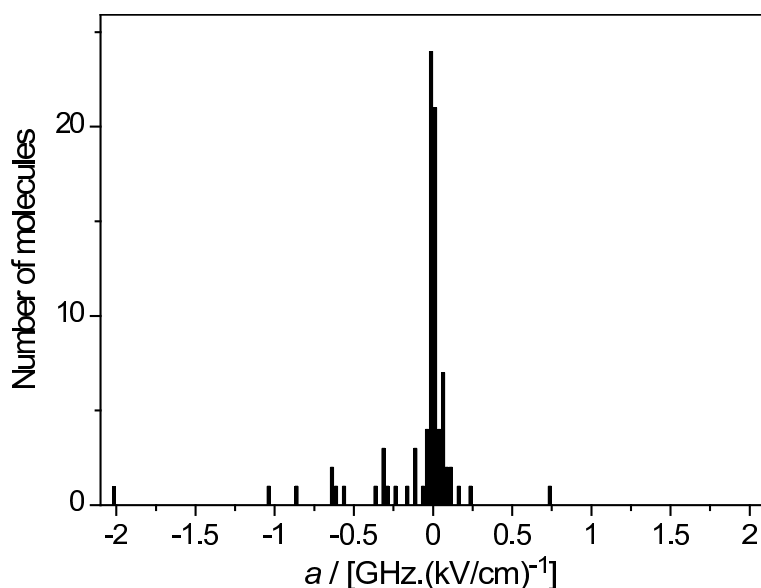


**Figure 6.3:** Distribution of the linear ‘contact-Stark’ coefficient for 70 molecules of the red site. The bin size is 25 MHz/(kV/cm).

indicated arrows. Similar broad distributions have been reported for single N vacancies in diamond [76], where the matrix was directly connected to the electrodes. As a conclusion, we do see effects of charges inside the crystal. However, it is rather difficult to draw any conclusion from such a measurement but the fact that it is possible to inject charges. Repeating similar experiments in a well defined micro-structure, where it is possible to control the charge injection, is a necessary step towards a better understanding of the electric transport phenomena in an organic crystal.

## 6.2 Transistors and single-molecule

We now concentrate on experiments performed in the FET configuration. The main difference between the previous experiment and a FET configuration resides in the transverse gate electrode that allows us to vary the density of charge carriers at the interface between silica and crystal. The samples have been described in Chapter 5, and the optical setup is the same as in Chapter 3. We performed experiments in both dc- and ac-regimes.

### 6.2.1 DC regime

Figure 6.4 shows the drift of the absorption frequencies of several single molecules as a function of time. The gate voltage was set at  $-40$  V during the whole experiment. Before starting the measurement, we set  $V_{sd}$  at  $50$  V during a few minutes. We switched it off when starting the laser scans. After 60 minutes, we set it back to  $50$  V, and finally switched it off again after 30 minutes. We can clearly see two different regimes. One without any source-drain voltage (parts one and three of the Graph 6.4), and one, more noisy, when  $V_{sd}$  had been switched on (the middle part of the graph).

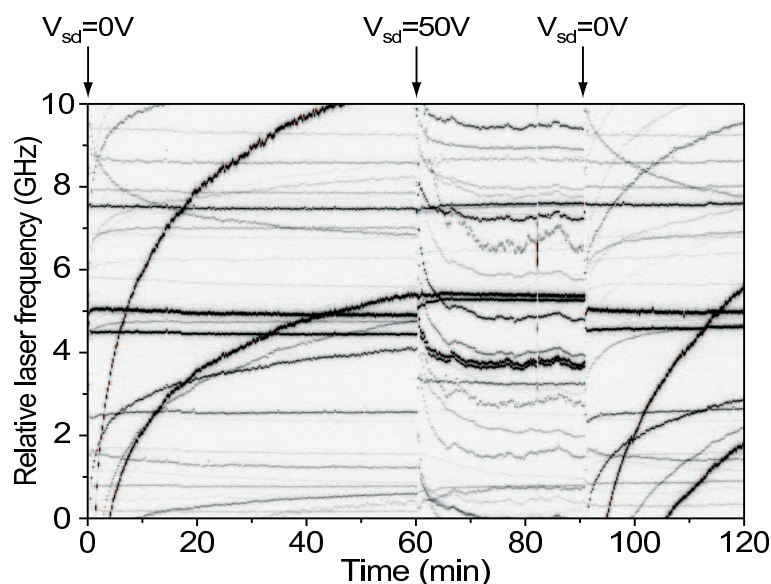


**Figure 6.4:** Single-molecule lines. The laser is scanned over 10 GHz.  $V_g$  is kept at  $-40$  V during the whole experiment.  $V_{sd}$  was set at  $50$  V during 2 minutes before starting the experiment. At  $t = 0$ , the source-drain voltage was switched off. After 1 hour, we set it to  $50$  V and switched it off again after 30 minutes.

The first regime exhibits molecules drifting towards a new spectral position over time scales of the order of a few hours (at least). These very slow drifts cover a range exceeding 10 GHz. In contrast with this, some molecules do not show any shift of their absorption frequencies. Similar effects had been reported in a former single-molecule study on silicon carbide (SiC) [21, 22]. However, in this study, the charges were not present in the matrix (which was a Shpol'skii  $n$ -hexadecane matrix) but onto the surface of SiC, a large

band-gap semiconductor used as insulator. The authors fitted the creeping motion of the molecule lines with biexponential-functions. In order to better understand the mechanism of these relaxations, we replotted the first and the last parts of Fig. 6.4 on a logarithmic time scale and applied a time dilation factor so as to obtain identical figures (see Fig. 6.5). We found a time dilation factor equal to about four.

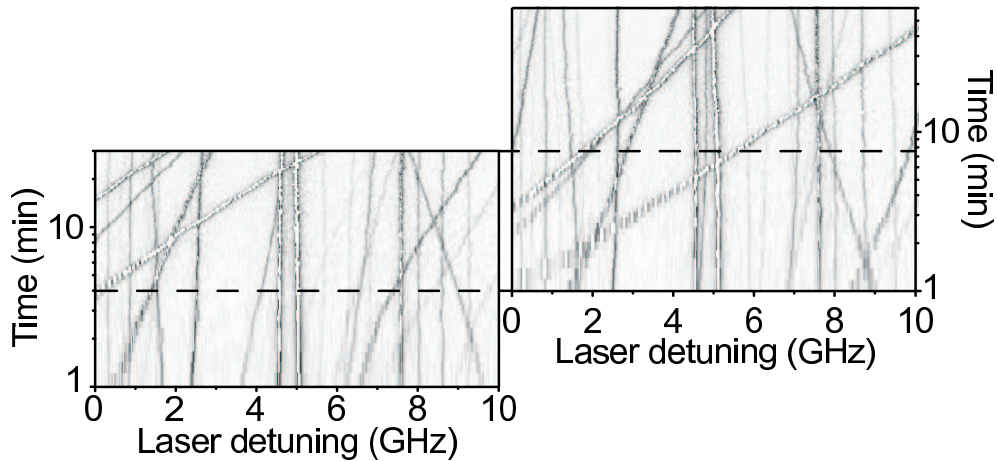


**Figure 6.5:** Comparison between part 1 (on the right) and part 3 (on the left) of Fig. 6.4, replotted on a log-scale. Most of the lines exhibit a linear drift varying as  $\ln(t)$ . After a time dilation by a factor of 4, the parts in between the dashed-lines are nearly identical.

The first striking feature of these semi log-plots is the fair linearity of most of the line shifts. We can notice the presence of a slower part at the beginning of the measurements, though. This slow part might be an artefact due to a lack of time resolution at the beginning of the experiment, which has an important effect at this short time-scale. The main shift is almost perfectly fitted with a log-function, with different slopes from molecule to molecule. These different slopes are probably due to the strength and the orientation of the local fields created by charges in the surrounding of the molecules. For instance, this field can be perpendicular to the dipole moment of a molecule which, consequently, will not show any frequency shift. In other cases, this field can be parallel to the dipole moment, and the absorption frequency of the molecule will shift. Very interesting is the fact that, apart from the time shift, the slopes of the drifts for each particular molecule (on a log-scale) are exactly the same for the first and the last experiments. This feature indicates that we are in presence of

the same relaxation process for all molecules, which is probably macroscopic (in the area of the focal laser spot, i.e.  $\sim 1 \mu\text{m}^2$ ). The time dilation between the two parts under consideration shows that we do not start the experiments from the same initial conditions. Indeed, we waited only a few minutes before the first experiment, while a source-drain voltage at 50 V was applied during 30 minutes before the last one. In Chapter 5, we showed that for the couple of values  $V_{sd}=50$  V and  $V_g=-40$  V, we always detected a significant current. Applying a source-drain voltage acts as a driving force that pushes charge carriers from one electrode towards the other one, changing consequently the distribution of trapped charges.

We showed in Section 6.1 that in the configuration of the ‘contact-Stark’ measurements, charge injection results in a breaking of the centro-symmetry and, as a consequence, in the presence of very high values of the linear component of the Stark coefficients. We can then write the spectral shift of the absorption frequency of the molecules as proportional to the local electric field  $E(t)$ , which is proportional to the amount of charges  $Q(t)$  as a function of time:

$$\Delta\nu_i(t) = \gamma_i E(t), \quad (6.1)$$

where  $\Delta\nu_i(t)$  represents the spectral position of the absorption line of the molecule  $i$  as a function of time  $t$ , and  $\gamma_i$  is a constant that takes into account the characteristics of molecule  $i$ .

### Model with a single jump

We present now a first phenomenological model, based on the assumption that each charge will tunnel in a single jump. Let us assume that we have trapped charges inside the crystal or in the  $\text{SiO}_2$ , close to one electrode. We also assume that the volume density  $\rho$  depends only on one coordinate, the depth  $z$ . We can write the electric field  $E(t)$  as  $E(t) \sim \sigma(t)/\epsilon_0\epsilon_r$ , where  $\sigma(t)$  is the surface density,  $\epsilon_0$  is the permittivity of free space, and  $\epsilon_r$  is the dielectric constant of Ac. We have  $\sigma(t) = \int_0^\infty \rho(z, t) dz$  (where  $z$  is the distance between the charge and the electrode). At  $t = 0$ , we assume  $\rho(z) = 0$ . We can define a decay-function as the probability to have tunnelling events of charges through the electrode as a function of time, which will induce changes in the volume density as:  $\rho(t) \propto \exp(-\lambda(z)t)$  (the probability to decay  $\lambda(z) = \lambda_0 \exp(-z/z_0)$ , depends on the distance between the charge and the electrode). We can then write:



$$\sigma = \int_0^{\infty} \exp(-\lambda_0 t \exp(\frac{-z}{z_0})) dz. \quad (6.2)$$

If we change the integration variable to  $G$  as  $G = \exp(-z/z_0)$ , we can rewrite the equation as  $\sigma \sim z_0 \int_0^1 \exp(-\lambda_0 G t) \frac{dG}{G}$ . We want to consider the short time-scale and the long time-scale. We obtain the conditions  $\exp(-\lambda_0 G t) = 1$  for  $t < 1/\lambda_0 G$  and  $\exp(-\lambda_0 G t) = 0$  for  $t > 1/\lambda_0 G$ , which give the condition  $G < 1/\lambda_0 t$ . If we then define a cut-off, we have:

$$\sigma = \sigma_0 - \beta \ln(\lambda_0 t). \quad (6.3)$$

As a consequence, one could describe the time evolution of  $E$  as:  $E(t) \propto E(0) + \beta \ln(t)$ , where  $E(0)$  depends on the initial amount of charges at the beginning of the experiment, and  $\beta$  is a constant. Applying a source-drain voltage will change the distribution of charges. When we switch the source-drain voltage off, the charges will relax slowly and get trapped again, which explains the slow observed drifts:

$$\nu(t) = \nu_0 + \beta \ln(t). \quad (6.4)$$

The initial conditions (i.e. the amount of charges already trapped when we start an experiment) will then depend on how long we applied the driving force. If we consider the first and the second experiments, we have different amounts of charges at the beginning of the two experiments. This difference induces a variation of the position of the absorption frequency of a molecule between experiment 1 and experiment 2 such as  $\Delta\nu_{exp1}(t) = \Delta\nu_{exp2}(\alpha t)$ , which is consistent with the time dilation previously mentioned between the first and the last experiments.

We performed similar experiments, varying the source-drain voltage with  $V_g = -50$  V (see Figure 6.6). Each measurement lasted 10 minutes. We plotted the spectral position of the molecule line as a function of the log of time. We obtained straight lines. We then fitted the measured spectral shifts with Eq. 6.4 and plotted the parameter  $\beta$  as a function of the previously applied source-drain voltage (see inset in Fig 6.6). We find the parameter  $\beta$  proportional to the previously applied field, which seems to indicate no interactions between injected charges.

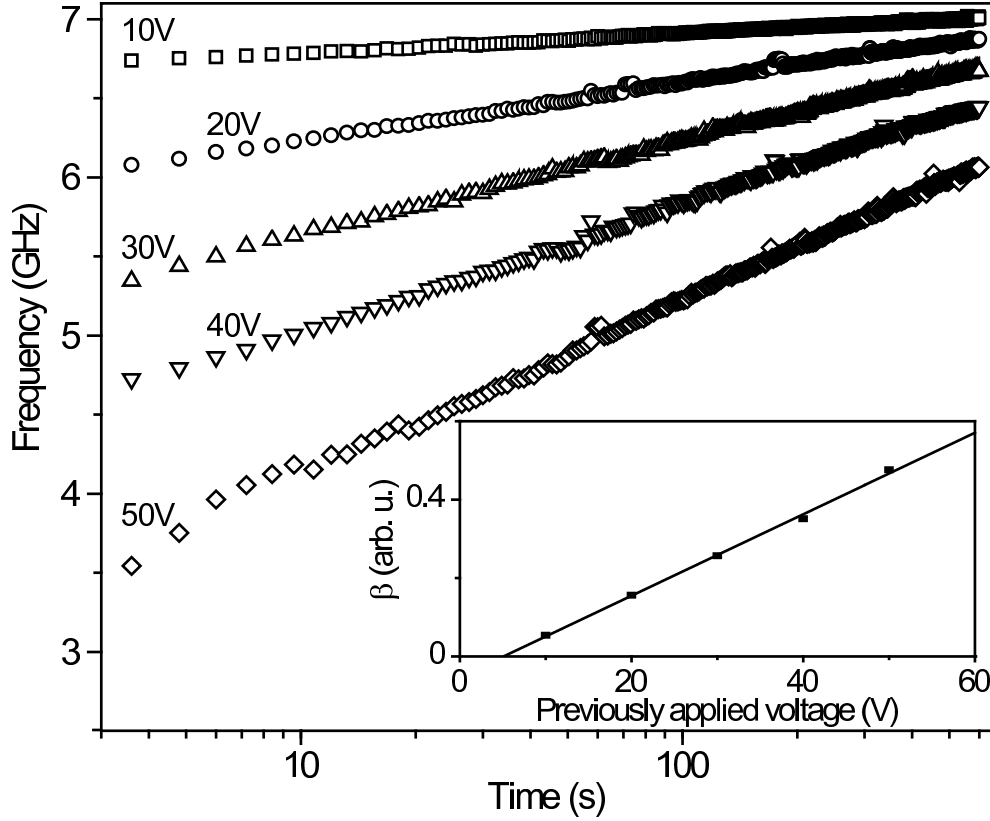


**Figure 6.6:** Spectral shift of a molecule line as a function of the log of time. We previously applied different source-drain voltages for 10 minutes and measured the spectral position of the molecule during 10 minutes. We applied a gate voltage  $V_g = -50$  V during the whole experiment. We fitted the shift with Eq. 6.4. The inset shows the plot of  $\beta$  as a function of the previously applied  $V_{sd}$  (from 10 to 50 V). The solid line is a guide for the eye.

The presented first phenomenological model assumed that the charges get trapped or detrapped in only one jump. A more realistic model should take into account the possibilities to have several jumps, such as the Scher and Montroll model [133–136], presented in the following part.

### The continuous-time random walk

The shift of the absorption frequency of the molecule lines while applying a gate voltage can be related to the shift of the threshold voltage under a gate

bias applied over an extended period of time. In a previous study, it has been shown that this shift is directly connected to a decrease of the measured current in the device [137]. This decrease of the current is a well-known phenomenon in disordered solids and diverse attempts to give a physical explanation have been conducted. Among them, the continuous-time random-walk (CTRW) theory, developed by Scher and Montroll [136], gives the following dependence of the current as a function of time:

$$\begin{aligned} I &\propto t^{-(1-\alpha)} & \text{for } t < t_\tau, \\ I &\propto t^{-(1+\alpha)} & \text{for } t > t_\tau, \end{aligned} \tag{6.5}$$

where the parameter  $\alpha$  ( $0 < \alpha < 1$ ) characterises the dispersion and  $t_\tau$  is the transit time. This model has been successful in describing experimental data in the case of dispersive carrier transport in amorphous solids. In the Scher-Montroll model, the transport is represented as a chain of hopping events, based on a distribution of waiting times ( $\psi(t) \sim t^{-(1+\alpha)}$ ). In that case, all of the essential features of dispersive transport can be described. Small variations of the hopping distance will then introduce a broad distribution in hopping times. Similarly, in the case of multiple trapping transport, broad release time distributions can be obtained for small variations in the trap depth. It has also been shown that hopping between sites which are exponentially distributed in energy also gives rise to dispersive transport [138]. The main difference between these explanations resides in the fact that, in some cases, the dispersion coefficient  $\alpha$  will be strongly temperature dependent (for models based on activated transport with energy distribution of the traps) or independent (in case of tunnelling with distances distribution). At cryogenic temperatures, we expect to have rather a temperature independent process.

Yet, we cannot directly apply the models on the transient current. Indeed, the CTRW model, as it is formulated, describes pulse measurements, where the charges are injected at once at the beginning of the experiment. However, in the case of our measurements, we inject charges continuously. Let us consider the Scher and Montroll model in the case where  $t > t_\tau$  (see Eq. 6.5). It corresponds to the situation where the injected charges start to reach one electrode. We have to calculate the number of charges  $Q(t) \propto \int_0^t I(t')dt'$ . We then obtain:  $Q(t) \propto t^{-\alpha}$ .

According to these considerations, we measured the shift of a molecule line for different source-drain voltages, while applying a gate voltage  $V_g = -50$  V. We then fitted the curves with a power law of time (see Fig. 6.7):

$$\nu(t) = \nu(0) + B(t - t_0)^{-\alpha}, \quad (6.6)$$

where  $\nu(0)$  is the initial absorption frequency of the molecule and  $t_0$  is the initial time of the experiment. We found a dispersion parameter  $\alpha$  ranging from 0.3 to 0.5 for different molecules. It has to be mentioned that it is not easy to obtain accurate values when fitting a power law with many fit parameter ( $\nu_0$ ,  $t_0$ ,  $B$  and  $\alpha$ ). We measured the temperature dependence and found no significant dependence for the parameter  $\alpha$ , which points to a distribution of the distances of the traps rather than to an energy distribution. We did not find any dependence of the parameter when changing the applied voltage. This seems to indicate that we do not reach a limitation due to Coulomb repulsion. However, the parameter  $B$  shows some saturation with an increase of the voltage (see inset in Fig. 6.7).

We saw that the applied voltage has a strong influence on the dynamics of the shift of the spectral position of the molecule line. We expect a dependence on the time duration of the applied voltages. We measured the spectral position of a molecule after applying a source-drain voltage of 50 V for different durations, ranging from 1 s to 15 minutes ( $V_g$  was kept at -50 V). We then fitted the curves with Eq. 6.6 and plotted the parameter  $B$  as a function of time (see Fig. 6.8).

We see a variation of the parameter  $B$ , which seems to reach saturation for long durations of the applied voltage. We plan, in the future, to measure this curve for shorter durations in order to be able to compare it with pulse experiments.

As shown in Figure 6.4, the shifts of the molecule lines depend strongly on the history. Indeed, the relaxation of charges is so slow a process that we do not reach the equilibrium of the system when doing a second experiment. As a consequence, it is rather difficult to perform a second experiment with the same initial conditions, each experiment being a non-negligible perturbation of the system.

One of the remaining questions is to know where exactly the charges get trapped. It is not obvious whether they are inside the crystal or rather in the SiO<sub>2</sub> layer. However, measurements for molecules on top of electrodes seems to indicate that these molecules are less prone to slow relaxations, possibly pointing to the presence of trapped charges inside the SiO<sub>2</sub> layer. Additionally, we did not measure any blinking of the molecules, while we would expect that some of them would act as traps for the moving charges, thereby losing their fluorescence. A maybe more convincing argument comes from our previous

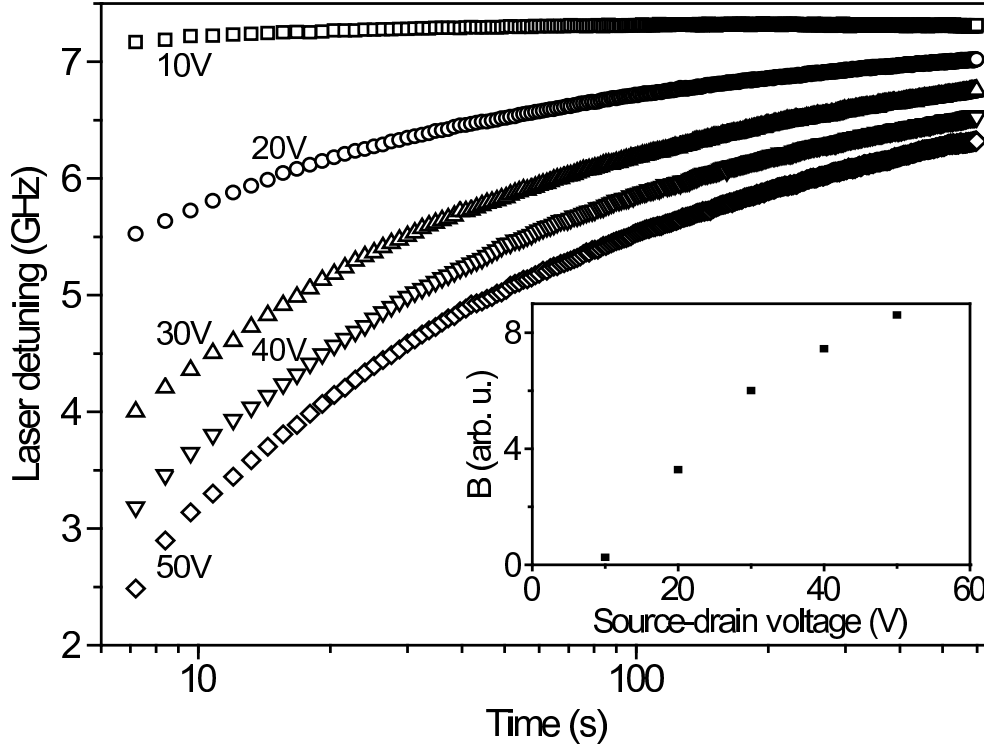


**Figure 6.7:** Log-log plot of the spectral shift of a molecule line as a function of time. We applied different source-drain voltages (from 10 to 50 V) and measured the spectral position of the molecule during 10 minutes. We applied a gate voltage  $V_g = -50$  V during the whole experiment. We fitted the shift with Eq. 6.6. The inset shows the plot of  $B$  as a function of applied  $V_{sd}$ .

measurements on the contact-Stark effect, which had been performed without  $\text{SiO}_2$  layer and where no drift had been detected. As a consequence, we think that the build-up of charges probably takes place in the  $\text{SiO}_2$  layer.

A last feature that can be seen in Figure 6.4 is the strong correlation between sudden jumps of the spectral position of the absorption lines from molecule to molecule at a shorter time-scale. We think that it shows correlated movements of group of charges. This feature is particularly pronounced when applying a source-drain voltage (middle part of Figure 6.4). Some single-molecule time-traces are almost parallel amidst rather chaotic shifts of the lines. In this regime, we expect hopping conduction. The charges have a certain probability to jump to another defect of the crystal. But each movement induces a reor-

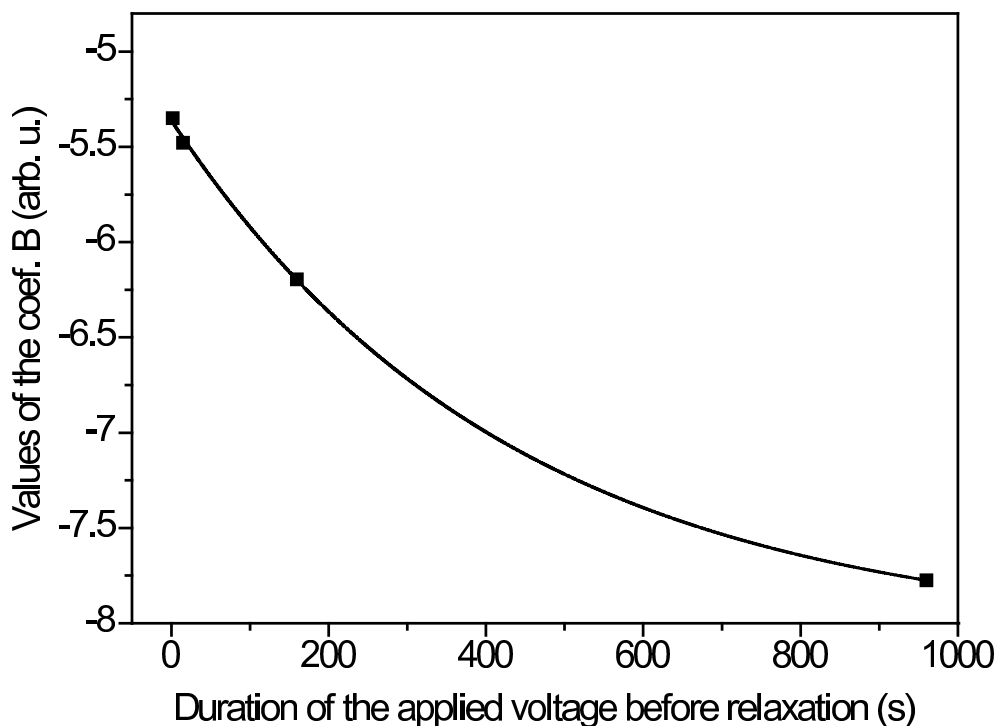


**Figure 6.8:** Plot of the parameter  $B$  as a function of the duration of the previously applied source-drain voltage. The solid line is a guide for the eye.

organisation of the charge distribution in the surroundings. Consequently, this regime shows more complex features than the one without any source-drain voltage. This complex feature is not always visible, which can be understood if the molecule is not close enough to the path of charges. This is an evidence of the heterogeneity of the current inside the crystal.

In order to understand the phenomena better, we shall measure the exact position of different molecules and, by means of a triangulation [115], we could determine precisely the position of these defects and make a map of their distribution in the crystal. Studying then the same phenomena at very low voltage might allow us to get new insight into charge carrier transport in organic crystal, and maybe to trace the percolation paths of charges if we correlate them with the detected source-drain current.

### 6.2.2 AC regime

In an ac-regime, we modulate the voltage as a sinusoidal function. This modulation splits the Lorentzian line of the molecules to a "cat's ears"-like shape (see Fig. 6.9). We can define a splitting of the Lorentzian as the distance between the two maxima of the new curve [139].

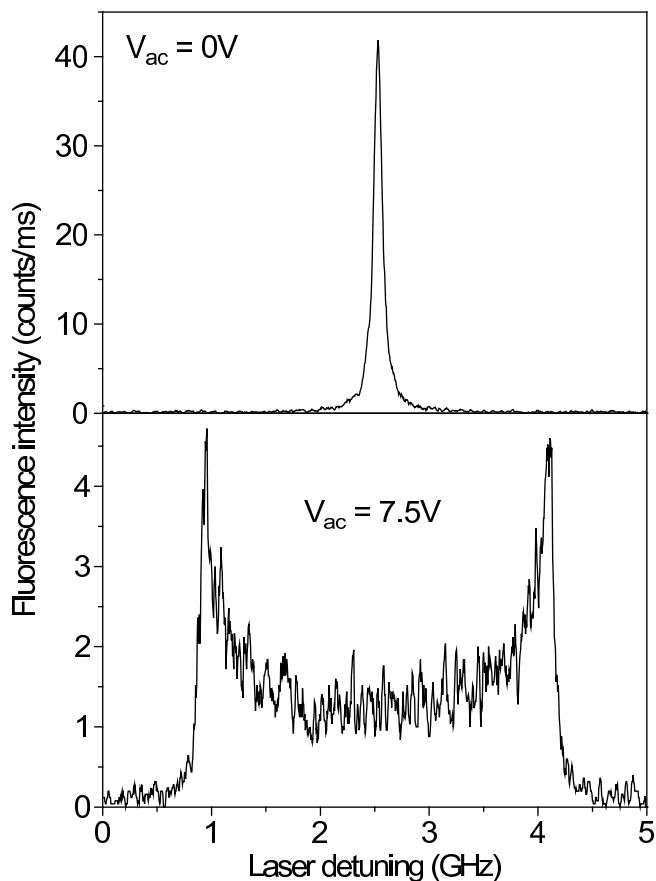


**Figure 6.9:** At zero voltage, the absorption of a single molecule has a Lorentzian shape. Under a sinusoidal modulation of the voltage (with a frequency of 10 kHz), we observe a splitting of the line to a "cat's ears" shape, result of the integration over time of the modulation of the Stark shift with the Lorentzian.

In principle, this splitting depends only on the applied voltage (at low enough frequencies, when the modulation frequency is much smaller than the linewidth of the molecule [140]). Figure 6.10 shows the voltage dependence

of the splitting of the Lorentzian from 0 to 10 V, with an excitation modulated at a frequency of 10 kHz. We have a linear dependence in the explored range (except at the very beginning, when the splitting is comparable to the linewidth of the molecule).

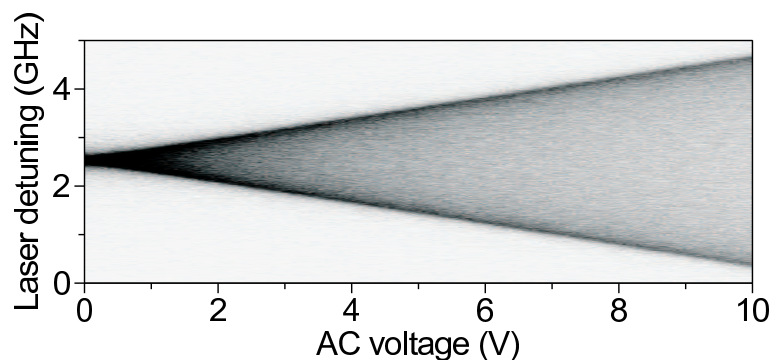


**Figure 6.10:** Splitting from Lorentzian to "cat's ears" shape as a function of the voltage at a frequency of 10 kHz.

### Resonances

The ac-signal is characterised by a voltage and by a frequency (we always apply a sine wave as a modulation). We already showed the voltage dependence of the splitting of the Lorentzian. Although we do not expect any change with frequency, the ac-field allows us to vary this additional parameter as well. Surprisingly, we observed abnormally large splittings for specific frequencies. These resonances appear for typical frequencies in the range from a few tens to a few hundreds of kHz. Similar effects had been already observed [19,20] with TBT molecules in *n*-hexadecane on an ITGO substrate, which is a completely different system. Figure 6.11 shows a typical example of resonances for a frequency ranging from 1 kHz to 1 MHz.

The typical spectrum of Figure 6.11 shows several resonances at 207, 415, 755, 813 and 909 kHz. We attributed the most intense resonance at  $\omega_0 = 415$  kHz as the fundamental frequency of an oscillator. The resonance at 207 kHz is equal to  $\omega_0/2$  and we probably have  $2\omega_0 = 830 \sim 813$  kHz. We cannot easily link the two other resonances to  $\omega_0$ . In most of the cases, the harmonics had a frequency a bit below the one expected, which probably indicates the non-linearity of the phenomenon. Moreover, we did not always find all harmonics (for instance, the third harmonic was often absent in the



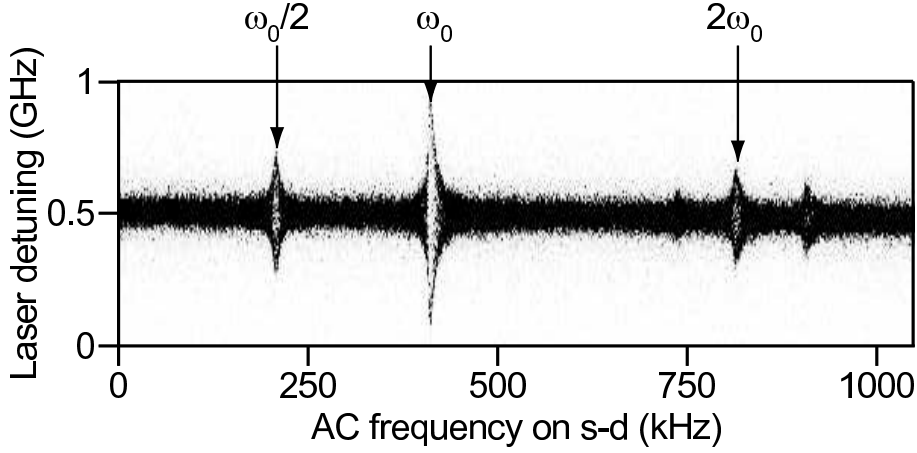


**Figure 6.11:** Scan over the ac-frequencies for a given voltage. For specific frequencies, we can see a sudden increase of the splitting, as resonances. The positions of the main frequencies (see text) are indicated with arrows.

spectrum). We can define a quality factor as  $q = \omega/\Gamma$ , where  $\omega$  is the frequency of the resonance and  $\Gamma$  its FWHM. For the previous resonances, we have respectively 20, 34, 125, 101, and 90. It has to be mentioned that in some cases, it was difficult to analyse the spectra because of the presence of fine structures in some range of the spectra. Figure 6.12 shows a typical example of this feature in a frequency range from 33 to 53 kHz.

Looking at several molecules over large areas revealed that all molecules in a few hundreds of  $\mu\text{m}^2$  exhibit similar spectra with resonances at the same frequencies. This result is very different from the one reported previously [19, 20] on ITGO films, where each molecule in the laser spot had different resonance frequencies (with domains of about  $100 \text{ nm}^2$ ). The observed resonance frequencies are not affected by the intensity nor by the polarisation of the laser.

Figure 6.13 presents the amplitude of a resonance as a function of the ac-voltage. For high enough voltage, the variation of the amplitude with the ac-field looks as  $A = a(V - V_0)$ . We observed indications of saturation when applying higher voltages. More remarkable is the presence of an apparent threshold (voltage  $V_0$ ) below which it is not possible to reach the resonant regime. We did not observe any significant broadening of the resonances as a function of the applied ac-voltage.

We studied the temperature dependence of the amplitude (see Fig. 6.14) and the width of the resonances. The dependence of the phenomenon on

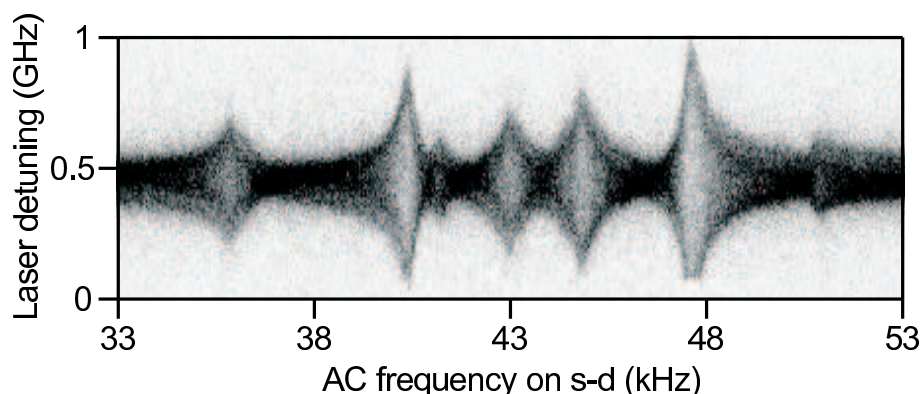


**Figure 6.12:** Fine structure of resonances in the range from 33 to 53 kHz. We can see resonances with frequencies of: 35.8, 40.3, 41.2, 43, 44.8, 47.5, and 50.8 kHz. The respective quality factors are: 44, 89, 205, 85, 99, 79, and 112.

temperature is very steep and we could not detect any resonances after passing the  $\lambda$ -transition superfluid-liquid He. The results could be fitted with a power law of  $T$ . We found  $A \propto T^{-\gamma}$  for the amplitude  $A$ , with an exponent  $\gamma$  ranging between 6 to 10. In the case of the width, the same law was found, but with a smaller exponent, close to half of the one for the amplitude (from 3 to 5). However, because of the very small range of temperatures explored (from 1.4 to 2.2 K), large errors in the fits are possible and fits by exponential laws are equally good.

We looked at the influence of a gate-voltage over the resonances. A variation of the gate voltage changes the amplitude of the resonance, but does not affect its frequency.

In order to prevent contact of the crystal with the environment and to isolate the probe molecules from superfluid He, we covered the sample with a PMMA layer with a thickness of several hundreds  $\mu\text{m}$ . In this new configuration, we observed the same behaviour of the sample as without any layer of polymer, with resonating phenomena occurring in the same range of frequencies.

We also performed the experiment with DBT molecules in a Shpol'skii matrix (*n*-dodecane). The choice of this material was motivated by its very poor conducting properties. No resonance was detected under this configuration.

Finally, we prepared a polycrystalline sample of Ac with DBT by spin-coating [141, 142]. In case of spin-coating sample, we did not obtain a single crystal but rather a layer of micro-crystals. The main differences expected from the two samples are the dimensions of the crystals. We then performed

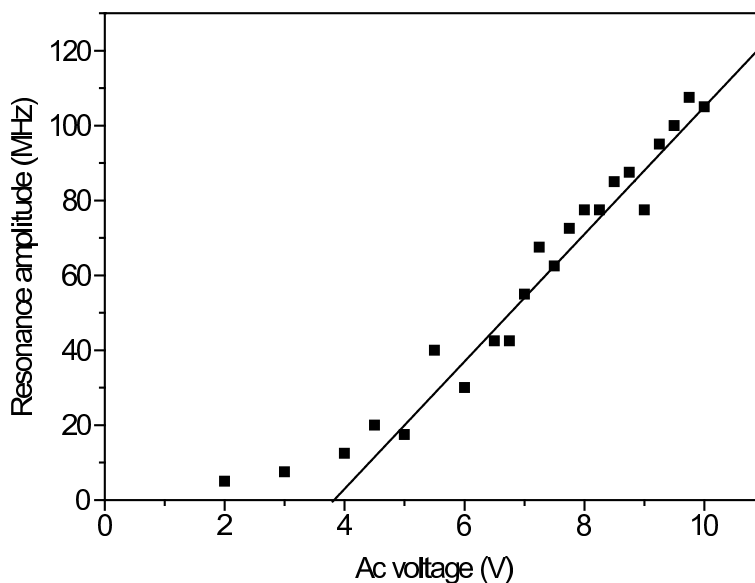


**Figure 6.13:** Amplitude of a resonance as a function of the voltage. We can see a linear part, and the presence of a threshold.

the same experiment. Resonances were observed in the typical frequency range of 1 to 2.5 MHz. No resonances below 1 MHz have been observed.

### Discussion

We now consider several possible mechanisms causing the resonance phenomenon.

(i) It is possible to inject charges into liquid He and create so-called He-bubbles [143]. These bubbles, having a charge, might react to an ac-field and start to oscillate and, eventually, lead to resonating phenomena.

(ii) Two other mechanisms had been proposed by Caruge *et al.* [19, 20, 139] which involve charges in semiconductor materials. For instance, resonating phenomena at low frequencies over large areas (a few mm) have been observed in doped semiconductors at low temperatures, involving current filaments [144]. Another explanation presented by Caruge *et al.* involves recharging waves [145, 146]. Recharging waves arise from the exchange of charges between the free carrier gas and impurities. Because the trapping rates can be low (times longer than ms), these waves can travel at very low velocities, and could lead to localised resonances.

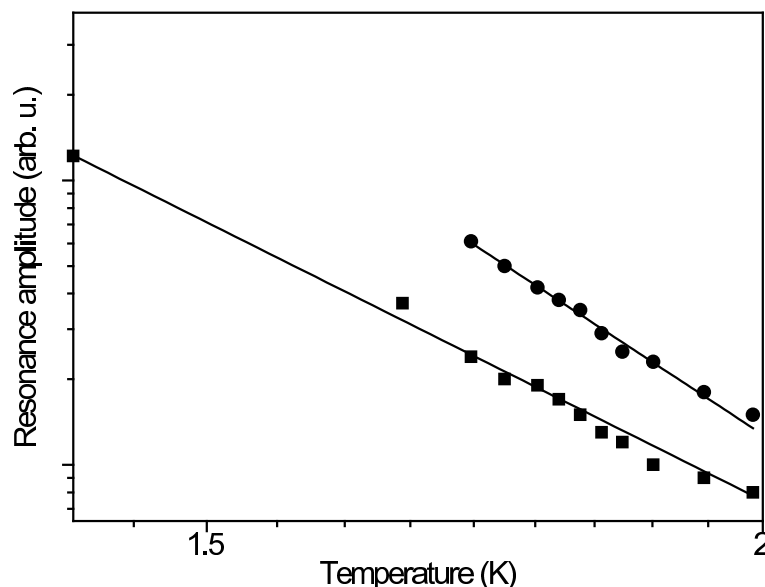


**Figure 6.14:** Temperature dependence of the amplitude of a resonance. The temperatures vary from 1.4 to 2 K. The solid lines show a power-law fit  $A \propto T^{-\gamma}$ , with  $\gamma$  equal 8 and 10.

(iii) Finally, we can also consider global or local vibrations of the lattice. The ac-field can create a driving force on charges inside the crystal. In the case of trapped charges, the latter cannot move. Yet, these charges can transmit the force to the lattice, which can start to vibrate. If the ac-frequency is close to the natural frequency of the crystal or of some local mode of the crystal, the latter will be prone to resonate.

The fact that the phenomenon disappears around the  $\lambda$ -point might indicate the predominant role of He. Considering the possibility to inject charges in superfluid He, which leads to the formation of He-bubbles, one could imagine that these bubbles can form at the interface He/Ac. In that case, we would get a possible resonating charged system. We performed temperature cycles, crossing the  $\lambda$ -point several times and observed the same frequencies of resonances before and after temperature cycles. It seems unlikely to have a bubble formed at a certain position and to have this bubble being formed exactly with the same characteristics after the temperature cycle. Additionally, we covered the sample with a few hundreds  $\mu\text{m}$  thick layer of PMMA. The large thickness should completely isolate the crystal to the possible bubbles. At least, the detected effect (amplitude at resonance) should be much lower. However, we

observed the same qualitative behaviour of the sample as without the PMMA layer. We think that this experiment rules out the possible involvement of He.

The two next hypotheses are similar in the sense that they both consider a mechanism involving only charges in the semiconductor. However, we know that the density of charges is very sensitive to any gate-bias. One would expect that applying a gate-voltage will dramatically change the charge density and that the resonances will probably shift in frequency or disappear. The frequencies being unaffected by the gate-bias, we consider these two hypothesis as unlikely.

However, ruling out the last two hypotheses which involved only charges, does not mean that charges do not play a role. We tried to measure the phenomenon in a poor conducting matrix, as *n*-dodecane and did not observe any resonances. This result points to the involvement of charges in the process. Another way to see the problem is not to consider charges as the vibrating system (detected by the probe molecules), but as anchorage points which allow us to induce vibrations of the lattice or of quasi-local-modes which are going to be detected by the probe molecules. We can picture a possible mechanical vibration of the whole crystal, or, as we detected different zones of a few hundreds of  $\mu\text{m}^2$  with the same resonance frequencies, of a large part of the crystal. Consistently, we observed higher frequencies in spin-coated Ac which might indicate either a smaller volume of the vibrating system, in case of micro-crystals, or a smaller spread of local modes through the matrix. Quasi-local-modes occur normally in amorphous materials (glass [147], polymer, random crystalline systems [148]) characterised by disorder [149]. The anomalous enhanced vibrational density of states in the low-frequency spectral range over that predicted by Debye is called the boson peak. The physical origin of this peak is still unclear. Yet, the boson peak is in the spectral range of THz. The low frequency resonances which we detected might be a far low frequency tail of this peak. So far, this last hypothesis is the only one which is not contradicted by experimental facts.

### 6.3 Conclusion

We studied charge-transport phenomena in an Ac crystal at cryogenic temperatures under dc and ac-voltages. We first showed that it is possible to inject charges into Ac, and that we can detect them via the presence of abnormally large linear shifts of the absorption frequencies of some probe DBT molecules. We then conducted similar experiments with OFET under dc-regime. This regime exhibits large 'creeping' of the absorption frequencies of the molecules

when we inject charges via the gate bias. Following the CTRW model, we fitted the shifts of the molecule lines with a power law and found exponents ranging from 0.3 to 0.5. The exponents are temperature and voltage independent, which tends to indicate a distance distribution of traps rather than an energy distribution. The fitted parameter  $\beta$  or  $B$  is proportional to the previously applied  $V_{sd}$  when we switch off the source-drain voltage, but seems to undergo saturation when applying a  $V_{sd}$ . Clear correlation between several time-traces of different molecules are present in the spectra, when applying a source-drain voltage, pointing to correlated changes of the local electric fields. Additional measurements are required, correlating the events with the precise position of the molecules involved, for different source-drain bias.

We have also studied the ac-regime. Surprisingly, resonance phenomena appear for typical frequencies ranging from a few tens to a few hundred of kHz. We studied several aspects of these resonances, changing the applied voltage, the temperature, the environment and the matrix. All these results seem to point to the presence of quasi-local-modes over a range of a few hundred of  $\mu\text{m}^2$  in Ac (and a few tens of nm in *n*-hexadecane on ITGO), driven by the charges which are trapped inside the Ac crystal and react to the ac-field.



## 7 Conclusions and perspectives

Besides their numerous applications in electronic devices, organic materials present a large interest for fundamental investigations of the electrical transport mechanisms, as many of these processes are still under discussion. Particularly, the charge injection and charge carrier transport processes in poorly conducting materials are still disputable. Some experimental results point to different possible interpretations and, in some cases, the experimental procedures do not allow one to really distinguish between different theoretical models. In this context, using non-conventional tools and methods might bring new insight. We proposed to study these phenomena by means of single-molecule spectroscopy, which is expected to give access to local information at the nanometer scale.

In Chapter 2 of this thesis, we studied the photophysics of single terrylene molecules in an anthracene crystal. We showed that the intersystem-crossing can be dramatically enhanced by an intermolecular mechanism when the triplet of the host is in between the singlet and the triplet of the guest. Shifting the energy levels of the chromophore with respect to the matrix, we proposed another guest-host system, which consisted of dibenzoterrylene molecules in an anthracene crystal. We studied the photophysics of these chromophores (Chapter 3) as well as their insertion into the Ac crystal (Chapter 4). This system is very favourable for single-molecule spectroscopy at cryogenic temperatures, with intense and narrow zero-phonon lines and a very low intersystem-crossing yield. Two dominant insertion sites were found and attributed to the replacement of three molecules of anthracene by one of dibenzoterrylene, almost oriented along the 'b'-axis of the crystal. Finally, we investigated the Stark effect, which turned out to have a strong quadratic component.

We then studied the anthracene field-effect transistor. The obtained  $I - V$  characterisations follow a power law, which is typical for trap-filling in the space-charge limited conduction regime. We extrapolated a value of the mobility and plotted it as a function of temperature (ranging from 4.2 to 290 K). Below 10 K, the mobility reaches a temperature independent plateau, indicating a tunnelling regime. Compared to other systems, the values of the mobility obtained for the anthracene field-effect transistor at low temperatures are reasonable and show a substantial amount of mobile charges inside the crystal,



indicating the possibility to investigate the charge transport phenomena in this system.

In Chapter 6, we investigated the response of single molecules in a field-effect transistor under different biases. We performed experiments in both dc- and ac-regimes. In the dc-regime, we observed drifts of the absorption frequencies of the probe molecules on extended durations. We believe that the accumulation of charges is in the SiO<sub>2</sub> layer. Using the continuous-time random walk model, developed by Scher and Montroll for dispersive current in disordered materials, we fitted these shifts with a power law of time. We found a dispersion parameter ranging from 0.3 to 0.5, apparently temperature and voltage independent. In the ac-regime, we observed resonances for specific frequencies. These resonances are temperature- or pressure-dependent, and the damping increases very steeply with these parameters. We performed a series of experiments, changing the matrix of the system (in *n*-dodecane, in spin-coated anthracene), and varying the two voltages of the field-effect transistor (source-drain and gate). A consistent explanation seems to involve charges trapped inside the matrix, which allow one to excite over large areas (several  $\mu\text{m}^2$  in the case of a single crystal of anthracene) quasi-local modes of the crystal.

We would like now to discuss future experiments that have to be performed and what we expect to learn from those. Let us first consider the dc-regime. We have two distinct phenomena. About the drifts of the frequency of the molecule lines, we would have to do the same experiments for many molecules so as to obtain enough statistics in order to access to macroscopic values via the distributions of the different parameters. This will allow us to compare the experiments with previous studies in a more reliable way. Additionally, we would like to investigate the heterogeneities of the local field in the crystal. Measuring the drifts at different places in the sample will give us a clearer idea of these inhomogeneities and might eventually show the sizes of the conduction paths and their distribution. The performed experiments showed a dependence in voltage and in pulse duration. However, we saw that the data were strongly connected to previous perturbations of the system (history dependence). Hence, repeating these measurements for lower voltages and various pulse durations will give us a more quantitative picture of these dependences. Moreover, it will tell us whether the voltage dependence exhibit a threshold or not. The second particularity of these measurements concerns the additional noisy dynamics in the drifts when one applies a source-drain voltage. In that case, we could first subtract the general drift and then investigate the correlation of the spectral position of the molecular lines. This will probably give

---

us specific times which, we believe, are directly connected to jumps of charges. We will have to correlate these dynamics for different molecules as well. Applying different gate and source-drain biases will allow us to investigate the voltage dependence of these phenomena.

Concerning the ac-regime and the resonances, we would like first to perform the same experiments on a glass substrate, in order to see how critically the phenomenon depends on the presence of a gate electrode and of the SiO<sub>2</sub> layer. We presented the voltage dependence of the amplitude of the resonance. But it is not clear yet whether this dependence is the same for all components of the spectrum or not. We will have to measure these thresholds for different frequencies. Setting the wavelength at a specific spectral position and studying correlation and Fourier transform of the response of the molecule might show us the different frequency components present when we excite the system at a given frequency. Indeed, preliminary results seem to indicate that (considering  $\Omega$  as the fundamental frequency) the system vibrates at the frequency  $\Omega$  when excited at  $\Omega/2$  or  $2\Omega$ , clear indication to an anharmonic oscillator [150].

In summary, we have shown that single-molecule spectroscopy and microscopy allow one to investigate local properties of electrical transport in organic crystals via the spectral displacement of the molecular absorption frequencies. These techniques are specially powerful when applied in a field-effect transistor, a device which confines the conduction paths in a well-defined area and permits to vary the number of charges inside the material. The studies presented in this thesis are very promising for further investigations to reveal new aspects of electrical processes in organic materials.



## Bibliography

- [1] C. K. Chiang, C. R. Fincher, Y. W. Park, A. J. Heeger, H. Shirakawa, E. J. Louis, S. C. Gau and A. G. Macdiarmid, “Electrical-Conductivity in Doped Polyacetylene”, *Phys. Rev. Lett.* **39**, 1098 (1977); *Phys. Rev. Lett.* **40**, 1472 (1978).
- [2] T. Holstein, “Studies of Polaron Motion. I. The Molecular-Crystal Model”, *Ann. Phys.* **8**, 325 (1959).
- [3] T. Holstein, “Studies of Polaron Motion. II. The Small Polaron”, *Ann. Phys.* **8**, 343 (1959).
- [4] R. W. I. de Boer, M. E. Gershenson, A. F. Morpurgo and V. Podzorov, “Organic single-crystal field-effect transistors”, *Phys. Status Solidi A-Appl. Res.* **201**, 1302 (2004).
- [5] F. Jelezko, B. Lounis and M. Orrit, “Pump-probe spectroscopy and photophysical properties of single di-benzanthanthrene molecules in a naphthalene crystal”, *J. Chem. Phys.* **107**, 1692 (1997).
- [6] S. Kummer, F. Kulzer, R. Kettner, Th. Basché, C. Tietz, C. Glowatz and C. Kryschi, “Absorption, excitation, and emission spectroscopy of terrylene in *p*-terphenyl: Bulk measurements and single molecule studies”, *J. Chem. Phys.* **107**, 7673 (1997).
- [7] D. Walser, G. Zumofen, A. Renn and T. Plakhotnik, “Line broadening and line shifts in one- and two-photon single-molecule spectra”, *J. Phys. Chem. A* **105**, 3022 (2001).
- [8] M. Croci, H. J. Müschenborn, F. Güttler, A. Renn and U. P. Wild, “Single-molecule spectroscopy: pressure effect on pentacene in *p*-terphenyl”, *Chem. Phys. Lett.* **212**, 71 (1993).
- [9] A. Müller, W. Richter and L. Kador, “Pressure effects on single molecules of terrylene in *p*-terphenyl”, *Chem. Phys. Lett.* **241**, 547 (1995).

- [10] J. Wrachtrup, C. von Borczyskowski, J. Bernard, M. Orrit and R. Brown, "Optical-Detection of Magnetic-Resonance in a Single Molecule", *Nature* **363**, 244 (1993).
- [11] J. Köhler, J. A. J. M. Disselhorst, M. C. J. M. Donckers, E. J. J. Groenen, J. Schmidt and W. E. Moerner, "Magnetic-Resonance of a Single Molecular Spin", *Nature* **363**, 242 (1993).
- [12] J. Wrachtrup, A. Gruber, L. Fleury and C. von Borczyskowski, "Magnetic resonance on single nuclei", *Chem. Phys. Lett.* **267**, 179 (1997).
- [13] A. C. J. Brouwer, E. J. J. Groenen and J. Schmidt, "Detecting magnetic resonance through quantum jumps of single molecules", *Phys. Rev. Lett.* **80**, 3944 (1998).
- [14] U. P. Wild, F. Güttler, M. Pirotta and A. Renn, "Single molecule spectroscopy: Stark effect of pentacene in *p*-terphenyl", *Chem. Phys. Lett.* **193**, 451 (1992).
- [15] M. Orrit, J. Bernard, A. Zumbusch and R. I. Personov, "Stark-Effect on Single Molecules in a Polymer Matrix", *Chem. Phys. Lett.* **196**, 595 (1992); *Chem. Phys. Lett.* **199**, 408 (1992).
- [16] C. Brunel, Ph. Tamarat, B. Lounis, J. C. Woehl and M. Orrit, "Stark effect on single molecules of dibenzanthanthrene in a naphthalene crystal and in a *n*-hexadecane Shpol'skii matrix", *J. Phys. Chem. A* **103**, 2429 (1999).
- [17] F. Kulzer, R. Matzke, C. Bräuchle and Th. Basché, "Nonphotochemical hole burning investigated at the single-molecule level: Stark effect measurements on the original and photoproduct state", *J. Phys. Chem. A* **103**, 2408 (1999).
- [18] P. Bordat, M. Orrit, R. Brown and A. Würger, "The anomalous Stark effect of single terrylene molecules in *p*-terphenyl crystals", *Chem. Phys.* **258**, 63 (2000).
- [19] J. M. Caruge and M. Orrit, "Probing local currents in semiconductors with single molecules", *Phys. Rev. B* **6420**, 205202 (2001).
- [20] J. M. Caruge and M. Orrit, "Investigations of local currents in a semiconductor by single-molecule spectroscopy", *J. Lumin.* **98**, 1 (2002).

- 
- [21] M. Bauer and L. Kador, "Stark spectroscopy of single molecules in the Shpol'skii matrix *n*-hexadecane", *J. Lumin.* **98**, 75 (2002).
- [22] M. Bauer and L. Kador, "Microscopic heterogeneities in the electrical properties of SiC as studied with single-molecule spectroscopy", *J. Phys. Chem. B* **107**, 14301 (2003).
- [23] W. E. Moerner and L. Kador, "Optical-Detection and Spectroscopy of Single Molecules in a Solid", *Phys. Rev. Lett.* **62**, 2535 (1989).
- [24] M. Orrit and J. Bernard, "Single Pentacene Molecules Detected by Fluorescence Excitation in a *p*-Terphenyl Crystal", *Phys. Rev. Lett.* **65**, 2716 (1990).
- [25] J. Bernard, L. Fleury, H. Talon and M. Orrit, "Photon bunching in the fluorescence from single molecules: A probe for intersystem crossing", *J. Chem. Phys.* **98**, 850 (1993).
- [26] W. P. Ambrose, Th. Basché and W. E. Moerner, "Detection and spectroscopy of single pentacene molecules in a *p*-terphenyl crystal by means of fluorescence excitation", *J. Chem. Phys.* **95**, 7150 (1991).
- [27] R. Brown and M. Orrit, *Single-Molecule Optical Detection, Imaging and Spectroscopy* (VCH, Weinheim, Germany, 1997).
- [28] P. Bordat and R. Brown, "Correspondence between electronic origins and substitution sites in pentacene/*p*-terphenyl mixed crystals by molecular modelling", *Chem. Phys. Lett.* **291**, 153 (1998).
- [29] P. Bordat and R. Brown, "Elucidation of optical switching of single guest molecules in terrylene/*p*-terphenyl mixed crystals", *Chem. Phys. Lett.* **331**, 439 (2000).
- [30] V. Podzorov, E. Menard, A. Borissov, V. Kiryukhin, J. A. Rogers and M. E. Gershenson, "Intrinsic charge transport on the surface of organic semiconductors", *Phys. Rev. Lett.* **93**, 086602 (2004).
- [31] G. Horowitz, "Organic thin film transistors: From theory to real devices", *J. Mater. Res.* **19**, 1946 (2004).
- [32] A. N. Aleshin, J. Y. Lee, S. W. Chu, J. S. Kim and Y. W. Park, "Mobility studies of field-effect transistor structures based on anthracene single crystals", *Appl. Phys. Lett.* **84**, 5383 (2004).

- [33] M. Banasiewicz, I. Deperasińska, D. Fabjanowicz and B. Kozankiewicz, “Excited singlet state relaxation yields of pentacene in Shpol’skii matrices”, *Chem. Phys. Lett.* **356**, 541 (2002).
- [34] R. Zondervan, F. Kulzer, M. A. Kol’chenko and M. Orrit, “Photobleaching of rhodamine 6G in poly(vinyl alcohol) at the ensemble and single-molecule levels”, *J. Phys. Chem. A* **108**, 1657 (2004).
- [35] A. M. van Oijen, J. Köhler, J. Schmidt, M. Müller and G. J. Brakenhoff, “Far-field fluorescence microscopy beyond the diffraction limit”, *J. Opt. Soc. Am. A* **16**, 909 (1999).
- [36] P. J. Walla, F. Jelezko, Ph. Tamarat, B. Lounis and M. Orrit, “Perylene in biphenyl and anthracene crystals: an example of the influence of the host on single-molecule signals”, *Chem. Phys.* **233**, 117 (1998).
- [37] G. S. Harms, T. Irngartinger, D. Reiss, A. Renn and U. P. Wild, “Fluorescence lifetimes of terrylene in solid matrices”, *Chem. Phys. Lett.* **313**, 533 (1999).
- [38] Winchell, *The Optical Properties of Organic Compounds* (Academic Press Inc., New York, 1954), 2 edn.
- [39] I. Rebane, “Spontaneous emission rates of a single impurity molecule in a uniaxial host crystal”, *Opt. Commun.* **217**, 265 (2003).
- [40] A. B. Myers, P. Tchénio, M. Z. Zgierski and W. E. Moerner, “Vibronic Spectroscopy of Individual Molecules in Solids”, *J. Phys. Chem.* **98**, 10377 (1994).
- [41] Ph. Tamarat, F. Jelezko, B. Lounis and M. Orrit, *Shpol’skii Spectroscopy and Other Site-Selection Methods* (Wiley Interscience, New York, 2000).
- [42] S. Kummer, Th. Basché and C. Bräuchle, “Terrylene in *p*-terphenyl: A novel single-crystalline system for single-molecule spectroscopy at low-temperatures”, *Chem. Phys. Lett.* **229**, 309 (1994); *Chem. Phys. Lett.* **232**, 414 (1995).
- [43] M. A. Kol’chenko, B. Kozankiewicz, A. Nicolet and M. Orrit, “Intersystem crossing mechanisms and single molecule fluorescence: Terrylene in anthracene crystals”, *Opt. Spectrosc.* **98**, 681 (2005).

- 
- [44] T. Plakhotnik, W. E. Moerner, V. Palm and U. P. Wild, "Single-Molecule Spectroscopy: Maximum Emission Rate and Saturation Intensity", *Opt. Commun.* **114**, 83 (1995).
- [45] B. Kozankiewicz, M. Banasiewicz, J. Dresner and M. Orrit, "Intersystem crossing of single pentacene molecules in Shpol'skii matrices", *Chem. Phys. Lett.* **343**, 71 (2001).
- [46] M. Orrit, J. Bernard, R. Brown and B. Lounis, "Optical spectroscopy of single molecules in solids", *Prog. Opt.* **35**, 61 (1996).
- [47] R. A. L. Vallée, M. Van der Auweraer, F. C. De Schryver, D. Beljonne and M. Orrit, "A microscopic model for the fluctuations of local field and spontaneous emission of single molecules in disordered media", *Chem. Phys. Chem.* **6**, 81 (2005).
- [48] E. A. Donley, V. Burzomato, U. P. Wild and T. Plakhotnik, "The distribution of line widths of single probe molecules in a crystalline host at milliKelvin temperatures", *J. Lumin.* **83-4**, 255 (1999).
- [49] B. Kozankiewicz, J. Bernard and M. Orrit, "Single-Molecule Lines and Spectral Hole-Burning of Terrylene in Different Matrices", *J. Chem. Phys.* **101**, 9377 (1994).
- [50] H. Zimmermann, D. Stehlik and K. H. Hausser, "Excitation of Triplet Excitons in Aromatic Single Crystals by Guest-Host Energy Transfer", *Chem. Phys. Lett.* **11**, 496 (1971).
- [51] G. C. Smith, "Triplet Exciton Phosphorescence in Crystalline Anthracene", *Phys. Rev.* **166**, 839 (1968).
- [52] H. Bach, A. Renn, G. Zumofen and U. P. Wild, "Exciton dynamics probed by single molecule spectroscopy", *Phys. Rev. Lett.* **82**, 2195 (1999).
- [53] R. E. Kellogg, "Second Triplet State of Anthracene", *J. Chem. Phys.* **44**, 411 (1966).
- [54] J. B. Birks, *Organic Molecular Photophysics*, vol. 1 (Wiley-Interscience, London and New York, 1973).
- [55] D. S. McClure, "Excited Triplet States of Some Polyatomic Molecules I.", *J. Chem. Phys.* **19**, 670 (1951).



- [56] C. Hofmann, A. Nicolet, M. A. Kol'chenko and M. Orrit, "Towards nanoprobe for conduction in molecular crystals: Dibenzoterrylene in anthracene crystals", *Chem. Phys.* **318**, 1 (2005).
- [57] W. E. Moerner and M. Orrit, "Illuminating single molecules in condensed matter", *Science* **283**, 1670 (1999).
- [58] Ph. Tamarat, A. Maali, B. Lounis and M. Orrit, "Ten years of single-molecule spectroscopy", *J. Phys. Chem. A* **104**, 1 (2000).
- [59] A. M. Boiron, Ph. Tamarat, B. Lounis, R. Brown and M. Orrit, "Are the spectral trails of single molecules consistent with the standard two-level system model of glasses at low temperatures?", *Chem. Phys.* **247**, 119 (1999).
- [60] C. Hofmann, H. Michel, M. van Heel and J. Köhler, "Multivariate analysis of single-molecule spectra: Surpassing spectral diffusion", *Phys. Rev. Lett.* **94**, 195501 (2005).
- [61] A. V. Naumov, Y. G. Vainer, M. Bauer and L. Kador, "Dynamics of a doped polymer at temperatures where the two-level system model of glasses fails: Study by single-molecule spectroscopy", *J. Chem. Phys.* **119**, 6296 (2003).
- [62] H. P. Lu and X. S. Xie, "Single-molecule kinetics of interfacial electron transfer", *J. Phys. Chem. B* **101**, 2753 (1997).
- [63] N. Karl, J. Marktanner, R. Stehle and W. Warta, "High-Field Saturation of Charge Carrier Drift Velocities in Ultrapurified Organic Photoconductors", *Synth. Met.* **42**, 2473 (1991).
- [64] A. L. Briseno, S. C. B. Mannsfeld, M. M. Ling, S. H. Liu, R. J. Tseng, C. Reese, M. E. Roberts, Y. Yang, F. Wudl and Z. N. Bao, "Patterning organic single-crystal transistor arrays", *Nature* **444**, 913 (2006).
- [65] G. Horowitz, F. Garnier, A. Yassar, R. Hajlaoui and F. Kouki, "Field-effect transistor made with a sexithiophene single crystal", *Adv. Mater.* **8**, 52 (1996).
- [66] V. Podzorov, V. M. Pudalov and M. E. Gershenson, "Field-effect transistors on rubrene single crystals with parylene gate insulator", *Appl. Phys. Lett.* **82**, 1739 (2003).

- 
- [67] V. Y. Butko, X. Chi, D. V. Lang and A. P. Ramirez, "Field-effect transistor on pentacene single crystal", *Appl. Phys. Lett.* **83**, 4773 (2003).
- [68] R. W. I. de Boer, T. M. Klapwijk and A. F. Morpurgo, "Field-effect transistors on tetracene single crystals", *Appl. Phys. Lett.* **83**, 4345 (2003).
- [69] V. Y. Butko, X. Chi and A. P. Ramirez, "Free-standing tetracene single crystal field effect transistor", *Solid State Commun.* **128**, 431 (2003).
- [70] N. Karl, *Crystals, Growth, Properties and Applications*, vol. 4 (Springer-Verlag, Berlin, 1980).
- [71] A. M. Boiron, B. Lounis and M. Orrit, "Single molecules of dibenzanthanthrene in *n*-hexadecane", *J. Chem. Phys.* **105**, 3969 (1996).
- [72] A. Nicolet, M. A. Kol'chenko, B. Kozankiewicz and M. Orrit, "Intermolecular intersystem crossing in single-molecule spectroscopy: Terryrene in anthracene crystal", *J. Chem. Phys.* **124**, 164711 (2006).
- [73] B. Lounis and M. Orrit, "Single-photon sources", *Rep. Prog. Phys.* **68**, 1129 (2005).
- [74] F. Jelezko, Ph. Tamarat, B. Lounis and M. Orrit, "Dibenzoterryrene in naphthalene: A new crystalline system for single molecule spectroscopy in the near infrared", *J. Phys. Chem.* **100**, 13892 (1996).
- [75] Th. Basché, W. E. Moerner, M. Orrit and H. Talon, "Photon Antibunching in the Fluorescence of a Single Dye Molecule Trapped in a Solid", *Phys. Rev. Lett.* **69**, 1516 (1992).
- [76] Ph. Tamarat, T. Gaebel, J. R. Rabeau, M. Khan, A. D. Greentree, H. Wilson, L. C. L. Hollenberg, S. Prawer, P. Hemmer, F. Jelezko and J. Wrachtrup, "Stark shift control of single optical centers in diamond", *Phys. Rev. Lett.* **97**, 083002 (2006).
- [77] B. R. Henry and W. Siebrand, *Organic Molecular Photophysics*, vol. 1 (Wiley-Interscience, London and New York, 1973).
- [78] N. Abasbegovic, N. Vukotic and L. Colombo, "Raman Spectrum of Anthracene", *J. Chem. Phys.* **41**, 2575 (1964).
- [79] V. Coropceanu, J. Cornil, D. A. da Silva, Y. Olivier, R. Silbey and J. L. Brédas, "Charge transport in organic semiconductors", *Chem. Rev.* **107**, 926 (2007).

- [80] A. Bloëß, Y. Durand, M. Matsushita, R. Verberk, E. J. J. Groenen and J. Schmidt, "Microscopic structure in a Shpol'skii system: A single-molecule study of dibenzanthanthrene in *n*-tetradecane", *J. Phys. Chem. A* **105**, 3016 (2001).
- [81] Th. Basché and W. E. Moerner, "Optical Modification of a Single Impurity Molecule in a Solid", *Nature* **355**, 335 (1992).
- [82] S. Mais, J. Tittel, Th. Basché, C. Bräuchle, W. Göhde, H. Fuchs, G. Müller and K. Müllen, "Terrylenediimide: A novel fluorophore for single-molecule spectroscopy and microscopy from 1.4 K to room temperature", *J. Phys. Chem. A* **101**, 8435 (1997).
- [83] A. C. Wirtz, C. Hofmann and E. J. J. Groenen, "Spin-coated polyethylene films probed by single molecules", *J. Phys. Chem. B* **110**, 21623 (2006).
- [84] R. Kettner, J. Tittel, Th. Basché and C. Bräuchle, "Optical Spectroscopy and Spectral Diffusion of Single Dye Molecules in Amorphous Spin-Coated Polymer-Films", *J. Phys. Chem.* **98**, 6671 (1994).
- [85] A. Zumbusch, L. Fleury, R. Brown, J. Bernard and M. Orrit, "Probing Individual Two-Level Systems in a Polymer by Correlation of Single Molecular Fluorescence", *Phys. Rev. Lett.* **70**, 3584 (1993).
- [86] M. Pirotta, A. Renn, M. H. V. Werts and U. P. Wild, "Single molecule spectroscopy, perylene in the Shpol'skii matrix *n*-nonane", *Chem. Phys. Lett.* **250**, 576 (1996).
- [87] M. Vacha, Y. Liu, H. Nakatsuka and T. Tani, "Inhomogeneous and single molecule line broadening of terrylene in a series of crystalline *n*-alkanes", *J. Chem. Phys.* **106**, 8324 (1997).
- [88] T. Plakhotnik, D. Walser, M. Pirotta, A. Renn and U. P. Wild, "Nonlinear spectroscopy on a single quantum system: Two-photon absorption of a single molecule", *Science* **271**, 1703 (1996).
- [89] M. Vacha and T. Tani, "Single-molecule spectroscopy of benzodiphenanthrobisanthene in a Shpolskii matrix", *J. Phys. Chem. A* **101**, 5027 (1997).
- [90] Y. Durand, A. Bloëß, J. Köhler, E. J. J. Groenen and J. Schmidt, "Spectral diffusion of individual pentacene, terrylene, and dibenzanthanthrene molecules in *n*-tetradecane", *J. Chem. Phys.* **114**, 6843 (2001).

- 
- [91] W. E. Moerner, T. Plakhotnik, T. Irngartinger, M. Croci, V. Palm and U. P. Wild, "Optical Probing of Single Molecules of Terrylene in a Shpol'skii Matrix - A Two-State Single-Molecule Switch", *J. Phys. Chem.* **98**, 7382 (1994).
- [92] S. Kummer, C. Bräuchle and Th. Basché, "Optical spectroscopy of single pentacene molecules in a naphthalene crystal", *Mol. Cryst. Liq. Cryst. Sci. Technol. Sect. A-Mol. Cryst. Liq. Cryst.* **283**, 255 (1996).
- [93] L. Kador, T. Latychevskaia, A. Renn and U. P. Wild, "Absorption spectroscopy on single molecules in solids", *J. Chem. Phys.* **111**, 8755 (1999).
- [94] F. Kulzer, S. Kummer, R. Matzke, C. Bräuchle and Th. Basché, "Single-molecule optical switching of terrylene in *p*-terphenyl", *Nature* **387**, 688 (1997).
- [95] P. Bordat and R. Brown, "A molecular model of *p*-terphenyl and its disorder-order transition", *Chem. Phys.* **246**, 323 (1999).
- [96] D. Hsu and J. L. Skinner, "Nonperturbative Theory of Temperature-Dependent Optical Dephasing in Crystals .II. Pseudolocal Phonons", *J. Chem. Phys.* **83**, 2097 (1985).
- [97] D. Hsu and J. L. Skinner, "Nonperturbative Theory of Temperature-Dependent Optical Dephasing in Crystals .III. Comparison with Experiment", *J. Chem. Phys.* **83**, 2107 (1985).
- [98] W. H. Hesselink and D. A. Wiersma, "Optical dephasing and vibronic relaxation in molecular mixed-crystals: A picosecond photon-echo and optical study of pentacene in naphthalene and *p*-terphenyl", *J. Chem. Phys.* **73**, 648 (1980).
- [99] F. Güttler, M. Croci, A. Renn and U. P. Wild, "Single molecule polarization spectroscopy: Pentacene in *p*-terphenyl", *Chem. Phys.* **211**, 421 (1996).
- [100] N. Neto, M. Scrocco and S. Califano, "A simplified valence force field of aromatic hydrocarbons-I Normal co-ordinate calculations for C<sub>6</sub>H<sub>6</sub>, C<sub>6</sub>D<sub>6</sub>, C<sub>10</sub>H<sub>8</sub>, C<sub>10</sub>D<sub>8</sub>, C<sub>14</sub>H<sub>10</sub> and C<sub>14</sub>D<sub>10</sub>", *Spectrochim Acta* **22**, 1981 (1966).
- [101] G. Filippini, M. Simonetta and C. M. Gramaccioli, "A Simplified Force-Field for Non-Planar Vibrations in Aromatic Polycyclic-Hydrocarbons", *Mol. Phys.* **51**, 445 (1984).

- [102] G. Filippini and C. M. Gramaccioli, "Lattice-Dynamical Calculations for Tetracene and Pentacene", *Chem. Phys. Lett.* **104**, 50 (1984).
- [103] D. E. Williams, "Nonbonded Potential Parameters Derived from Crystalline Aromatic Hydrocarbons", *J. Chem. Phys.* **45**, 3770 (1966).
- [104] M. J. Frisch, G. W. Trucks, H. B. Schlegel, G. E. Scuseria, M. A. Robb, J. R. Cheeseman, V. G. Zakrzewski, J. A. Montgomery, R. E. Stratmann, J. C. Burant, S. Dapprich, J. M. Millam, A. D. Daniels, K. N. Kudin, M. C. Strain, O. Farkas, J. Tomasi, V. Barone, M. Cossi, R. Cammi, B. Mennucci, C. Pomelli, C. Adamo, S. Clifford, J. Ochterski, G. A. Petersson, P. Y. Ayala, Q. Cui, K. Morokuma, P. Salvador, J. J. Dannenberg, D. K. Malick, A. D. Rabuck, K. Raghavachari, J. B. Foresman, J. Cioslowski, J. V. Ortiz, A. G. Baboul, B. B. Stefanov, G. Liu, A. Liashenko, P. Piskorz, I. Komaromi, R. Gomperts, R. L. Martin, D. J. Fox, T. Keith, M. A. Al-Laham, C. Y. Peng, A. Nanayakkara, M. Challacombe, P. M. W. Gill, B. Johnson, W. Chen, M. W. Wong, J. L. Andres, C. Gonzalez, M. Head-Gordon, E. S. Replogle and Pople J. A., *Gaussian98*, Gaussian, Inc., Pittsburgh PA (2001).
- [105] P. Bordat and R. Brown, "Molecular mechanisms of photo-induced spectral diffusion of single terrylene molecules in *p*-terphenyl", *J. Chem. Phys.* **116**, 229 (2002).
- [106] H. J. C. Berendsen, J. P. M. Postma, W. F. van Gunsteren, A. Dinola and J. R. Haak, "Molecular-Dynamics with Coupling to an External Bath", *J. Chem. Phys.* **81**, 3684 (1984).
- [107] W. Smith and T. R. Forester, *The DLPOLY User Manual*, CCLRC, Daresbury Laboratory, England (2001).
- [108] A. A. L. Nicolet, C. Hofmann, M. A. Kol'chenko, B. Kozankiewicz and M. Orrit, "Single Dibenzoterrylene Molecules in an Anthracene Crystal: Spectroscopy and Photophysics", *Chem. Phys. Chem.* **8**, 1215 (2007).
- [109] G. Horowitz, "Organic field-effect transistors", *Adv. Mater.* **10**, 365 (1998).
- [110] C. D. Dimitrakopoulos and P. R. L. Malenfant, "Organic thin film transistors for large area electronics", *Adv. Mater.* **14**, 99 (2002).
- [111] M. E. Gershenson, V. Podzorov and A. F. Morpurgo, "Colloquium: Electronic transport in single-crystal organic transistors", *Rev. Mod. Phys.* **78**, 973 (2006).

- 
- [112] J. H. Burroughes, D. D. C. Bradley, A. R. Brown, R. N. Marks, K. Mackay, R. H. Friend, P. L. Burn and A. B. Holmes, "Light-Emitting-Diodes Based on Conjugated Polymers", *Nature* **347**, 539 (1990); *Nature* **348**, 352 (1990).
- [113] P. P. Infelta, M. P. D. Haas and J. M. Warman, "Study of Transient Conductivity of Pulse Irradiated Dielectric Liquids on a Nanosecond Timescale Using Microwaves", *Radiat. Phys. Chem.* **10**, 353 (1977).
- [114] P. Prins, F. C. Grozema, J. M. Schins, S. Patil, U. Scherf and L. D. A. Siebbeles, "High intrachain hole mobility on molecular wires of ladder-type poly(p-phenylenes)", *Phys. Rev. Lett.* **96**, 146601 (2006).
- [115] T. Plakhotnik, "Single-molecule dynamic triangulation", *ChemPhysChem* **7**, 1699 (2006).
- [116] R. W. I. de Boer, *Organic single-crystal field-effect transistors*, Ph.D. thesis, Technische Universiteit Delft (2005).
- [117] D. J. Gundlach, L. L. Jia and T. N. Jackson, "Pentacene TFT with improved linear region characteristics using chemically modified source and drain electrodes", *IEEE Electron Device Lett.* **22**, 571 (2001).
- [118] R. W. I. de Boer, N. N. Iosad, A. F. Stassen, T. M. Klapwijk and A. F. Morpurgo, "Influence of the gate leakage current on the stability of organic single-crystal field-effect transistors", *Appl. Phys. Lett.* **86**, 032103 (2005).
- [119] P. Mark and W. Helfrich, "Space-Charge-Limited Currents in Organic Crystals", *J. Appl. Phys.* **33**, 205 (1962).
- [120] G. Vaubel and H. Baessler, "Determination of Band-Gap in Anthracene", *Phys. Lett. A* **27**, 328 (1968).
- [121] M. Pope and C. E. Swenberg, "Electronic Processes in Organic-Solids", *Annu. Rev. Phys. Chem.* **35**, 613 (1984).
- [122] J. A. Geurst, "Theory of Insulated-Gate Field-Effect Transistors Near and Beyond Pinch-Off", *Solid-State Electron.* **9**, 129 (1966).
- [123] J. A. Geurst, "Theory of Space-Charge-Limited Currents in Thin Semiconductor Layers", *phys status solidi* **15**, 107 (1966).

- [124] R. Zuleeg and P. Knoll, "Space-Charge-Limited Currents in Heteroepitaxial Films of Silicon Grown on Sapphire", *Appl. Phys. Lett.* **11**, 183 (1967).
- [125] O. D. Jurchescu and T. T. M. Palstra, "Crossover from one- to two-dimensional space-charge-limited conduction in pentacene single crystals", *Appl. Phys. Lett.* **88**, 122101 (2006).
- [126] A. Rose, "Space-Charge-Limited Currents in Solids", *Phys. Rev.* **97**, 1538 (1955).
- [127] P. W. M. Blom, M. J. M. de Jong and M. G. van Munster, "Electric-field and temperature dependence of the hole mobility in poly(p-phenylene vinylene)", *Phys. Rev. B* **55**, R656 (1997).
- [128] J. Frenkel, "On Pre-Breakdown Phenomena in Insulators and Electronics Semi-Conductors", *Phys. Rev.* **54**, 647 (1938).
- [129] H. Bässler, "Charge Transport in Disordered Organic Photoconductors - A Monte-Carlo Simulation Study", *Phys. Status Solidi B-Basic Res.* **175**, 15 (1993).
- [130] G. W. Kang, K. M. Park, J. H. Song, C. H. Lee and D. H. Hwang, "The electrical characteristics of pentacene-based organic field-effect transistors with polymer gate insulators", *Curr. Appl. Phys.* **5**, 297 (2005).
- [131] V. C. Sundar, J. Zaumseil, V. Podzorov, E. Menard, R. L. Willett, T. Someya, M. E. Gershenson and J. A. Rogers, "Elastomeric transistor stamps: Reversible probing of charge transport in organic crystals", *Science* **303**, 1644 (2004).
- [132] J. Pflaum, J. Niemax and A. K. Tripathi, "Chemical and structural effects on the electronic transport in organic single crystals", *Chem. Phys.* **325**, 152 (2006).
- [133] E. W. Montroll and G. H. Weiss, "Random Walks on Lattices. II.", *J. Math. Phys.* **6**, 167 (1965).
- [134] H. Scher and M. Lax, "Stochastic Transport in a Disordered Solid. I. Theory", *Phys. Rev. B* **7**, 4491 (1973).
- [135] H. Scher and M. Lax, "Stochastic Transport in a Disordered Solid. II. Impurity Conduction", *Phys. Rev. B* **7**, 4502 (1973).

- 
- [136] H. Scher and E. W. Montroll, “Anomalous Transit-Time Dispersion in Amorphous Solids”, *Phys. Rev. B* **12**, 2455 (1975).
- [137] S. G. J. Mathijssen, M. Colle, A. J. G. Mank, M. Kemerink, P. A. Bobbert and D. M. de Leeuw, “Scanning Kelvin probe microscopy on organic field-effect transistors during gate bias stress”, *Appl. Phys. Lett.* **90**, 192104 (2007).
- [138] M. Silver, G. Schoenherr and H. Baessler, “Dispersive Hopping Transport from an Exponential Energy-Distribution of Sites”, *Phys. Rev. Lett.* **48**, 352 (1982).
- [139] J. M. Caruge, *Étude du transport local de charges dans des couches semi-conductrices désordonnées par spectroscopie à une molécule*, Ph.D. thesis, Université de Bordeaux I (2001).
- [140] L. Kador, T. Latychevskaia, A. Renn and U. P. Wild, “Radio-frequency Stark effect modulation of single-molecule lines”, *J. Lumin.* **86**, 189 (2000).
- [141] E. ten Grotenhuis, J. C. van Miltenburg and J. P. van der Eerden, “Preparation of anthracene micro-crystals by spin-coating and atomic force microscopy study of the molecular packing”, *Chem. Phys. Lett.* **261**, 558 (1996).
- [142] R. J. Pfab, J. Zimmermann, C. Hettich, I. Gerhardt, A. Renn and V. Sandoghdar, “Aligned terrylene molecules in a spin-coated ultrathin crystalline film of *p*-terphenyl”, *Chem. Phys. Lett.* **387**, 490 (2004).
- [143] J. Tempere, I. F. Silvera and J. T. Devreese, “Effect of pressure on statics, dynamics, and stability of multielectron bubbles”, *Phys. Rev. Lett.* **87**, 275301 (2001).
- [144] A. Brandl and W. Prettl, “Chaotic Fluctuations and Formation of a Current Filament in N-Type Gaas”, *Phys. Rev. Lett.* **66**, 3044 (1991).
- [145] R. F. Kazarino, R. A. Suris and B. I. Fuks, “Thermal-Current Instability in Compensated Semiconductors”, *Sov. Phys. Semicond.* **6**, 500 (1972).
- [146] R. F. Kazarino, R. A. Suris and B. I. Fuks, “Waves of Spatial Charge-Exchange and Thermoelectric Current Instability in Compensated Semiconductors”, *Sov. Phys. Semicond.* **7**, 102 (1973).



## Bibliography

---

- [147] A. I. Chumakov, I. Sergueev, U. van Bürk, W. Schirmacher, T. Asthalter, R. Ruffer, O. Leupold and W. Petry, “Collective Nature of the Boson Peak and Universal Transboson Dynamics of Glasses”, *Phys. Rev. Lett.* **92**, 245508 (2004).
- [148] J. Jäckle, *Amorphous Solids: Low Temperature Properties* (Springler-Verlag, Berlin, 1981).
- [149] Y. G. Vainer, A. V. Naumov, M. Bauer and L. Kador, “Experimental evidence of the local character of vibrations constituting the Boson peak in amorphous solids”, *Phys. Rev. Lett.* **97**, 185501 (2006).
- [150] L. D. Landau and E. M. Lifshitz, *Course of Theoretical Physics: Mechanics* (Pergamon Press, 1976).

# Individuele Molekules in Organische Veld-effecttransistoren Sonderen

Dit proefschrift gaat over molekulen, licht en elektronisch transport in organische kristallen. Het is de bedoeling de spectroscopische eigenschappen van individuele molekulen die in een organisch kristal worden opgenomen te gebruiken om de heterogeniteit van het elektrisch veld te onderzoeken dat door ladingen binnen het materiaal wordt gecreëerd. Dit wordt gedaan in een veld-effecttransistor en maakt het mogelijk om ladingen in het kristal te injecteren.

## Molekulen en kristalen

Laten we eerst verscheidene noodzakelijke concepten bekijken om het volgende te begrijpen. Een molekuul is een voldoende stabiele groep van minstens twee atomen in een welomlijnde structuur samengebonden. Een kristal is een vast lichaam dat door groepen atomen of moleculen wordt gevormd die een regelmatig basispatroon vormen dat in alle dimensies kan worden herhaald. De organische molekulen zijn gebaseerd op koolstof (C) atomen. Echter, om historische redenen worden enkele samenstellingen die koolstofelementen bevatten niet als organisch beschouwd. Het gebruik van het woord 'organische' dateert uit de 19<sup>de</sup> eeuw toen men geloofde dat de organische moleculen slechts door levende organismen met behulp van de *vis vitalis* konden worden samengesteld. Dit onderscheid is niet meer correct in een tijd waar plastics, met een organische samenstelling, in industriële processen worden vervaardigd. Desalniettemin, de benaming bleef.

In het vervolg zullen wij een molekulaair kristal dat van organische molekulen is gemaakt, beschouwen. Deze molekulen worden anthraceen genoemd, een molekuul dat 14 koolstof atomen en 10 waterstof atomen bevat (de chemische formule is:  $C_{14}H_{10}$ ). Merk op dat het mogelijk is om andere molekulen binnen een dergelijk kristal op te nemen. Als het aantal van deze andere molekulen laag genoeg is, beschouwen we ze enkel als onzuiverheden en bijgevolg blijft het kristal een anthraceen kristal. Maar alvorens op deze overwegingen dieper in te gaan, moeten wij verscheidene punten over de interactie tussen licht en materie uitleggen.

## Spectroscopie aan individuele molekulen

Materie bestaat uit atomen en molekulen. Een atoom is een kern (bestaand uit protonen en neutronen) omringd door een wolk van negatief geladen elektronen. Deze elektronen kunnen slechts duidelijk omliggende energiewaarden hebben. Wanneer niets gebeurt, zijn zij in de zogenaamde grondtoestand, het laagste energieniveau dat zij kunnen bereiken. Maar een elektron kan een hoger energieniveau hebben wanneer het met licht in aanraking komt. Om dit te kunnen bewerkstelligen, moet de energie van het licht, dat we dan als een stroom van foton deeltjes kunnen beschouwen, de juiste waarde hebben gelijk aan het verschil tussen beide energieniveaus van het elektron. In dat geval, zeggen wij dat het deeltje zich in een aangeslagen toestand bevindt. Deze aangeslagen toestand is niet stabiel (het heeft een levensduur), en het elektron zal naar zijn grondtoestand teruggaan door dezelfde energie in de vorm van een foton uit te zenden. Een dergelijk proces vindt plaats wanneer men wat zout (natriumchloride) op het fornuis zet en de vlam geel wordt. Na het absorberen van wat energie uit de vlam, zullen de elektronen van het natrium naar hun grondtoestand teruggaan door die gele fotonen uit te zenden. Dit fenomeen wordt fluorescentie genoemd. In de praktijk verstemmen wij langzaam de golflengte van een laser. Wanneer de golflengte precies in resonantie is met de overgang van het molekuul (wat betekent dat de fotonen precies de hoeveelheid energie hebben bestaande uit het verschil van energieniveaus), zal het licht geabsorbeerd worden en kunnen wij de fluorescentie van het molekuul detecteren.

Laten we terugkomen op onze discussie met betrekking tot onzuiverheden waar we een kristal met een kleine concentratie van andere molekulen (als onzuiverheden) beschouwen. Wij kunnen de molekulen van het kristal de gastheer en de onzuiverheden de gast noemen. Indien goed gekozen, kunnen deze gastmolekulen bij een bepaalde golflengte fluorescentie vertonen. In het geval van een molekuul dat in een kristal wordt opgenomen, zal het emissiespectrum wegens de interactie van dit molekuul met de molekulen van het kristal wat complexer zijn. Voorts, zal elk gastmolekuul van een gegeven type een iets verschillende interactie met de omgevende gastheermolekulen vertonen. Bijgevolg, zullen zij op verschillende golflengten licht uitzenden. Wanneer men vele molekulen waarneemt, ziet men een overlapping van signalen van alle individuele molekulen, wat betekent dat men een breed spectrum zal waarnemen. Wanneer het aantal molekulen klein genoeg is, kan men een situatie creëren waar deze overlapping zal verdwijnen. In dat geval kan men de emissie van licht van één enkel molekuul ontdekken. Het emissiespectrum van zo'n enkel molekuul zal veel smaller zijn dan dat van het ensemble van molekulen.

Een fluorescerend molecuul kan zeer gevoelig zijn voor kleine storingen in zijn omgeving. Deze storingen kunnen worden ontdekt door de spectrale positie van de absorptie van het licht van het molecuul te bepalen. Omdat de spectrale positie met een hoge nauwkeurigheid kan worden gemeten, kunnen fluorescerende molekulen worden gebruikt om kleine variaties in het lokale veld bij het aanleggen van een uitwendig elektrisch veld af te tasten. De elektronen, die een lading hebben, zijn namelijk gevoelig voor een elektrisch veld en dit zal sommige veranderingen in hun energieniveaus veroorzaken en bijgevolg in het absorptiespectrum van het gastmolecuul. Het bestuderen van de fluorescentie van één molecuul is de basis van wat men de ‘single-molecule’ spectroscopie noemt. Dit is de techniek die wij gebruiken. De experimenten worden gedaan in vloeibaar helium, bij een temperatuur van  $-271.75\text{ }^{\circ}\text{C}$  (1.4 K).

In Hoofdstuk 2 karakteriseerden wij een systeem voor de ‘single-molecule’ spectroscopie. Dit systeem bestaat uit terryleen molekulen (als fluorescerende molekulen) die worden opgenomen in een kristal van anthraceen. Een combinatie gast-gastheer is een goed systeem als de fluorescerende molekulen een grote hoeveelheid fluorescentiefotonen uitzenden en de geëxciteerde moleculelijn (dit wordt de nul-fonon lijn genoemd) zeer smal en spectraal stabiel is. Wij kunnen een fluorescentiefoton detecteren wanneer het molecuul een directe overgang van de aangeslagen toestand naar een andere toestand van lagere energie ondergaat (het uitgezonden foton heeft een energie die overeenkomt met het verschil van energieën van die twee toestanden). Met terryleen, wordt de fluorescentie opgewekt door de overgang tussen twee zogenaamde ‘singlet’ toestanden. Het woord verwijst naar bepaalde symmetrie eigenschappen van de desbetreffend elektronische toestand, geralateerd aan de spin van de elektronen. De spin is één van de intrinsieke eigenschappen van deeltjes zoals de massa of de lading (een elektron heeft een spin  $s=1/2$ ). Evenwel, tussen de grondtoestand en de fluorescerende toestand ligt in ons geval (en vrijwel alle andere organische molekulen) nog een andere elektronische toestand die ‘triplet’ genoemd wordt. Deze toestand heeft een andere spin dan de eerder vermelde ‘singlets’. De overgangen tussen toestanden van verschillende ‘multiplicities’ (d.w.z. van verschillende spinwaarden, bijvoorbeeld van ‘singlet’ naar ‘triplet’) zijn, in het algemeen, weinig waarschijnlijk. Dergelijke overgangen worden ‘intersystem-crossing’ genoemd. Wanneer de door ons beschouwde molekulen zich in die ‘triplet’ toestand bevinden, absorberen of emitteren ze geen fotonen. Deze ‘triplet’ toestand wordt daarom vaak een donkere toestand genoemd. Bijgevolg, zou een goed systeem een zeer lage ‘intersystem-crossing’ frequentie moeten hebben. In het geval van terryleenmolekulen in een anthraceen kristal toonden wij aan dat deze ‘intersystem-crossing’ sterk door

een intermolekulaire proces wordt verhoogd. De anthraceen molekulen hebben eveneens een ‘triplet’ toestand. Deze ‘triplet’ toestanden bevinden zich, in energietermen, beide tussen de aangeslagen ‘singlet’ en de ‘triplet’ van de terryleenmolekulen. Dit heeft als gevolg dat de excitatie via de ‘triplet’ van anthraceen wordt overgedragen naar de ‘triplet’ van terryleen. Bijgevolg is het fluorescentiesignaal zeer zwak en het systeem niet geschikt voor ‘single-molecule’ spectroscopie.

Om dit probleem op te lossen, kozen wij een ander systeem dat een aangeslagen ‘singlet’ heeft met een lagere energie dan de ‘triplet’ van de anthraceen molekulen. De nieuwe fluorescerende molekulen heten dibenzoterryleen. In Hoofdstuk 3 karakteriseerden wij de fotofysica van dit systeem. De combinatie van dibenzoterryleen in een anthraceen kristal bleek een zeer goed systeem voor de spectroscopie van individuele molekulen, met een intense fluorescentie en een smalle en spectraal stabiele nul-fonon lijn. In dit geval, is de ‘intersystem-crossing’ frequentie zeer laag. Deel twee van de karakterisering wordt besproken in Hoofdstuk 4. Wij onderzochten de toevoeging van de gastmolekulen in het kristal, en vergeleken de experimentele resultaten met sommige simulaties. Wij vonden twee verschillende manieren om de molekulen op te nemen in het kristal. We stelden vast dat één molekkel van dibenzoterryleen drie molekulen van anthraceen vervangt.

## **Elektronisch transport en transistoren**

Wij gaan nu het geleidingsfenomeen bespreken. De materialen kunnen in twee extreme gevallen worden geclassificeerd. Enerzijds zijn er materialen waarin ladingen kunnen bewegen. Wij zullen hen geleiders noemen. Anderzijds, zijn er isolatoren, waarin de ladingen gelokaliseerd zijn en niet kunnen bewegen. Daartussen zijn er materialen die, in bepaalde omstandigheden, ofwel een geleider of isolator kunnen zijn. Zij worden halfgeleiders genoemd. Zij zijn van groot belang omwille van hun talrijke technologische toepassingen. Organische kristallen, die slechte geleiders zijn, kunnen in bepaalde mate als halfgeleiders beschouwd worden. De geleidingsprocessen van deze materialen worden niet zo goed begrepen. Daarom is er behoefte aan verder onderzoek. Dit kan door middel van een veldeffecttransistor gedaan worden.

Een veldeffecttransistor bestaat uit drie elektroden die aan een halfgeleider worden vastgehecht. Twee van de elektroden (de ‘source’ en de ‘drain’) worden direct verbonden met de halfgeleider terwijl de laatste (de ‘gate’) door een isolatielaag wordt gescheiden. Het toepassen van een elektrisch spanningsverschil tussen de twee eerste elektroden veroorzaakt een verplaatsing van ladingen bin-

nen het kristal. Deze verplaatsing van ladingen wordt stroom genoemd. Het toepassen van een spanning op de derde elektrode (de ‘gate’) kan het aantal ladingen binnen de halfgeleider verhogen of verminderen en bijgevolg wordt de mogelijke stroom verhoogd of verminderd (als wij eveneens het eerdergenoemde spanningsverschil toepassen). Transistoren worden algemeen gebruikt in elektronische apparaten zoals computers. Fundamenteel onderzoek eraan is belangrijk om een goede controle te verzekeren over de stromen binnen het materiaal, die het mogelijk maakt de elektrische eigenschappen van de halfgeleider te karakteriseren. De elektrische eigenschappen worden gewoonlijk onderzocht door de mobiliteit, dit is het gemak waarmee de ladingen zich in het materiaal bewegen, te meten. De meting van deze parameter geeft aan welke mogelijke fysieke processen betrokken zijn bij het geleidingsfenomeen. Zijn temperatuurafhankelijkheid geeft belangrijke informatie over de energiedistributie van de ‘traps’ (de ladingen kunnen bewegen, maar kunnen ook gevangen worden door voornamelijk gebreken of onzuiverheden in het kristal). De ‘traps’ zijn een belangrijke belemmering in de geleidingsprocessen.

In Hoofdstuk 5 karakteriseren wij de anthraceen veldeffecttransistor door verschillende spanningen (aan de ‘drain’ en de ‘gate’) toe te passen en de stroom door het materiaal te meten. Wij vonden dat de stroom varieert als een ‘power law’,  $f(x) = x^n$ , met een exponent groter dan 2. Dit is typisch voor ‘trap-filling’ in het ‘space-charge’ beperkte geleidingsregime. Wij berekenden een waarde voor de mobiliteit en maten haar temperatuurafhankelijkheid. Onder  $-263.15$  °C (10 K), wordt de mobiliteit temperatuurafhankelijk.

Maar toch geeft het meten van de mobiliteit niet alle details van de geleiding weer. De mobiliteit is namelijk een macroscopische waarde die het gemiddelde is van vele individuele gebeurtenissen. Deze individuele gebeurtenissen op nanometrische schaal (een nanometer - nm - is een miljardste  $- 10^{-9}$  - meter) moeten begrepen worden. Daarom stelden wij voor om de voordelen van de veldeffecttransistor (voor een goede beheersing van het aantal ladingen in het kristal) met die ‘single-molecule’ spectroscopie (om een hoge gevoeligheid op kleine veranderingen vast te stellen) te combineren teneinde het lokaal elektrisch veld binnen het kristal te sonderen.

## Het elektronisch transport sonderen

In Hoofdstuk 6, gebruikten wij een veldeffecttransistor gebaseerd op een kristal van anthraceen waarin wij enkele fluorescerende onzuiverheden (dibenzoterrylene moleculen) als sondes opnamen. Zo verwachten wij een goede controle te hebben over de stroom binnen het kristal en kunnen wij de geleidingsprocessen

door middel van de ‘single-molecule’ spectroscopie plaatselijk bestuderen.

Wij bestudeerden eerst het systeem door een gelijkspanning (dus constant spanningverschil) aan te leggen. Na lange tijd, stelden wij afwijkingen van de absorptiefrequenties van de sondemolekulen vast. Een accumulatie van ladingen wekt een potentiaal op. Wij denken dat deze accumulatie van ladingen in de SiO<sub>2</sub> laag (de isolatie die het kristal scheidt van de ‘gate’ elektrode) plaatsvindt. Wij beschreven deze afwijkingen met een machtswet van tijd. Wij kunnen de gegevens begrijpen door gebruik te maken van het ‘continuous-time random walk’ model, ontwikkeld door Scher en Montroll om de stroom in wanordelijke materialen te beschrijven. Wij vonden een dispersieparameter van 0.3 tot 0.5, blijkbaar temperatuur- en spanningonafhankelijk. De geleidingsprocessen kunnen als een ketting van verspringende gebeurtenissen worden gezien, die gebaseerd zijn op een distributie van wachttijden, waarschijnlijk te wijten aan een distributie van afstanden tussen de ‘traps’.

In het wisselspanning experiment (wat betekent dat de spanningsverschil niet meer constant is, maar een periodieke modulatie volgt), pasten wij een sinusmodulatie van de spanning toe. In dat geval, is de absorptie lijn van het molecuul gesplitst in twee lijnen, met een afstand tussen de twee maxima afhankelijk van de spanning. Wanneer wij de frequentie van de modulatie veranderden, namen wij onverwachte resonanties voor specifieke frequenties waar (de afstand tussen de twee lijnen wordt plotseling groter). Deze resonanties zijn temperatuur- of drukafhankelijk. De demping neemt sterk toe met zowel temperatuur als druk. Wij voerden een reeks experimenten uit in andere gastheer systemen: een polykrystallijne *n*-dodecaan matrix of ‘spin-coated’ anthraceen in plaats van een anthraceen eenkristal). Een coherente verklaring van de resultaten is dat de ladingen die binnen de matrix worden gevangen toestaan om quasi-lokale ‘phonon modes’ in het kristal op lange afstanden op te wekken.

## List of publications

- A. A. L. Nicolet, P. Bordat, C. Hofmann, M. A. Kol'chenko, B. Kozankiewicz, R. Brown, M. Orrit, "Single Dibenzoterrylene Molecules in an Anthracene Crystal: Main Insertion Sites", *ChemPhysChem* **8**, in press (2007).
- A. A. L. Nicolet, C. Hofmann, M. A. Kol'chenko, B. Kozankiewicz, M. Orrit, "Single Dibenzoterrylene Molecules in an Anthracene Crystal: Spectroscopy and Photophysics", *ChemPhysChem* **8**, 1215 (2007).
- A. Nicolet, M. A. Kol'chenko, B. Kozankiewicz, M. Orrit "Intermolecular inter-system-crossing in single-molecule spectroscopy: Terrylene in anthracene crystal" *J. Chem. Phys.* **124**, 164711 (2006).
- C. Hofmann, A. Nicolet, M. A. Kol'chenko, M. Orrit "Towards nano-probes for conduction in molecular crystals: Dibenzoterrylene in anthracene crystals" *Chem. Phys.* **318**, 1 (2005).
- M. A. Kol'chenko, B. Kozankiewicz, A. Nicolet, M. Orrit "Intersystem Crossing Mechanisms and Single-Molecule Fluorescence. Terrylene in Anthracene Crystals" *Opt. Spect.* **98**, 681 (2005).
- B. Desplanques, A. Nicolet, L. Theussl "Relationship of the  $^3P_0$  decay model to other strong decay models", 9<sup>th</sup> International Conference on the Structure of Baryons, Newport News, Virginia, USA, 3-8 March 2002: Proceedings edited by C.E. Carlson, B.A. Mecking *World Scientific*, 421 (2003).





## Curriculum vitae

Aurélien Armel Louis Nicolet, born in La Tronche (France), the 9<sup>th</sup> of November 1977.

Aurélien Nicolet obtained his baccalauréat in 1995 in the Académie of Grenoble (France). He then started to study Physics at the University Joseph Fourier (Grenoble). In 2000, he worked as an intern at the “Institut des Sciences Nucléaires” of Grenoble in the “Laboratoire de Physique Théorique” under the supervision of Prof. Bertrand Deplanques on *A Study of the Baryonic Resonances Decays*. The same year, he followed a Master of Sciences (Diplôme d’Études Approfondies : “Particules, Noyaux, Atomes et Photons”) at the University Claude Bernard in Lyon. During this period, he joined again the “Institut des Sciences Nucléaires” of Grenoble for another internship where he continued his studies on the baryonic resonances (*a “Microscopic” Study of the Model  $^3P_0$* ). He graduated in Lyon in 2001. He followed then a second Master of Sciences (DEA : “Chimie Physique Moléculaire et Structurale”) at the University Joseph Fourier in Grenoble. During this period, he worked as an intern at the “Laboratoire Louis Néel” in Grenoble. His research was then focused on *The Optical Detection of Molecular Magnetic Moments*, a collaboration project with the group of Prof. Michel Orrit from the University of Leiden. After graduating, he decided to join the University of Leiden in 2003 as an ‘Onderzoeker In Opleiding’ and started a Ph.D. on *Probing charge transport in molecular crystals*. From 2004 to 2006, he also worked as a Teaching Assistant for the Second Year Practicum at the University of Leiden. There, he was responsible for the ‘radioactivity’ and ‘Michelson Interferometer’ experiments. Aurélien Nicolet defended his Ph.D. in October 2007.



## Nawoord

This is the very end of my thesis. Yet, it would not be complete without expressing my gratitude to everyone without whom this work would not have been possible.

I would like to thank all members of the electronic department, especially Arno van Amersfoort, for running our computer network with dedication, René Overgauw and Leendert Prevo, who were always ready to help, with enthusiasm and professionalism. Working at low temperatures would not have been possible without the members of the cryogenic department. I would also like to thank Harmen van der Meer and Jos Disselhorst who liked to share their knowledge and competencies. Their wonderful work was always done with quality and aestheticism. Henriëtte van Leeuwen, Daniëlle van Raaij and, Riet Nieuwenhuijzen made certain that we could concentrate on our research. Without them, the group would probably have been very different.

It is difficult to forget the other members of the group, Markus and Alexander, for the pleasant atmosphere they created, Rob and Rogier, who were always there to dispute about any subject, Florian, who helped everyone with patience, and Robin, for these very interesting conversations about language, for her kindness, and her help. At the end of my Ph.D., I shared my office with Meindert. This cohabitation was very nice. I would like to thank him for these long discussions during the evenings in Veldhoven or Lunteren. I would especially like to thank Silvia and Edo, who have this incredible ability to share their enthusiasm about every thing, from sport to food, passing by culture and politics. I will definitely miss you! I have been very pleased to meet Anna with whom I shared worries and joys of the laboratory. Her presence was a great help to find a balance during the last period of my work.

Naast de mensen die ik al genoemd heb, ben ik nog veel dank verschuldigd aan Matthias, Michiel, Henriëtte en Prof. van der Waals. Met name voor hun ondersteuning bij de moeilijk totstandkoming van de samenvatting in het Nederlands.

I am also grateful to Mikhail Kol'chenko, who came back after his post-doc in the group and helped me with the measurements. I am deeply indebted to Clemens Hofmann, who taught me all about the work of an experimentalist. He did not only work with me, but also shared a friendship. His presence in

---

the group brought in a lot of life.

Finally, are the others, maybe the most important ones, incommensurable number of people who shared pieces of their lives with me and showed me the beauty of this country, who made my stay a wonderful adventure, Jessica, Peter and Miryam with whom I shared the tango, all people from Geversstraat and the surroundings, Lenie, Denis, Djamel, Gülhan, Umut, and the different room mates with whom we shared this small house and its events... Un gran gracias a Javier por todos esos años juntos. Era un gran placer ! Avant de terminer, je voudrais accorder encore quelques pensées à ceux, sans qui rien ne serait arrivé, à ceux qui m'ont guidé et aidé durant toutes ces années. Ces pensées vont à ma famille, à mon père et à ma mère, qui m'ont toujours soutenu dans mes choix, sans jugement et sans a priori. Je leur dois tout et jamais ne l'exprimerai-je assez. Ces pensées vont enfin à ceux, qui depuis une éternité m'ont procurer leur affection, Damián, Sophie, Matthieu, Jean-Philippe et, bien sûr, mon frère. Je ne saurais dire combien je vous dois... Dans mes attitudes, mes choix et mes goûts, toujours, je retrouve ces instants partagés avec vous. Ils sont pour moi préludes à bien des sourires, immarcescibles souvenirs... Je termine cette thèse en pensant à Anna. Ton amour a été d'une inestimable aide durant ces dernières années, source de réconfort et saveur du quotidien. Il apporte la beauté au jour levant et l'espoir des lendemains.